GEC·92

45th Annual Gaseous Electronics Conference

October 27–30, 1992 • Boston, Massachusetts

GTE Laboratories

45th Annual Gaseous Electronics Conference

27–30 October 1992 • Boston, Massachusetts

Program and Abstracts

A Sponsored Conference of the
American Physical Society
Division of Atomic, Molecular, and Optical Physics

Hosted by
GTE Laboratories Incorporated, Waltham, Massachusetts

Executive Committee

Chun C. Lin
Chairman
University of Wisconsin

Pablo A. Vicharelli
Secretary
GTE Laboratories Incorporated

James T. Dakin
Chairman-Elect
GE Lighting

W. Lowell Morgan
Treasurer
Kinema Research

Michel Moisan
Secretary-Elect
University of Montreal

David B. Graves
University of California

Harold M. Anderson
University of New Mexico

John Heidenreich
IBM — T.J. Watson Research Center

Kurt H. Becker
City College of New York

Fred W. Meyer
Oak Ridge National Laboratory

Local Committee

Diane Vrattos
Kathryn Bailey
Wojciech Byszewski

Timothy Fohl
Yan Ming Li
Robert Piejak

This book was prepared by the
Publication and Presentation Services Department
at
GTE Laboratories Incorporated.

Acknowledgments

The Gaseous Electronics Conference gratefully acknowledges the support of GTE Laboratories Incorporated. Financial support for the Gaseous Electronics Conference has been provided by:

Government Agency

The National Science Foundation

Major Corporate Sponsors

IBM — International Business Machines Corporation
GTE Products Corporation
The General Electrical Company

The Gaseous Electronics Conference is sponsored by the American Physical Society, Division of Atomic, Molecular, and Optical Physics.

Contents

Technical Program

45th Annual Gaseous Electronics Conference

Registration and Reception

6:00 – 9:00 p.m., Monday, October 26, 1992
Park Plaza Hotel, Stanbro Room, Boston, Massachusetts

Session AA — Streamers and Time Dependent Discharges

8:00 – 10:00 a.m., Tuesday, October 27, Georgian Room
Chair: Y.M. Li, GTE Laboratories Incorporated

8:00 –	8:30	AA-1	Models of Low-Current, Low-Pressure Hydrogen Discharges A.V. Phelps, Z.Lj. Petrovic, and B.M. Jelenkovic
8:30 –	8:45	AA-2	Multidimensional Nonequilibrium Fluid Models for Streamers J.-M. Guo and C.-H. Wu
8:45 –	9:00	AA-3	Observation of a Hysteresis Effect in Chaotic Behavior of a He Discharge D.F. Hudson
9:00 –	9:15	AA-4	On the Physics of the Pendulum Effect in a Hollow Cathode H. Eichhorn, K.H. Schoenbach, R.P. Joshi, and T. Tessnow
9:15 –	9:30	AA-5	Streamers in a 13 cm Gap W. Yi, P.F. Williams, and F.E. Peterkin
9:30 –	9:45	AA-6	Electrical Discharge Initiation and a Circuit Model for Formative Time Lags W.B. Maier II, A. Kadish, C.J. Buchenauer, and R.T. Robiscoe
9:45 –	10:00	AA-7	A Fast and Accurate Kinetic Method — A Generalized Monte Carlo Flux Method — for Spatio-Temporal Varying Fields C. Li and C.-H. Wu

Session AB — Plasma Modeling

8:00 – 10:00 a.m., Tuesday, October 27, Arlington Room
Chair: J. Margot, University of Montréal

8:00 –	8:30	AB-1	Monte Carlo Modeling of RF Nonequilibrium Plasma in Monosilane H. Tagashira, A. Yokozawa, K. Kitamori, and Y. Sakai *(Invited Paper)*

8:30 – 8:45 AB-2 Modeling the Helical Resonator in the Presence of Large Sheaths
K. Niazi, A.J. Lichtenberg, M.A. Lieberman, and D.L. Flamm

8:45 – 9:00 AB-3 A 2D Diffusion Model of Transport in Plasma Processing Reactors
R.A. Stewart, B. Troyanovsky, and M.A. Lieberman

9:00 – 9:15 AB-4 A Monte Carlo Simulation of Remote Plasma Reactors Using Equivalent Representations for Electrons, Ions and Excited States
F.Y. Huang and M.J. Kushner

9:15 – 9:30 AB-5 The Effects of Nonthermal Charge Exchange on Ion Energy Distributions for Multicomponent Gas Mixtures in RF Discharges
H.H. Hwang and M.J. Kushner

9:30 – 9:45 AB-6 Self-Consistent Glow Discharge Model Including Neutral Transport and Reaction
D.J. Economou and D. Lymberopoulos

9:45 – 10:00 AB-7 Multi-dimensional Kinetic Models of the Radial and Axial Flow in RF Glow Discharges
J.H. Tsai and C.-H. Wu

Session BA — Atomic and Molecular Collisions

10:15 a.m. – 12:00 noon, Tuesday, October 27, Georgian Room
Chair: J. Paulson, Phillips Laboratory

10:15 – 10:30 BA-1 Mixing of the Cd 5^3P Fine-Structure States Induced by Hg Collisions
J. Supronowicz, J. Hinek, J.B. Atkinson, and L. Krause

10:30 – 10:45 BA-2 Guided-Ion Beam Study of the Reactions of Ar^+ and NO
R.A. Dressler, S. Graul, S. Williams, R.H. Salter, and E. Murad

10:45 – 11:00 BA-3 Collisional Detachment of I^- Using Pulsed ICR Spectrometry
K. Riehl and P. Haaland

11:00 – 11:15 BA-4 Energy Transfer Kinetics Between N_2 (X, v) and SiH_4
L.G. Piper

11:15 – 11:30 BA-5 Ion-Molecule Reactions at High Temperatures
M. Menendez-Barreto, J.F. Friedman, T.M. Miller, A.A. Viggiano, R.A. Morris, A.E.S. Miller, J.M. van Doren, and J.F. Paulson

11:30 – 11:45 BA-6 Temperature, Kinetic Energy and Internal Energy Dependences of the Rate Constants for the Reaction O_2^- with SF_6
A.A. Viggiano, R.A. Morris, J.M. van Doren, and J.F. Paulson

11:45 – 12:00 BA-7 High Energy Asymptotic Forms for Partial Derivatives of Phase Shifts with Respect to Momentum and Angular Momentum
W.J. Romo and S.R. Valluri

Session BB — RF Discharge Modeling and GEC Reference Cell
10:15 a.m. – 12:15 p.m., Tuesday, October 27, Arlington Room
Chair: J. Gerardo, Sandia National Laboratories

10:15 – 10:30 BB-1 Measuring the Distribution of RF Current in the GEC Reference Cell
M.A. Sobolewski

10:30 – 10:45 BB-2 Dependence on Excitation Symmetry of Electrical Parameters and Radial Currents in a Parallel-Plate RF Discharge
P.A. Miller, K.E. Greenberg, G.A. Hebner, P.D. Pochan, and J.T. Verdeyen

10:45 – 11:00 BB-3 Measurement of Atomic Hydrogen Concentration Profile in GEC Reference Cell
B.L. Preppernau, T.A. Miller, P. Bletzinger, B.N. Ganguly, and A. Garscadden

11:00 – 11:15 BB-4 Comparison of Experiment and Theory for Helium RF Discharge
M.E. Riley, K.E. Greenberg, G.A. Hebner, and P.J. Drallos

11:15 – 11:30 BB-5 A Two-Dimensional Simulation of the GEC RF Reference Cell Using a Hybrid Fluid-Monte Carlo Method
H. Pak and M.E. Riley

11:30 – 11:45 BB-6 Modeling of RF Glow Discharges in SF_6 by RCT Model
N. Nakano, N. Shimura, Z. Lj. Petrovic, and T. Makabe

11:45 – 12:00 BB-7 Kinetic Modeling of the α to γ Transition in RF Discharges
W.N.G. Hitchon, G.J. Parker, and J.E. Lawler

12:00 – 12:15 BB-8 Comparison of a 2D Hybrid Fluid-PIC Simulation to Experimental Results
H.M. Persing, R.K. Porteous, A.J. Perry, B.A. Nelson, and R.W. Boswell

Session CA — Electron Molecule Collisions

1:30 – 3:30 p.m., Tuesday, October 27, Georgian Room

Chair: G. Victor, Harvard-Smithsonian Center for Astrophysics

1:30 – 1:45 CA-1 Low Energy Elastic Scattering from Molecular Ions
A.E. Orel

1:45 – 2:00 CA-2 Differential Cross Sections for Elastic Scattering of Electrons from N_2
X. Shi, T.M. Stephen, and P.D. Burrow

2:00 – 2:15 CA-3 Electron Scattering from C_2H_2 Molecules in the Energy Range of 0.01–20 eV
I. Khurana and A. Jain

2:15 – 2:30 CA-4 Low-Energy Electron-H_2S Scattering
B.H. Lengsfield III and T.N. Rescigno

2:30 – 2:45 CA-5 Relative Electron Excitation Efficiencies for Vibrations of O_3, CO_2, and N_2O
K. Holtzclaw, K.L. Carleton, B.L. Upschulte, B.D. Green, S. Lipson, and W. Blumberg

2:45 – 3:00 CA-6 Generalized Oscillator Strengths of Valence and Carbon K Shell Excitations of Freons
J.F. Ying, C.P. Mathers, and K.T. Leung

3:00 – 3:15 CA-7 Optical Pumping of the $b^4\Sigma$-$X^2\Pi$ Transition in NO
M.J. Dyer, G.W. Faris, P.C. Cosby, D.L. Huestis, and T.G. Slanger

3:15 – 3:30 CA-8 Valence Shell Electronic Structures of Cis-, Trans-, and Iso-Butene by Symmetric Noncoplanar (e, 2e) Spectroscopy and Synchrotron Radiation Photoelectron Spectroscopy
C.P. Mathers, J.F. Ying, B.N Gover, and K.T. Leung

Session CB — High Density Plasmas

1:30 – 3:30 p.m., Tuesday, October 27, Arlington Room

Chair: J. Heidenreich, IBM — T.J. Watson Research Center

1:30 – 1:45 CB-1 Hollow Anode Discharge Based High Efficiency RF Triode Reactor
B. Singh, V. Patel, S. Sun, E. Whittaker, R. Kerns, and J. Maher

1:45 – 2:00 CB-2 RF Production of Dense Plasma Columns
F.F. Chen and G. Chevalier

2:00 – 2:15 CB-3 Comparison of Electrostatic Shielded and Unshielded Inductive Coupled Plasma Sources
W. Johnson

2:15 – 2:30 CB-4 RF Induction/Multipole Plasma for Etching
J.H. Keller, M.S. Barnes, J.C. Forster, T. Wicker, and R. Lindquist

2:30 – 2:45 CB-5 Hybrid Models of Low Pressure Inductively Coupled Plasma Sources for Etching
P.L.G. Ventzek and M.J. Kushner

2:45 – 3:00 CB-6 Inductive Low Pressure RF Discharges: Model and Experiment
R.B. Piejak, V.A. Godyak, and B.M. Alexandrovich

3:00 – 3:15 CB-7 Model Study of ECR Reactors
H.M. Wu, D.B. Graves, R.K. Porteous, and J.D. Bukowski

3:15 – 3:30 CB-8 Hybrid Model of an ECR Etching System
R.E.P. Harvey, W.N.G. Hitchon, E.R. Keiter, and K.M. Kramer

Session D — Posters
3:30 – 5:30 p.m., Tuesday, October 27, Castle
Chair: H. Anderson, University of New Mexico

Heavy Particle Collisions

DA-1 Reflection of N_2 Metastables at the Boundary
S. Suzuki, H. Itoh, H. Sekizawa, and N. Ikuta

DA-2 Influence of Excited Oxygen Atoms (O^1D) to Wall Recombination Coefficient
S. Wickramanayaka, N. Hosokawa, and Y. Hatanaka

DA-3 Absorption Cross Section Measurements of Schumann-Runge Continuum of O_2 at 78 K and 295 K
W.H. Parkinson, J.R. Esmond, and K. Yoshino

DA-4 EUV Absorption Spectroscopy of Supersonic-Jet-Cooled-Molecules: CO Bands in the Wavelength Region Near 97 nm
P.L. Smith, G. Stark, K. Yoshino, K. Ito, and J.R. Esmond

DA-5 OH (v, N) Populations Determined from High-Resolution Spectra of the Airglow. Kinetic Model for State-to-State Dynamics
J.A. Dodd, W.A.M. Blumberg, S.J. Lipson, J.R. Lowell, P.S. Armstrong, D.R. Smith, R.M. Nadile, N.B. Wheeler, E.R. Huppi, S.M. Adler-Golden, W.J. Marinelli, K.W. Holtzclaw, and B.D. Green.

DA-6 Electron Thermalization Processes in After Glow Plasma
Y. Sakai, S. Sawada, and H. Tagashira

DA-7 Electron Attachment to Silicon Hydride and Silicon Fluoride Species
H.H. Michels and R.H. Hobbs

DA-8 Empirical Potentials for the Interaction of Electronically Excited Atoms
D. Hudson

DA-9 Single-Particle Potential for Photo-excited States of Open-Shell Atoms
J.J. Boyle

DA-10 X-ray Double Ionization of Helium Isoelectronic Sequence
A. Dalgarno and H.R. Sadeghpour

DA-11 Model for Ion Trapping in Dusty Plasmas
J. Goree

DA-12 Effect of Ion-Neutral Collisions on the Perpendicular Ion Temperature in Argon
R.K. Porteous, S. Defauconpret, H.B. Smith, and R.W. Boswell

DA-13 Quenching and Energy Transfer in $B^3\Pi$ State of N_2
C. Scripter and J. Borysow

DA-14 Radiative Association and Inverse Predissociation of Oxygen Atoms
J.F. Babb, A. Dalgarno, and J. Yeh

DA-15 Chemiluminescence in Suprathermal Reactive Collisions of O^+ and Ar^+ with Monomethylhydrazine
J.A. Gardner, R.A. Dressler, R.H. Salter, and E. Murad

DA-16 Three-Body Conversion of He^{++} Ions in Helium
R.E. Tosh and R. Johnsen

Diagnostics

DB-10 Mass Spectroscopy and Molecular-Beam Deposition from Hydrocarbon Arcjet Plasmas that Produce Diamond
W. Homsi and K.R. Stalder

DB-11 Miniature Retarding Grid Ion Energy Analyzer
G.W. Gibson, Jr., and H.H. Sawin

DB-12 The Diagnostics of RF Glow Discharges with Particulates by Using Spatiotemporal Spectroscopy and Mie Scattering
S. Kakuta, T. Kamata, and T. Makabe

DB-13 Artificial Neural Networks for Plasma Spectroscopy Analysis
W.L. Morgan, J.T. Larsen, and W.H. Goldstein

DB-14 Application of CARS to the Study of Surface Deactivation of Vibrationally Excited Homonuclear Diatomic Molecules
P.P. Yaney, K.A. Rimkus, and B. Ganguly

DB-15 Laser Induced Fluorescence Measurement of Ion Velocity Distributions in a Pulsed Plasma Sheath
M.J. Goeckner, M. Shamim, R.A. Breun, and J.R. Conrad

DB-16 Laser Induced Fluorescence Measurements of the Sheath Thickness in a Magnetron Sputtering Discharge
M. Bowden, T. Nakamura, Y. Yamagata, B.W. James, K. Muraoka, and M. Maeda

DB-17 Measurement of Magnetic Presheath in Collisional ECR Plasma
G.-H. Kim and N. Hershkowitz

DB-18 Emission Spectroscopy in DC C_3H_8-H_2 Discharges Generated in a Plasma Carburizing Furnace
G. Sultan, G. Baravian, E. Denisse, P. Jacquot, and G. Dervieux

DB-20 Detection of O and H Atoms by Laser Induced Fluorescence and Stimulated Emission in a DC Glow Discharge
J. Amorim, G. Baravian, J. Jolly, and M. Touzeau

DB-21 Laser and Spectroscopic Studies of RF-Excited Hydrogen Discharges
A.T. Young, P. Chen, K.N. Leung, L.C. Pan, D.M. Ponce, and H.F. Döbele

Plasma Surface Interactions

DC-2 Modeling of Microwave Plasmas for Applications to CVD of Thin Diamond Films
B. Lane, E. Hyman, K. Tsang, A. Drobot, and R. Post

DC-3 Characterization of Thin Film-Diamond and DLC Producing Discharges
R.C. Cheshire, M.J. Higgins, T. Morrow, and W.G. Graham

DC-4 Thin Film Ceramics for Improved Performance of Repetitively-Pulsed High-Power Microwave Sources
C.B. Fleddermann, E. Schamiloglu, J. Gahl, D. Shiffler, B. Wroblewski, L. Moreland, and T. Cavazos

DC-5 Secondary Electron Emission from Electrode Surface Covered with Hydrogenated Amorphous Silicon
Y. Matsuda, H. Kawasaki, S. Yang, and H. Fujiyama

DC-6 SiO_2 Deposition by TEOS and Selected Oxygen Atoms
S. Wickramanayaka, A. Matsumoto, Y. Nakanishi, and Y. Hatanaka

DC-7 Spectroscopic and Actinometric Investigation of SiO_2 Etching Chemistry in the Helicon Reactor
H. Persing, A.J. Perry, and R.W. Boswell

DC-8 Molecular Dynamics Simulations of Fluorine Etching Silicon in the Presence of Ion Bombardment
M.E. Barone, T. Schoolcraft, B. Garrison, and D.B. Graves

DC-9 Above-Surface Neutralization of Multicharged Ions Incident on a Cesiated Au Target
F.W. Meyer, I.G. Hughes, S.H. Overbury, D.M. Zehner, and P.A. Zeijlmans van Emmichoven

DC-10 An Industrial-Scale Plasma Source Ion Implantation Facility
J.T. Scheuer, B.P. Wood, W.A. Reass, R.H. Olsher, M.A. Nastasi, and D.J. Rej

DC-11 Fabrication and Characterisation of Schottky Diodes Obtained by Deposition of TiN on Si Substrates
K.F. Al-Assadi, M. Boudiaf, and N.M.D. Brown

DC-12 Volume and Surface Effects Upon Oxygen Addition to YBaCuO Thin Film Producing Discharges
B.F. Burns and W.G. Graham

DC-13 Trapped Dust in Rare Gas Plasmas
B. Ganguly, A. Garscadden, and P. Haaland

DC-14 A Self-Consistent Study of the Plasma-Particulate Interface in Dusty Glow Discharges
S.J. Choi and M.J. Kushner

DC-15 Particulate Transport in ECR Discharges
M.D. Kilgore, J.E. Daugherty, R.K. Porteous, H.M. Wu, and D.B. Graves

Session EA — Electronic and Atomic Collision Processes
8:00 – 10:00 a.m., Wednesday, October 28, Georgian Room
Chair: K. Becker, City College of New York

8:00 – 8:30 EA-1 Electron-Atom Scattering Using Atomic Recoil
B. Bederson *(Invited Paper)*

8:30 – 9:00 EA-2 Collisional Deexcitation of Excited Rare Gas Atoms by Molecules Containing Group IV Elements
Y. Hatano *(Invited Paper)*

9:00 – 9:15 EA-3 The Production and Extraction of Polarized Electrons from an Optically Pumped Helium Discharge
R.J. Vandiver, L.D. Schearer, and T.J. Gay

9:15 – 9:30 EA-4 Electron Drift in Alkali-Metal Vapors
I.I. Fabrikant

9:30 – 9:45 EA-5 First-Order Distorted-Wave Calculation for the Excitation of Hydrogen Using Stark States
J.L. Peacher, D.H. Madison, and K. Taulbjerg

9:45 – 10:00 EA-6 Application of the Complex Kohn Method to the Calculation of Photoionization Cross Sections
T.N. Rescigno, B. Elza, B.H. Lengsfield III, and A.E. Orel

Session EB — Radiation, Metastables, and Lasers
8:00 – 10:00 a.m., Wednesday, October 28, Arlington Room
Chair: J.T. Dakin, GE Lighting

8:00 – 8:15 EB-1 Ionization Balance in the Negative Glow of a Hg-Ar Hot Cathode Discharge
R.C. Wamsley, K. Mitsuhashi, and J.E. Lawler

8:15 – 8:30 EB-2 A Monte Carlo Simulation of Resonance Radiation Transport in a Rare-Gas-Mercury Positive Column
T.J. Sommerer

8:30 – 8:45 EB-3 Behavior of Excited Atoms in High Density Plasma
K. Kadota, A. Miyata, T. Fujimoto, T. Ni-Imi, and Y. Hara

8:45 – 9:00 EB-4 Are Metastable Ions in High Density Glow Discharges Significant?
K.P. Giapis, R.A. Gottscho, N. Sadeghi, J. Margot, and T.C. Lee

9:00 – 9:15 EB-5 Influence of Metastables on the Discharge Structure in Ar
F. Tochikubo, T. Kamata, and T. Makabe

9:15 – 9:30 EB-6 Parametric Studies of the Neon Recombination Laser at 585 nm Using Electron Beam Pumping
R.L. Rhoades, L. Little, and J.T. Verdeyen

9:30 – 9:45 EB-7 Modeling of the Atomic Ne Laser in He/Ne/Ar Gas Mixtures
J.W. Shon and M.J. Kushner

9:45 – 10:00 EB-8 The Ar-Xe Laser: Efficiency as a Function of Xe Partial Pressure and Energy Loading
S.F. Fulghum, T.T. Perkins, R.L. Watterson, and J.H. Jacob

Session F — Plenary Lecture
10:30 – 11:30 a.m., Wednesday, October 28, Georgian Room
Chair: L.W. Anderson, University of Wisconsin

10:30 – 11:30 F-1 Laser Spectroscopy on the Cathode Fall and Negative Glow
J.E. Lawler

Session G — Business Meeting
11:30 a.m. – 12:00 noon, Wednesday, October 28, Georgian Room
Chair: C.C. Lin, University of Wisconsin

Session HA — Surface Interactions
1:30 – 3:00 p.m., Wednesday, October 28, Georgian Room
Chair: L. Christophorou, Oak Ridge National Laboratory

1:30 – 2:00 HA-1 The Physics and Chemistry of Large Carbon Clusters
R.N. Compton and R.L Hettich *(Invited Paper)*

2:00 – 2:30 HA-2 Interaction Dynamics of Hydrogen at a Cu (111) Surface
D.J. Auerbach, C.T. Rettner, and H.A. Michelsen *(Invited Paper)*

2:30 – 2:45 HA-3 Real Time, In Situ Monitoring of Surface Reactions During Plasma Processing
E.S. Aydil, Z.H. Zhou, K.P. Giapis, R.A. Gottscho, V.M. Donnelly, Y. Chabal, and J.A. Gregus

2:45 – 3:00 HA-4 Spatially and Temporally Resolved Detection of H Atoms in RF Plasmas
A. D. Tserepi and T.A. Miller

Session HB — Novel Plasma Applications
1:30 – 3:00 p.m., Wednesday, October 28, Arlington Room
Chair: R. Piejak, GTE Laboratories Incorporated

1:30 – 1:45 HB-1 Uranium Atomic Vapor Laser Isotope Separation (AVLIS)
R.G. Beeler and G.M. Heestand

1:45 – 2:00 HB-2 Plasmolysis of Ammonia
G.P. Miller and J.K. Baird

2:00 – 2:15 HB-3 Plasma Remediation of Gas Streams Contaminated by Trichloroethylene
D. Evans, M.J. Kushner, L.A. Rosocha, G.K. Anderson, and J.J. Coogan

2:15 – 2:30 HB-4 Optical Diagnostics of Corona Discharges as Envisaged for NO_x Removal from Flue Gas
T.H. Teich

2:30 – 2:45 HB-5 Emission of UV to Visible Radiation Produced by Pulsed RF Excitation of Ionizing Radiation Particle Tracks in a Gas
S.R. Hunter and W.A. Gibson

2:45 – 3:00 HB-6 Modeling and Temperature Measurement of a DC Plasma Torch Discharging into Air
A.B. Murphy

Session J — Posters

3:30 – 5:30 p.m., Wednesday, October 28, Castle

Chair: J.T. Verdeyen, University of Illinois

Glow Discharges

JA-1 Cathode Fall Development in Low-Pressure Hydrogen Discharges
B.M. Jelenkovic and A.V. Phelps

JA-2 A Model of the Cathode Spot Glow Discharge for a Cathode with Inclusions of Low Work Function Material
L. Pekker

JA-3 Frequency Dependent Effects in Parallel-Plate Argon RF Discharges
M.J. Colgan, Y. Li, and D.E. Murnick

JA-4 Characterization of Strange Attractor in Electrical Discharges in N_2 at 30 to 800 Pa
T. Akitsu, E. Ogawa, and H. Matsuzawa

JA-5 Suppression of Oscillations in Low Current Hydrogen Discharges
Z. Lj. Petrovic and A.V. Phelps

Electron Transport

JB-1 Electron Drift Velocities in Hydrogen-Argon Gas Mixtures
D.L. Mosteller, J.D. Clark, and A. Garscadden

JB-2 Electron Drift Velocities in Boron Trichloride in Argon and Helium Gas Mixtures
D.L. Mosteller, J.D. Clark, and A. Garscadden

JB-3 Electron Transport in Gases at High Densities
E.E. Kunhardt

JB-4 Monte Carlo Simulation of Electrons Including e-e Collisions
M. Chung and E.E. Kunhardt

JB-5 Relating Scattering Cross Sections to Swarm Data
E.E. Kunhardt

JB-6 Comparative Study of Positron and Electron Transport in Neon
P.J. Drallos and J.M. Wadehra

JB-7 Transport of Electrons in Hydrocarbon Gases at High E/N
A.A. Sebastian, P.J. Drallos, and J.M. Wadehra

JB-8 RF Electron Swarm Transport in Ar and HCl by Direct Numerical Method of the Boltzmann Equation
K. Maeda and T. Makabe

JB-9 Characteristic Energy of Electrons in NO at Moderate E/N
W. Roznerski, J. Mechlinska-Drewko, and Z. Lj. Petrovic

JB-10 Nonequilibrium Kinetics of Nitrogen Under Plasma Conditions: An Improvement
C. Gorse and M. Capitelli

Ion Transport

JC-1 Accurate Analysis of Transport Property of Ions by FTI Method for Isotropic Scattering in CM Frame
E. Nishi, E. Holcomb, and N. Ikuta

JC-2 Mobility Curves of Gaseous Ions with a Hump
E. Nishi and N. Ikuta

JC-3 Constant Mobilities of Gaseous Ions in Low Field
N. Ikuta and E. Nishi

JC-4 The Influence of Charge Transfer on Plasma Balance
T.E. Gist, W.F. Bailey, and A. Garscadden

JC-5 Combined Diffusion Coefficients in a Partially Ionized Binary Gas Mixture
A.B. Murphy

JC-6 Direct Experimental Observation of Velocity Component Correlations and Transport Properties of Ba^+ Drifting in Ar
M.J. Bastian, V.M. Bierbaum, and S.R. Leone

JC-7 Ne_2^+ Dissociative Recombination Products in Metastable Ne Effusing from a Ne Gas Discharge
A. Barrios, W. Chism, J. Li, J.W. Sheldon, K.A. Hardy, and J.R. Peterson

JC-8 Mobility of $C_2H_5^+$ in Methane
J. de Urquijo, I. Alvarez, C. Cisneros, and H. Martinez

Laser Kinetics

Lamps and Switching Arcs

Electron Collisions: Theory

JF-11 Recommended Set of Cross Sections for Modeling of RF Discharges in Argon: Excited State Kinetics
Z. Lj. Petrovic, J. Jovanovic, S. Vrhovac, and J.T. Broad

JF-12 Electron Driven Chemistry for the CF_4 Chemical System as a Function of Electron Temperature
R.E.P. Harvey

JF-13 Mechanisms, Cross Sections, and Rates for Dissociative Recombination
S.L. Guberman

JF-14 Collisional Excitation of $O(^1D)$ via the O_2 ($^1\Pi_g$) State
Y. Sun and A. Dalgarno

JF-15 Dissociative Recombination of Electrons with $ArXe^+$
A.P. Hickman, D.L. Huestis, and R.P. Saxon

JF-16 Monte Carlo Calculation of Illustrative Electron Trajectory Patterns in a Hollow Cathode Cylindrical Magnetron Discharge
B. Shi, Z. Yu, L. Li, and G.J. Collins

JF-17 Effective Radiative Recombination Coefficients of Atomic Oxygen
V. Escalante and G.A. Victor

JF-18 Rates for Electron Collisional Excitation of OII
B.M. McLaughlin and K.L. Bell

JF-19 Collisional Rates and Cooling within Atomic Hydrogen Plasmas
T.T. Scholz

JF-20 Angle-Differential and Momentum-Transfer Cross Sections for Low-Energy Electron-Cs Scattering
U. Thumm and D.W. Norcross

Breakdown

JG-1 Observation of the Breakdown in a Planar Hollow Cathode Discharge
M.P. Alberta and J. Derouard

JG-2 Low Density Breakdown Characteristics in the Presence of Magnetic Field
S. Popovic and E. Kunhardt

JG-3 The Morphology of Streamer Coronas
P.A. Vitello, B.M. Penetrante, and J.N. Bardsley

Session KA —Collisions of Laser Cooled Atoms
8:00 – 10:00 a.m., Thursday, October 29, Georgian Room
Chair: P.L. Gould, University of Connecticut

8:00 – 8:30 KA-1 Optical Manipulation of Ultracold Atomic Collisions
P.S. Julienne *(Invited Paper)*

8:30 – 9:00 KA-2 "Bright Beams" of Ne* Metastable Atoms
H.C.W. Beijerinck, H.J.L. Megens, M.P. Schuwer, M.D. Hoogerland, and K.A.H. van Leeuwen *(Invited Paper)*

9:00 – 9:30 KA-3 Collisions of Trapped Atoms
T. Walker *(Invited Paper)*

9:30 – 10:00 KA-4 Ultracold Collisions by Velocity Selection in an Atomic Beam
J. Weiner, Y. Wang, and D. Laman *(Invited Paper)*

Session KB — Sheaths and Cathodes
8:00 – 10:00 a.m., Thursday, October 29, Arlington Room
Chair: W. Byszewski, GTE Laboratories Incorporated

8:00 – 8:15 KB-1 Ion and Atom Temperatures in a Pulsed Vacuum Arc
I.S. Falconer, A.J. Studer, B.W. James, and D.R. McKenzie

8:15 – 8:30 KB-2 Measurement of the Electric Field in the Cathode Fall Region of a Hollow-Cathode Discharge from the Intensity of Forbidden Spectral Transitions
I.S. Falconer, L.Y. Montuno, and B.W. James

8:30 – 8:45 KB-3 Kinetics and Dynamics of Non-equilibrium Cathode Heating
W.L. Morgan, L.C. Pitchford, and S. Boisseau

8:45 – 9:00 KB-4 Sheath and Presheath in Plasmas of Co-axial and Concentric Geometries
H.-B. Valentini

9:00 – 9:15 KB-5 Monte-Carlo Simulation of Pulsating Dielectric Barrier Discharges-Stochastic Analysis
R.J. van Brunt, E.W. Cernyar, and P. von Glahn

9:15 – 9:30 KB-6 Nonequilibrium Ion Transport in a Collisional Sheath
J. Ingold

9:30 – 9:45 KB-7 A Unified Theory of Arc-Electrode Systems
P. Zhu, J.J. Lowke, and R. Morrow

9:45 – 10:00 KB-8 Investigation of Arc Spot Development on Cold Cathodes
J. Schein, R. Bayer, and J. Mentel

Session L — Posters

10:15 a.m. – 12:15 p.m., Thursday, October 29, Castle
Chair: J. McConkey, University of Windsor

Modeling

LA-1 Two Dimensional Calculations of the Free Radical Concentrations in an ECR Processing Plasma
K. Ashtiani, J.L. Shohet, and R.E.P. Harvey

LA-2 Modeling of ECR Processes
M. Meyyappan

LA-3 The RF Resonant Mode in an Elliptical Cavity
H.M. Wu and D.B. Graves

LA-4 Simulation of the Cathode Fall Region of a Cylindrical Magnetron Discharge
I.S. Falconer, T.A. Vander Straaten, B.W. James, and I.J. Donnelly

LA-5 Modelling an Improved Spiral Loop Antenna for Inductively Coupled Plasma Sources
T. Intrator, J. Menard, and H. Hershkowitz

LA-6 Simulation of an RF Inductively Coupled Reactor
R.K. Keinigs, T.A. Oliphant, H.M. Anderson, and R.C. Sierocinski

LA-7 RF Discharge Model Comparisons
T.E. Nitschke and D.B. Graves

LA-8 Semi Analytic, Hybrid Fluid-Particle Model of 1-D Glow Discharges
R. Bendahan, I. Peres, J.P. Boeuf, and L.C. Pitchford

LA-9 RF Discharge Modeling: Moment Equations Approach
M. Meyyappan and T.R. Govindan

LA-10 A Bounded Two Dimensional PIC-MCC Code for Simulating Processing Plasmas
V. Vahedi, C.K. Birdsall, M.A. Lieberman, G. Dipeso, T.D. Rognlien, J.R. Hiskes, and R.H. Cohen

LA-11 Bounded PIC-MCC Simulation of an Electronegative RF Discharge
V. Vahedi, M.A. Lieberman, C.K. Birdsall, T.D. Rognlien, J.R. Hiskes, and R.H. Cohen

LA-12 Single Particle Monte Carlo Models and Nonlinearity as Tools to Understand the Measured EEDF Shape in RF Discharges
S. Longo

LA-13 PIC Monte Carlo/Fluid Model Comparison for Low Pressure RF Glow Discharges
T.E. Nitschke, D.B. Graves, and M. Surendra

LA-14 A Highly Flexible Framework for Modeling of Plasma Processing
E.R. Keiter, K.M. Kramer, and W.N.G. Hitchon

LA-15 A Hydrodynamic-Monte Carlo Simulation for Neutral Radical Transport in Remote Plasma Reactors
M.J. Hartig and M.J. Kushner

LA-16 Numerical Simulation of Electrical Arc Including the Continuous Phase Transition (CPHT) Model
A. Kaddani, C. Delalondre, O. Simonin, and H. Minoo

LA-17 Two-Dimensional, Self-Consistent, Three-Moment Simulation of RF Glow Discharges
F. Young and C.-H. Wu

LA-18 2-D Fluid Model of Radio-Frequency Discharges
M. Dalvie and M. Surendra

LA-19 A Moment Analysis of Particle-in-Cell/Monte Carlo Simulations of RF Parallel-Plate Discharges
M. Surendra and M. Dalvie

LA-20 2-D Model of Low Pressure Glow Discharges in Plane-Plane and Rod-Rod Geometries
A. Fiala, L.C. Pitchford, and J.P. Boeuf

LA-21 Non-Linear Circuit Model of Plasma Loaded RF Electrodes
J. Forster

LA-22 Nonlinear Gaseous Electric Discharge — Mathematical Modeling
M. Kuman

High Density Plasma Sources and Applications

LB-1 Plasma Wave Fields in a Helicon Plasma Source
A.R. Ellingboe and R.W. Boswell

LB-2 Etching and Deposition in the Helicon Reactor with $SiCl_4$
M.A. Jarnyk, R.W. Boswell, K.G. Orrman-Rossiter, and J.S. Williams

LB-3 Theoretically Exploring the Experimentally Observed V-B Transition Between the Conventional Magnetron and Anode Obstructed Hollow Cathode Discharge Modes
B. Shi, Z. Yu, L. Li, and G.J. Collins

LB-4 Large Area ECR Plasma Source with a New Type of Microwave Window Utilizing a Multipolar Line Cusp Magnetic Field
W. Getty and J. Geddes

LB-5 Extended Pressure Range for Planar Inductive RF Processing Discharges Through Pulsed Operation
A.E. Wendt, L.J. Mahoney, and J.L. Shohet

LB-6 A Comparison Between Inductively-Coupled Hydrogen and Argon RF Discharges
C.S. Cui, R.K. Porteous, and R.W. Boswell

LB-7 ECR Microwave Power Absorption in Plasma Deposition and Etching Devices
R. Veerasingam, C.A. Outten, J.C. Barbour, R.B. Campbell, and R.T. McGrath

LB-8 Investigation of Spatial and Temporal Plasma Uniformity in an ECR Plasma Etch Tool
J.E. Stevens, Y.C. Huang, and J.L. Cecchi

LB-9 Comparison Between Measured and Predicted Spatial Variation of Plasma Parameters in an ECR Reactor
R.A. Stewart, H.-M. Wu, M.A. Lieberman, and D.B. Graves

LB-10 Ion Transport in a Non Diverging Magnetically Assisted Surface-Wave Produced Plasma (SWP) Under ECR Conditions
J. Margot and C. Barbeau

LB-11 Electrical Characterization of Low Pressure Inductive RF Discharges in Argon
V.A. Godyak, R.B. Piejak, and B.M. Alexandrovich

LB-12 Self-Accelerating Electric Field in Gridless ECR Ion Source
T. Akitsu, E. Ogawa, and H. Matsuzawa

LB-13 Modeling Plasma-Natural Interactions in a High Density ECR Argon Discharge
R.K. Porteous and R.W. Boswell

LB-14 A Cesium Plasma Ion Source
A.J.T. Holmes, M. Inman, and E. Surrey

GEC Reference Cell

LC-1 GEC Reference Cell to Model Comparisons
T.E. Nitschke and D.B. Graves

LC-2 Importance of Boundary Conditions for Breakdown in the Helium RF Discharge
M.E. Riley, K.E. Greenberg, and G.A. Hebner

LC-3 A Comparison of Etching Results of the GEC Reference Cell with a Commercial Etcher
J. Pender, M. Buie, M. Beauvais, M. Brake, and M. Elta

LC-4 Measurement of Ion Kinetic Energy Distributions from an Argon Discharge in the GEC RF Reference Cell
J.A. Rees, J.K. Olthoff, R.J. van Brunt, and S.B. Radovanov

LC-5 Spatial Distribution of Densities of the Metastable $3p^5$ 4s State of Argon in a GEC Reference Cell
E. Augustyniak, S. Filimonov, and J. Borysow

LC-6 Comparison of Microwave Interferometer and Langmuir Probe Results in the GEC Reference Reactor
M. Hopkins and L.J. Overzet

LC-7 Spatial Argon Optical Emission Distributions in the GEC RF Reference Cell
S. Djurovic and J. Roberts

Electron Collisions: Experiment

LD-1 Cross Sections for Electron Excitation of Singlet Levels from the 2^3S and 2^1S Metastable Levels of He
R.B. Lockwood, F.A. Sharpton, L.W. Anderson, and C.C. Lin

LD-2 Differential Vibrational and Electronic Excitation Cross Sections of Molecular Oxygen by Electron Impact
T.W. Shyn and C.J. Sweeney

LD-3 Further Studies of the Dissociative Excitation of CF_4
K. Becker, J. Dike, U. Müller, and G. Schulz

LD-4 Elastic Electron Scattering by Laser-Excited Sodium
C.H. Ying, Z. Shi, W. Tan, L. Vuskovic, and B. Bederson

LD-5 Elastic Electron Scattering by Hydrogen Sulphide
R.J. Gulley, S.J. Buckman, and M.J. Brunger

LD-6 Hydrogen Atom Yield in Surface-Wave-Sustained Hydrogen Discharges
L. St-Onge and M. Moisan

LD-7 Ion Chemistry of Tetra-Ethoxy Silane (TEOS)
J. Holtgrave, K. Riehl, and P. Haaland

LD-8 Optical Emissions from Electron-Impact Excited TEOS
M. Ducrepin, J. Dike, R.B. Siegel, and K. Becker

LD-9 Molecular Beam Profile Measurements — Investigating the Validity of the Relative Flow Normalisation Technique
R.J. Gulley, S. Bennett, and S.J. Buckman

LD-10 Electron Impact Ionization Covariance Mapping Spectroscopy of N_2
M.R. Bruce, L. Mi, and R.A. Bonham

LD-11 Triple Coincidence Measurements of Electron Impact Double Ionization
M.J. Ford, J.P. Doering, M.A. Coplan, J.W. Cooper, and J.H. Moore

LD-12 The Angular Distribution of Low-Energy Secondary Electrons in the Ionization-Excitation of N_2
J.P. Doering and J. Goembel

LD-13 Electron Impact Ionization of APSM (2 Acryloyloxy Propionic Acid Methylester)
R. Basner, M. Schmidt, H. Deutsch, H. Steinhauser, and A. Hartwig

LD-14 Electron Impact Ionization of WF_6
R. Basner, M. Schmidt, and H. Deutsch

LD-15 Electron-Impact Ionization of CF_x and NF_x ($x = 1 - 3$)
V. Tarnovsky, K. Becker, H. Deutsch, and T.D. Märk

LD-16 Electron Impact Ionization Cross Sections for NO and N_2O from Threshold to 1 keV
I. Iga, M.V.V.S. Rao, and S.K. Srivastava

LD-17 Electron-Impact Ionization Cross-Section Measurements for In^+ and Te^+ Using Crossed Beams
N. Duric, E. Bell, and G.H. Dunn

LD-18 Electron Recombination of $CO^+ \cdot CO$ and H_3O^+
R. Johnsen, Y.S. Cao, L.A. Weber, and M.F. Golde

LD-19 Dissociative Electron Attachment in S_2F_{10}, S_2OF_{10} and $S_2O_2F_{10}$
J.K. Olthoff, K.L. Stricklett, R.J. van Brunt, J.H. Moore, and I. Sauers

LD-20 Low-Energy Electron Attachment to Molecules Studied by Pulse Radiolysis Microwave Cavity Technique Combined with Microwave Heating
H. Shimamori, Y. Tatsumi, Y. Ogawa, and T. Sunagawa

LD-21 Neutral Metastable Fragments from Electron Collisions with Ar Clusters
P.J.M. van der Burgt and J.W. McConkey

LD-22 Angular Correlations Between Sequential Cascading Photons from n = 3 Atomic Hydrogen
J.F. Williams and M. Kumar

Session MA — Excited Atoms and Electron Collisions
1:30 p.m. – 3:30 p.m., Thursday, October 29, Georgian Room
Chair: W.A.M. Blumberg, Phillips Laboratory

1:30 – 2:00 MA-1 Electron Collisions with Excited Atoms
S. Trajmar, J.C. Nickel, K. Fujii, and M. Johnston *(Invited Paper)*

2:00 – 2:30 MA-2 Excitation from Metastable He Levels by Electron Impact
L.W. Anderson and C.C. Lin *(Invited Paper)*

2:30 – 2:45 MA-3 Distorted-Wave Approach for (e-2e) Scattering with the Proper Asymptotic Boundary Conditions
D.H. Madison and S. Jones

2:45 – 3:00 MA-4 The Use of Distorted Green's Functions for Electron Scattering from Heavy Atoms
D.H. Madison and J. Mitchell

3:00 – 3:15 MA-5 Electron Collision Cross Sections for He and Ar — Compilations of DCS
M. Hayashi

3:15 – 3:30 MA-6 Measurement of Dielectronic Recombination in a Known External Electric Field
D.W. Savin, L.D. Gardner, J.C. Raymond, D.B. Reisenfeld, and J.L. Kohl

Session MB — Plasma Etching
1:30 p.m. – 3:30 p.m., Thursday, October 29, Arlington Room
Chair: T. Sommerer, GE Corporate Research

1:30 – 1:45 MB-1 A Simple Rule for the Etch Rate of SiO_2 in CF_4 Plasmas
N. Hershkowitz and J. Ding

1:45 – 2:00 MB-2 Investigation of Ion-Enhanced Fluorocarbon Etching Kinetics at Near-Threshold Ion Energies
D.C. Gray and H.H. Sawin

2:00 – 2:15 MB-3 Microtrench Formation During Plasma Etching
T.J. Dalton, J.C. Arnold, H.H. Sawin, S. Swan, and D. Corliss

2:15 – 2:30 MB-4 Parametric Study of the Influence of the Wafer Biasing Frequency and Voltage Upon Etching of Polyimide
F. Bounasri, G. Sauve, and M. Moisan

2:30 – 2:45 MB-5 Spatially and Temporally Resolved Profiles of O Atoms in Etching Plasmas
A.D. Tserepi, B.L. Preppernau, and T.A. Miller

2:45 – 3:00 MB-6 High Sensitivity Absorption Spectroscopy for Low Pressure Plasma Etching Diagnostics
E.A. Whittaker, H.C. Sun, V. Patel, and B. Singh

3:00 – 3:15 MB-7 Surface Charging Effects During Plasma Etching
J.P. McVittie, S. Fang, and S. Murakawa

3:15 – 3:30 MB-8 Electron Collection at the Gate Edge During Overetching
S. Murakawa, S. Fang, and J.P. McVittie

Session NA — CF_4 Workshop
3:45 – 6:15 p.m., Thursday, October 29, Georgian Room
Chair: R.A. Bonham, Indiana University

3:45 – 4:00 NA-1 Cross Sections for Scattering of Low- and Intermediate-Energy Electrons from CF_4
M.A. Dillon, M. Kimura, L. Boesten, H. Tanaka, and A. Kobayashi

4:00 – 4:15 NA-2 Calculation of Elastic and Momentum Transfer Cross Sections for CF_4
C. Winstead, Q. Sun, and V. McKoy

4:15 – 4:30 NA-3 Dissociative Attachment and Ionic Dissociation Cross Sections of CF_4
S.K. Srivastava

4:30 – 4:45 NA-4 Dissociative Ionization Cross Sections for CF_4
M.R. Bruce and R.A. Bonham

4:45 – 5:00 NA-5 Measured and Calculated Cross Sections for the Electron-Impact Ionization of CF_3, CF_2, and CF
V. Tarnovsky, K. Becker, H. Deutsch, and T.D. Märk

5:00 – 5:15 NA-6 Dissociative Excitation of CF_4 Following Electron Impact
S. Wang, P.J.M. van der Burgt, L. Forand, and J.W. McConkey

5:15 – 5:30 NA-7 Polarization Calculations for Electron-Molecule Scattering Employing the Schwinger Multichannel Method with VGV Insertion
J.A. Sheehy and W.M. Huo

5:30 – 5:45 NA-8 Initial Modeling Results of RF Discharges in CF_4 Gas Mixtures Using a New Cross Section Set
H.H. Hwang, D.S. Thomas, and M.J. Kushner

5:45 – 6:15 Workshop Discussion

Session NB — Plasma Assisted Deposition
3:45 – 5:45 p.m., Thursday, October 29, Arlington Room
Chair: E. Kunhardt, Stevens Institute of Technology

3:45 – 4:00 NB-1 Absolute CH_3 Densities in a Diamond Growth Environment by Ultrasensitive Absorption Spectroscopy
K.L. Menningen, M.A. Childs, P. Chevako, N.W. Spellmeyer, L.W. Anderson, and J.E. Lawler

4:00 – 4:15 NB-2 Microwave Perturbation and Langmuir Probe Measurements in Methane/Hydrogen Discharges
C.B. Fleddermann and H.R. Snyder

4:15 – 4:30 NB-3 Ultraviolet Photoacoustic Detection of Gas Phase Precursors of Diamond
M.A. Childs, K.L. Menningen, P. Chevako, N.W. Spellmeyer, L.W. Anderson, and J.E. Lawler

4:30 – 4:45 NB-4 Oxidation and Reduction of Carbonous Impediments to the Low Temperature Growth of Diamond Films
F.V. Wells, R. Rodriguez, D.W. Warner, and S. Johnson

4:45 – 5:00 NB-5 A Comparison of $He/O_2/SiH_4$ and $He/N_2O/SiH_4$ Gas Mixtures for Remote Plasma Deposition of SiO_2
M.J. Kushner

5:00 – 5:15 NB-6 Low Temperature Plasma Assisted Deposition of Thick SiO_2 Layers Using the Helicon Reactor
H. Persing, G. Giroult-Matlakowski, S. Armand, and R. Boswell

5:15 – 5:30 NB-7 Deposition of a-Si:H Films by Glow Discharge Method with SiH_4-He System
Y. Nakamura, S. Sunago, Y. Sakai, N. Kutsuwada, and T. Sekine

5:30 – 5:45 NB-8 Time Dependent Analysis of Velocity Distribution and Transport Coefficients of Electrons in SiH_4 Under RF Field
S. Nakajima and N. Ikuta

Session PA — Recent Advances in Electron Atom Collisions
8:00 – 9:45 a.m., Friday, October 30, Georgian Room
Chair: D.H. Madison, University of Missouri

8:00 – 8:30 PA-1 Advances in the Theory of Electron-Atom Collisions
H.R.J. Walters *(Invited Paper)*

8:30 – 8:45 PA-2 Unpolarized Electron Scattering as a Stringent Test of Theory
L. Vuskovic

8:45 – 9:00 PA-3 Electron-Impact Excitation from Excited Atomic Systems
G. Csanak, D.C. Cartwright, R.E.H. Clark, and J. Abdallah, Jr.

9:00 – 9:15 PA-4 Polarized Electron-Noble Gas Collisions
T.J. Gay, J.E. Furst, and W.M.K.P. Wijayaratna

9:15 – 9:30 PA-5 R-Matrix Calculations for Electron-Impact Ionization of Complex Atoms
K. Bartschat

9:30 – 9:45 PA-6 Time-Dependent Approach to Electron-Hydrogen Collisions
D.R. Schultz, C. Bottcher, and D.H. Madison

Session PB — Electrical Characterization of Plasmas
8:00 – 10:00 a.m., Friday, October 30, Arlington Room
Chair: W. Lapatovich, GTE Laboratories Incorporated

8:00 – 8:15 PB-1 Probe Diagnostics of Non-Maxwellian Plasmas
V.A. Godyak, R.B. Piejak, and B.M. Alexandrovich

8:15 – 8:30 PB-2 Electron Energy Distribution Function in Plasma Etching System
K.F. Al-Assadi, M. Boudiaf, and N.M.D. Brown

8:30 – 8:45 PB-3 Mapping of Plasma Densities, Potentials, and Electron Energy Distribution Functions in a Low Pressure DC Discharge
R.C. Woods and I.D. Sudit

8:45 – 9:00 PB-4 A Study of the Accuracy of Various Cylindrical Probe Theories
I.D. Sudit and R.C. Woods

9:00 – 9:15 PB-5 Plasma-Sheath Approximate Solutions for Cylindrical Probes
O. Biblarz and G.S. Brown

9:15 – 9:30 PB-6 Electron Temperature Measurements in a Magnetized Surface-Wave-Produced Plasma (SWP) Under ECR Conditions
J. Margot, M. Moisan, and R. Grenier, M. Chaker, and F. Goldberg

9:30 – 9:45 PB-7 Charged Particle Dynamics Inside the Sheath of a Spherical Electrode in the Presence of Axial Magnetic Field
S. Popovic and E. Kunhardt

9:45 – 10:00 PB-8 Thomson Scattering Measurements of T_e and n_e in an ECR Discharge
M.D. Bowden, F. Kimura, K. Muta, K. Uchino, K. Muraoka, M. Maeda, Y. Manabe, M. Kitagawa, and T. Kimura

Session QA — Electron Attachment
10:15 – 11:15 a.m., Friday, October 30, Georgian Room
Chair: F.W. Meyer, Oak Ridge National Laboratory

10:15 – 10:30 QA-1 Enhanced Electron Attachment to Laser-Irradiated Molecular Hydrogen
L.A. Pinnaduwage and L.G. Christophorou

10:30 – 10:45 QA-2 Temperature Dependence of the Cross Section for Dissociative Attachment in Methyl Chloride
D.M. Pearl and P.D. Burrow

10:45 – 11:00 QA-3 Variation with Temperature of the Dissociative Electron Attachment to CH_3Br
P.G. Datskos, L.G. Christophorou, and J.G. Carter

11:00 – 11:15 QA-4 Effect of Temperature on the Autodetachment of C_6F_6
P.G. Datskos, L.G. Christophorou, and J.G. Carter

Session QB — Optical Diagnostics
10:15 a.m. – 12:00 p.m., Friday, October 30, Arlington Room
Chair: T. Fohl, Technology Integration Group

10:15 – 10:45 QB-1 Radical Density Measurements in RF Reactive Plasmas by IR Diode Laser Absorption Spectroscopy
T. Goto *(Invited Paper)*

10:45 – 11:00 QB-2 Spectroscopic Study of Metastable Oxygen in Point-to-Plane Corona Discharges
I.S. Falconer, G.P. Timms, L.Y. Montuno, B.W. James, and J.J. Lowke

11:00 – 11:15 QB-3 Time-Delayed Fluorescence from the 2px States of Pulse-Irradiated Argon and Neon: The Role of Subexcitation Electrons
M.A. Dillon, M. Kimura, and M.M. Burgers

11:15 – 11:30 QB-4 High Sensitivity Absorption Spectroscopy in Glow Discharge Plasmas
J.E. Lawler, K. Mitsuhashi, and R.C. Wamsley

11:30 – 11:45 QB-5 Optogalvanic Effect as a Probe for Plasma Processes
D. Kumar, R.R. Zinn, and S.P. McGlynn

11.45 – 12:00 QB-6 Temporal and Spectral Characteristics of Laser Optogalvanic Signals in an Argon RF Discharge
D. Kumar, R.R. Zinn, and S.P. McGlynn

Session AA

8:00 a.m. – 10:00 a.m.
Tuesday, October 27, 1992

Georgian Room

Streamers and Time Dependent Discharges

Chair
Y.M. Li, GTE Laboratories Incorporated

AA-1 Models of Low-Current, Low-Pressure Hydrogen Discharges.* A. V. PHELPS, Z. Lj. PETROVIĆ,** and B. M. JELENKOVIĆ** JILA, U. of Colorado and NIST. - Models of the transient and steady-state voltage and current for low-current (< 50 $\mu A/cm^2$), low-pressure ($0.3 \leq pd \leq 1$ Torr·cm), parallel-plane discharges in hydrogen are applied to dc, laser-perturbed, and pulsed discharges. The steady-state model includes electron- and ion-induced ionization, ion-induced electron emission at the cathode, ion-molecule reactions, and space charge effects. The transient model considers only one ion. A fit to voltage-current data at low currents adjusts the ion-induced electron yield; the positive ion transit time can be obtained by fitting one transient waveform; and the applied voltage or photocurrent pulse is set for a fit at some instant. The transient model then agrees quantitatively with experiment for the onset of spontaneous oscillations, for current and voltage following either a laser-induced photoelectron pulse or a voltage pulse, and for spontaneous oscillation waveforms. Numerical and analytical steady-state models give too large ($\geq$ x 2) negative differential resistances.

* Work supported in part by Air Force Wright Laboratories.
** Present address: Institute of Physics, Belgrade, Yugoslavia.

AA-2 Multidimensional Nonequilibrium Fluid Models for Streamers.* Jing–Ming Guo and Chwan–Hwa "John" Wu, Department of Electrical Engineering, Auburn University. The formation of ionizing channel and the propagation of Cathode– and anode–directed streamers in Nitrogen gas have been theorectically examined by a self–consistent, fully two–dimensional simulation, assuming a cylindrically symmetrical geometry. The dynamical model of the electron, considering the photoionization effect, is described by an equilibrium single moment equation and nonequilibrium two and three moment equations[1]. A More Accurate Flux Corrected Transport (MAFCT) technique, which guaratees the steep and varying gradient problem to be precisely solved, is used to solve the electron equations[2]. This is the first time that the gas pre–breakdown is investigated based on a nonequilibrium model which is more accurate than the equilibrium model. The spatial–temporal two–dimensional (r–z) simulation results of the development and propagation of streamers including the electron density, the space–change electric fields, the electron average velocity, and the electron mean energy are presented step by step from the initial condition to the ionizing channel bridging the gap.

*Work supported by NSF under ECS–9009395 and Advanced Manufacturing Technology Center at Auburn University.

[1]Michael S. Barnes, Tina J. Cotler, and Michael E. Elta, J. Comput. Phys. 77, 53 (1988).
[2]E. E. Kunhardt and C. Wu, J. Comput. Phys. 68, 127 (1987).

AA-3 Observation of a Hysteresis Effect in Chaotic Behavior of a He Discharge, D. Hudson, Naval Surface Warfare Center/ White Oak Laboratory - A continuing program concerned with the study of chaotic processes in gases, in particular He, has led to the observation of a hysteresis effect. As reported previously (1), increasing the current in a low pressure discharge in He results in the appearence of at least two independent oscillations, at about 12 and 100 kHz and their harmonics. At least two periods of oscillations occur separated by a region of chaotic behavior before transitioning to a pure chaotic state. A detailed study of the frequency of the 100 kHz peak revealed a weak frequency dependence on the discharge current. At the transition to chaos, this frequency suddenly increases by about 10 percent. Decreasing the current showed a sudden frequency decrease of about 10 percent but at a current 1-2 ma below that where the increase occured. This behavior is very reproducible and the jumps are extremly sharp.

(1) Hudson, D. 43d Gaseous Electronics Conference 1990

AA-4 On the Physics of the Pendulum Effect in a Hollow Cathode*, H. EICHHORN, K.H. SCHOENBACH, R.P. JOSHI and T. TESSNOW, Old Dominion University, Norfolk, VA - To study the pendulum effect, the development of the pre-discharge has been considered assuming stationary emission of the electrons at the cathode. The hollow cathode simulated consists of a cylindrical cathode and a coaxial grid anode. It has been found that due to the non-equilibrium behavior of the electrons within a few nanoseconds a maximum of the ionization rate υ develops followed by a pronounced minimum in the direction to the anode. The corresponding values of υ differ by about two orders of magnitude. This effect is the same on which has been applied by Franck and Hertz to show the quantum character of the atomic excitation. Discussing both aspects of the pendulum motion it has been shown that the sheath effect dominates and that it leads to an avalanche like ionization. After 7ns, the corresponding current is two orders of magnitude higher than in the corresponding glow discharge. From the physical results obtained conclusions are drawn concerning the modeling of hollow cathode discharges.

*Work supported by the Max-Kade Foundation

AA-5 Streamers in a 13 cm Gap,* W. YI, P.F. WILLIAMS, and F.E. PETERKIN, U. of Nebraska—High speed streak and shutter photography have been used to study streamers in a ~13 cm non-uniform field gap. We have data for streamers in pure N_2 and in mixtures of N_2 and O_2, at 760 Torr. Most data has been obtained with a gap consisting of nearly-uniform field electrodes with a short (<1 cm), sharp conducting point projecting from the surface of one. The polarity of the point was positive. The highest average field we have studied is 11.5 kV/cm (V = 150 kV, $E/N = 4.3 \times 10^{-16}$ V cm^2). For pure N_2 several streamers are initiated from the point, and they branch repeatedly during gap transit. Streamers were observed to propagate in average fields as low as 5 kV/cm (V = 60 kV, $E/N = 1.9 \times 10^{-16}$ V cm^2). Free electron density inside the streamers was about 10^{14} cm^{-3}, and streamer diameters were in the range of 1-2 mm. Streamer velocity varied with applied voltage from about 2×10^7 cm/sec at the minimum voltage to 10^8 cm/sec at the highest. In mixtures containing O_2 only a few streamers are observed, and branching is greatly reduced.

*Work supported by the Electric Power Research Institute and the Nebraska Energy Office

AA-6 Electrical Discharge Initiation and a Circuit Model for Formative Time Lags, WILLIAM B. MAIER II, A. KADISH, C. JERALD BUCHENAUER, Los Alamos National Laboratory, and R. T. ROBISCOE, Montana State University--Highly time-resolved (≈ 85 ps) data on discharge initiation between a spherical electrode and a plane suggests a simple model for formative time lags, t_d. The first phase of initiation lasts 1-3 ns and is dominated by leader phenomena. The second phase lasts a few ns and is characterized by rapid current fluctuation and removal of charge from the electrode gap. In the third phase, which lasts μs, current grows and causes a sudden voltage drop associated with observed t_d. t_d can be obtained from a simple model in which the current in the third phase heats the discharge channel to a critical temperature T_C at which the medium's electrical resistivity falls abruptly. We take t_d to be the time when the temperature of the medium reaches T_C, and we derive relations between t_d and θ, the fractional overvoltage applied before breakdown. For LTE in the channel, this relation is $d(\ln t_d)/d(\ln \theta) = -1$, which describes data for t_d over fairly wide ranges of θ.

AA-7 A Fast and Accurate Kinetic Method– A Generalized Monte Carlo Flux Method– for Spatio-Temporal Varying Fields,* Chihwen Li and Chwan-Hwa Wu, Dept. of E. E. Auburn Univ. – A new kinetic scheme, Generalized Monte Carlo Flux (GMCF) method, provides charged particle distribution functions for transport in a background gas under the influence of rapidly spatio-temporal varying fields. This method handles the computations similar to that of Boltzmann equation, but it uses a transition matrix to compute the collision transition in velocity space cells. The transition matrix, motivated by the Monte Carlo Flux method[1], is obtained by calculating the transitional probabilities for each velocity space cell from an initial impulse (δ) function of a charged particle distribution in velocity space. This transition matrix only has to be solved *once* for a gas. GMCF method contains the major characteristics of a multi-group fluid model proposed by Kunhardt[2]; however, the implementation of this scheme is more straightforward. The nonequilibrium electron distribution functions, $f(r, v, \mu)$, (r: space, v: speed, and μ: velocity angle) calculated by the GMCF method in helium gas are presented and compared with Monte Carlo simulation results. The new method gives a high resolution of the wings in the distribution function and conserves a significant amount of computational time. This method facilitates a way of solving multidimensional kinetic equations for modelling practical problems and can be fully vectorized/parallelized to take the advantage of supercomputers.

* Work supported by NSF under ECS-9009395.

1 G. Schaefer and P. Hui, J. Comput. Phys. 89, 1(1990).
2 E. E. Kunhardt, 44th Annual Gaseous Electronics Conf., 89(1991).

Session AB

8:00 a.m. – 10:00 a.m.
Tuesday, October 27, 1992

Arlington Room

Plasma Modeling

Chair
J. Margot, University of Montréal

AB-1 Monte Carlo Modeling of RF Non-equilibrium Plasma in Monosilane,* H.TAGASHIRA, A.YOKOZAWA, K.KITAMORI and Y.SAKAI, Dept. of Electrical Eng., Hokkaido Univ., Sapporo, Japan.-An rf non-equilibrium plasma between parallel plates in monosilane has been simulated by a Monte Carlo technique. The electric field is determined self-consistently with the densities of electrons and ions. The frequency of the total radical generation is obtained. This frequency is distributed to various radical species. Then, the diffusion equation representing the reaction and transport of radicals is solved considering the reaction of the radicals at the surface of the deposited amorphous silicon. For the deposition of the film, a simple Monte Carlo model is employed. All the simulations, i.e. for the charged species, for the radicals and for the film growth are integrated by feedback simulations. It is found that some radical density distributins are affected considerably by the feedback simulations, demonstrating the importance of the integration.

*Work supported in part by a Grant-in-Aid for Scientific Research of the Ministry of Education, Science and Culture, Japan.

AB-2 Modeling the Helical Resonator in the Presence of Large Sheaths, K. Niazi, A. J. Lichtenberg, M. A. Lieberman, D. L. Flamm, University of California, Berkeley -- Indirect observations on our helical resonator plasma source indicate that the sheath occupies a major portion of the plasma chamber under some common operating conditions. Once the sheath is large enough, power loss through electron-neutral collisions in the sheath can no longer be ignored. We have extended a previous theory of the helical resonator[1] and compare our results with experimental data, and with the unmodified theory where applicable.

[1] M. A. Lieberman, A. J. Lichtenberg, and D. L. Flamm, Memorandum No. UCB/ERL M90/10 (1990), Electronics Research Laboratory, College of Engineering, U. C. Berkeley.

AB-3 A 2D Diffusion Model of Transport in Plasma Processing Reactors. R. A. Stewart, B. Troyanovsky, and M. A. Lieberman, U.C. Berkeley – A two-dimensional model is presented that treats plasma transport as governed by ambipolar diffusion.[1] The ion diffusion equation is solved in cylindrical coordinates with an anisotropic diffusion tensor perpendicular to and parallel to spatially nonuniform magnetic field lines. Electron-ion generation is accounted for by a source term that can be either a pre-specified spatially varying function or the product of the ionization rate and the density. A mixed boundary condition is used that obtains from the one-dimensional momentum transport equation evaluated near the chamber wall, appropriately modified to include dependence on a reflection coefficient for the case of multi-polar confinement.[2] Spatial variations of plasma density in a downstream ECR process chamber and a transformer coupled plasma reactor are presented for a range of operating conditions, along with the effect of wafer holders of various sizes on radial uniformity.

[1]R. A. Stewart, B. Troyanovsky, and M. A. Lieberman, IEEE Conference of Plasma Science, June 1991.

[2]A. V. Phelps, J. Res. Natl. Inst. Stand. Technol. 95, 407 (1990).

AB-4 A Monte Carlo Simulation of Remote Plasma Reactors Using Equivalent Representations for Electrons, Ions and Excited States. Fredrick Y. Huang and Mark J. Kushner, University of Illinois, Dept. Elect. & Comp. Engr., Urbana, IL 61801 * – Models for low pressure plasmas must consider nonequilibrium and noncontinuum transport of charged species and neutral excited states. The transport of charged species is usually represented separately from neutrals; and separate algorithms are often used for electrons and ions. In principal heavy particles (ions and excited states) and free electrons have combined densities of states consisting of discrete negative energies (bound states) and positive energies (continuum electrons). Heavy particles are, then, electrons in bound states having large effective masses. Electron-excited state collisions can then be viewed as electron-electron collisions. We have developed a Monte Carlo simulation for the transport of electrons, ions and neutral excited states in which all species are treated equivalently as either free or bound states of electrons. This method is being applied to low pressure plasma deposition reactors. Results for excited state transport will be discussed for a selection of gas mixtures (He/N_2, He/SiH_4, NH_3/SiH_4).

* Work supported by the NSF, SRC, and IBM East Fishkill

AB-5 The Effects of Nonthermal Charge Exchange on Ion Energy Distributions for Multicomponent Gas Mixtures in rf Discharges, Helen H. Hwang and Mark J. Kushner, University of Illinois, Department of Electrical and Computer Engineering, Urbana, IL 61801 * - The ion energy distribution (IED) incident on electrodes in rf discharges is important in determining the isotropy of etching of microelectronic devices. In multicomponent gas mixtures, nonthermal charge exchange reactions occur in the sheaths where ions are accelerated to many 10s eV. A computer model has been developed to examine these issues. The model is based on a self-consistent hybrid Monte Carlo-fluid simulation for rf discharges to which Monte Carlo ion particles have been added. Elastic, thermally exothermic and endothermic charge exchange, ion-ion reassociation and electron-ion recombination reactions are included for the ion particles. Ion-charged particle reactions are included using a new technique whereby ion "holes", analogous to holes in semiconductors, are used. IEDs for etching ($He/CF_4/O_2$, $He/CF_4/H_2$) and deposition (SiH_4/N_2, SiH_4/NH_3) gas mixtures will be presented, which show "cut-off" IEDs at the inelastic charge exchange thresholds.

* Work supported by U. of Wisconsin ERC, SRC, NSF and IBM E. Fishkill

AB-6 Self-Consistent Glow Discharge Model Including Neutral Transport and Reaction, D.J. ECONOMOU and D. LYMBEROPOULOS, University of Houston. - A fluid model for charged particle transport in low pressure glow discharges has been extended to include mass conservation equations of neutral species. The system of coupled equations is integrated in time until a periodic steady-state is reached. Calculation time is shortened by an "acceleration" scheme that avoids direct time integration of the equations. A 13.56 MHz argon discharge including metastable species is examined as a case study. A parametric study of metastable density and other discharge variables as a function of operating conditions is carried out. Results are compared to lumped parameter models. The impact of using different boundary conditions on the fluid equations and of an "effective" ion electric field are also examined.

AB-7 Multi-dimensional Kinetic Models of the Radial and Axial Flow in RF Glow Discharges. J. H. TSAI and CHWAN-HWA "JOHN" WU, Electrical Engineering Department, Auburn University, Alabama 36849 - A two dimensional (2D), self-consistent, kinetic model of RF glow discharges, simulated by a Monte Carlo technique, has been developed. In the simulation, the low-pressure helium glow discharges between two parallel-plate electrodes, assuming cylindrically symmetric geometry, were used to illustrate the dynamic transport of the charged particle along the radial and axial directions. The exhibiting results show the spatio-temporal variations of the electron current densities, ionization rate, averaged electron energy, power deposition and induced space charge fields in *(r,z)* space. More importantly, observing the dynamic evolution of the electron current density from the 2D Monte Carlo simulation, and subsequently, the distributions of the plasma densities and the induced space charge field in the radial direction further illustrate the significant radial effect due to the radial wall of the reactor. However, because of the extensive computational time and the limitation of computer memory, an alternative methods by considering the radial effect, namely, one and half dimensional (1HD) Monte Carlo simulation was proposed. By considering an effective radial space charge field in the simulation, the 1HD Monte Carlo model was configured in a one dimensional model (axial direction), therefore, it will not only comprise the radial effect but also reduce the number of particle that required for the 2D Monte Carlo model. Results in the 1HD Monte Carlo simulation will be used to compare with the results from 2D and 1D Monte Carlo simulations.

Session BA

10:15 a.m. – 12:00 noon
Tuesday, October 27, 1992

Georgian Room

Atomic and Molecular Collisions

Chair
J. Paulson, Phillips Laboratory

BA-1 **Mixing of the Cd 5^3P fine-structure states induced by Hg collisions,*** J. SUPRONOWICZ, J. HINEK, J.B. ATKINSON and L. KRAUSE, Department of Physics, University of Windsor, Windsor, Ontario, Canada.--Inelastic mixing within the Cd 5^3P manifold, induced in Hg collisions, was studied by methods of LIF with time resolution. A quartz vapor-cell containing an Hg-Cd mixture was irradiated with consecutive pump and probe laser pulses. The pump pulses (326.1 nm) produced a population of Cd 5^3P_1 atoms whose collisions with ground-state Hg atoms caused the distribution of population among the ^3P fine-structure states. These were probed with 467.8 nm, 480 nm, or 508.6 nm laser radiation exciting the 6^3S_1 state which emitted fluorescence of intensity proportional to the respective ^3P_J population. The experiments were carried out over a range of temperatures and Hg densities, provided data on the time-evolution and kinetics of the excitation transfer processes, and yielded the rate constants for the various processes which also included HgCd excimer formation.[1]

* Supported by the Canadian Department of Defence and Natural Sciences and Engineering Research Council of Canada.

1 J. Supronowicz, D. Petro, J.B. Atkinson, and L. Krause, Phys. Rev. A, to be published (1992).

BA-2 Guided-Ion Beam Study of the Reactions of Ar^+ and NO_2. R. A. DRESSLER, S. GRAUL[a], S. WILLIAMS[b], R. H. SALTER, and E. MURAD, Phillips Lab, PL/WSSI, [a]Carnegie Mellon University, [b]Stanford University - Cross section and product ion time-of-flight measurements are presented for the Ar^+ + NO collision system over a collision energy range of 0.1 to 17 eV (c.m.). The experiments are carried out in an octopole guided-ion beam apparatus. Charge transfer is the main channel observed throughout the collision energy range. The charge transfer cross section has approximately an $E^{-0.5}$ dependence at low collision energies, and at higher energies decreases rapidly with energy. The high exothermicity (6.5 eV) enables access to the NO^+ $a^3\Sigma^+$ state in near-resonant charge transfer collisions. The time-of-flight measurements suggest that most product ions are produced in the $a^3\Sigma^+$ state, since little translational-to-internal energy transfer is observed. At higher collision energies, N^+, O^+, ArN^+ and ArO^+ are observed near the respective thermodynamic thresholds. The energy dependence of all observed cross sections will be presented as well as the analysis of the time-of-flight spectra.

BA-3 Collisional Detachment of I^- Using Pulsed ICR Spectrometry, K. RIEHL and P. HAALAND, Air Force Institute of Technology – Fourier Transform Mass Spectrometry has been adapted for the quantitative measurement of collisional detachment cross sections. I^- is formed via low energy dissociative attachment to CF_3I and excited into cyclotron motion with a well defined kinetic energy. Elastic and inelastic scattering lead to an exponentially damped image current at the I^- cyclotron frequency. The variation of this damping constant with I^- kinetic energy is used to calculate cross sections for collisional detachment

$$I^- + A \rightarrow I + e + A$$

where $A = Xe, Ne, CF_3I$, for lab frame energies of 0.5 eV–300 eV. Thresholds are complicated by the competition between elastic and inelastic scattering, but are resolved. The maximum value of the detachment cross sections are found to be of order 12, 2, and 2, $\AA^2$.

BA-4 Energy Transfer Kinetics between $N_2(X, v)$ and SiH_4.* L.G. PIPER, Physical Sciences Inc., Andover, MA, 01810-1022.

We have used discharge-flow techniques to measure rate coefficients for quenching $N_2(X, v)$ by SiH_4. The $N_2(X, v)$ source is a low power microwave discharge sustained in a flowing mixture of N_2 dilute in He with subsequent removal of atomic nitrogen and electronically excited metastables by passing the discharge effluent through a Ni screen. Detection of $N_2(X, v)$ at the down stream end of the flow reactor uses metastable transfer techniques. Metastable $He(2^3S)$ excitation of $N_2^+(B\text{-}X)$ emission serves to determine absolute number densities of $N_2(X, v=0\text{-}6)$ while $N_2(A)$ excitation of $N_2(B\text{-}A)$ emission is diagnostic of $N_2(X, v<5, v<13)$. Rate coefficients increase from 1.3×10^{-13} cm^3 $molecule^{-1}$ s^{-1} for quenching v=1 to about 6×10^{-13} cm^3 $molecule^{-1}$ s^{-1} for quenching vibrational levels 4 and above.

*Work sponsored by Air Force Wright Laboratory

BA-5 Ion-Molecule Reactions at High Temperatures. M. MENENDEZ-BARRETO, J.F. FRIEDMAN, T.M. MILLER, A.A. VIGGIANO, R.A. MORRIS, A.E.S. MILLER, J.M. VAN DOREN, and J.F. PAULSON, Phillips Laboratory, Geophysics Directorate, Hanscom, AFB - We have begun an investigation of ion-molecule reactions at high temperatures, using a flowing afterglow apparatus. Our initial work is on the classic reaction $Cl^- + CH_3Br \rightarrow Br^- + CH_3Cl$, which has been studied by many groups at room temperature; recent SIFT experiments[1] have shown that the reaction rate coefficient **k** decreases steadily with temperature in the range 200-560 K. We find that **k** passes through a minimum at about 550 K and then increases by two orders of magnitude, becoming nearly collisional at 1200 K. We will also discuss matters special to high-temperature measurements, *viz.*, alkali emission from the flow tube walls, and thermal dissociation of reactants.

[1]A.A. Viggiano, R.A. Morris, J.S. Paschkewitz, and J.F. Paulson, *J. Am. Chem. Soc.* (in press).

BA-6 Temperature, Kinetic Energy and Internal Energy Dependences of the Rate Constants for the Reaction of O_2^- with SF_6. A. A. VIGGIANO, ROBERT A. MORRIS, JANE M. VAN DOREN and JOHN F. PAULSON, Phillips Laboratory, Geophysics Directorate/GPID, Hanscom AFB - We have measured the rate constants for the reaction of O_2^- with SF_6 in a variable temperature selected ion flow drift tube over the temperature range 163 K to 550 K. The rate constants show a distinct minimum with temperature at approximately room temperature. Increasing kinetic energy monotonically decreases the rate constants, although kinetic energy dependences at high temperature are relatively flat. Internal energy dependences can be derived from the data. Low levels of internal excitation change the rate constants only slightly. Increasing amounts of internal energy are found to increase the rate constants dramatically. The increase with increasing internal energy may reflect that vibrational excitation in the SF_6 changes the geometry of SF_6 to be more like that of SF_6^- and therefore increases the Franck-Condon overlap.

BA-7

High Energy Asymptotic Forms for Partial Derivatives of Phase Shifts with Respect to Momentum and Angular Momentum.

W.J. Romo and S. R. Valluri, Carleton University and University of Western Ontario.

Asymptotic forms for the partial derivatives of the phase shifts δ_ℓ (k) with respect to momentum k and angular momentum l have been derived for the square well and square well and Coulomb tail potentials respectively. kR in current heavy ion experiments, where R is the short range radius of interaction, is typically 30 or more. This makes the exact analytical expressions for $\delta_\ell(k)$ and $\partial\delta_\ell/\partial\ell$ more analytically and numerically practicable and motivates our study. Such an approximation, to the best of our knowledge, has not been published and could be of practical value.

1. S.R. Valluri and W. J. Romo, Nucl. Phys. A492, 493 (1989)
2. W. J. Romo and S. R. Valluri, J.Phys. B23, 4223 (1990)

Session BB

10:15 a.m. – 12:15 p.m.
Tuesday, October 27, 1992

Arlington Room

RF Discharge Modeling and GEC Reference Cell

Chair
J. Gerardo, Sandia National Laboratories

BB-1 Measuring the Distribution of RF Current in the GEC Reference Cell. M.A. Sobolewski, NIST— RF glow discharges in the GEC Reference Cell are often characterized by measurements of current and voltage waveforms at the leads of the powered electrode. However, these measurements alone are not sufficient to fully characterize the electrical behavior of the discharge. Additional measurements are required to determine how the current flowing into the plasma distributes itself among the multiple grounded surfaces present in the cell (the grounded electrode, ground shields, and the walls of the cell).

By simultaneously monitoring the current at both the powered and the grounded electrode, we have obtained a less ambiguous characterization of the plasma. This method includes a correction for the effects of all cell parasitics. Measurements were performed on Ar plasmas at 13.56 MHz, at pressures of 0.05-1.00 Torr, at peak-to-peak voltages of 75-200 V. Under this range of conditions, the current drawn by the grounded electrode is only roughly half of the current supplied by the powered electrode; the remainder flows to other grounded surfaces.

The added information gained by this technique assists efforts to compare plasma conditions in cells with different designs. It also allows more accurate values of plasma properties (sheath widths and sheath voltages) to be obtained from the electrical data, as shown by comparisons with other diagnostic techniques.

BB-2 Dependence on Excitation Symmetry of Electrical Parameters and Radial Currents in a Parallel-Plate RF Discharge,* P.A. MILLER, K.E. GREENBERG, G.A. HEBNER, Sandia National Laboratories, P.D. POCHAN, Geo-Centers, and J.T. VERDEYEN, U. of Illinois. - Current probes were installed inside a GEC RF Reference Cell (10-cm-diam electrodes, 2.5-cm spacing, 13.56 MHz) in order to measure currents to the chamber walls and to the ground shields. An air-core transformer was used to achieve equal-amplitude opposite-phase excitation of the top and bottom electrodes. In 100-mTorr argon discharges with both electrodes powered, most of the current flowed between the two electrodes. With only one electrode powered, the largest current flow was from the powered electrode to the chamber wall. In both cases, other currents were significant and dc bias referred to the chamber walls was high. In both cases, the electrode voltage had little harmonic content but current waveforms were rich in harmonics. We will compare voltages, currents, and electron densities vs. drive symmetry.

* Work supported by the U.S. Department of Energy under contract DE-AC04-76-DP00789.

BB-3 Measurement of atomic hydrogen concentration profile in GEC reference cell, B.L. Preppernau, T. A. Miller, The Ohio State Univ., Peter Bletzinger, B. N. Ganguly and A. Garscadden, Wright-Patterson AFB -- The axial variation of ground state atomic hydrogen concentration has been measured with and without silicon wafer loading from 0.3 torr up to 5 torr pressure, using two-photon LIF. The measurements were performed at approximately constant discharge power with a dc self-bias that increased nonlinearly with decrease in pressure, exceeding 50 percent of the peak rf voltage at 0.3 torr. The atomic hydrogen concentrations exhibit a maximum near the powered electrode for all measured conditions with a gradual sloping decrease towards the ground electrode. The slope was observed to increase with pressure. The 3 inch silicon wafer loading on the ground electrode reduced the atomic hydrogen concentration axial non-uniformity. The electrical characteristics of the plasma were not measurably affected by the wafer loading.

BB-4 Comparison of Experiment and Theory for the Helium RF Discharge,* M. E. RILEY, K. E. GREENBERG, G. A. HEBNER, and P. J. DRALLOS, Sandia National Laboratories - Electron and metastable densities were measured for Helium discharges in a symmetrically driven "GEC Reference Cell." The electron density was determined using microwave interferometry. Spatially resolved singlet and triplet metastable profiles were determined using absorption spectroscopy. We compare these quantitative measurements with theoretical predictions of a 1D Boltzmann description of the system. The Boltzmann description of the electrons is used with a five-level model of He, including 14 electron-produced transitions. The ions and neutrals obey fluid equations. The Boltzmann calculations for the fast processes are used to compute rf-cycle-averaged rates and fields; these rates and fields drive the slow time-scale processes for the heavy particles, unrestricted by the rf time scale. In general we find the theoretical predictions of plasma density to be within a factor of four of the measured density. Comparisons of the measured spatial profiles of the metastable densities with theoretical predictions elucidates some of the discharge kinetics.

*This work was performed at Sandia National Laboratories and supported by the U.S. Department of Energy under contract No. DE-AC04-76DP00789.

BB-5 A Two-Dimensional Simulation of the GEC RF Reference Cell Using a Hybrid Fluid-Monte Carlo Method,* H. PAK and M.E. RILEY, Sandia National Laboratories - A two-dimensional fluid-Monte Carlo hybrid model is used to simulate the GEC reference cell. The 2-D model assumes azimuthal symmetry and accounts for the ground shield about the electrodes as well as the grounded chamber walls. The hybrid model consists of a Monte Carlo method for generating rates and a fluid model for transporting electrons and ions. In the fluid model, the electrons are transported using the continuity equation; and the electric fields are solved self-consistently using Poisson's equation. The Monte Carlo model transports electrons using the fluid-generated periodic electric field. The ionization rates are then obtained using the electron energy distribution function. An averaging method is used to speed the solution by transporting the ions in a time-averaged electric field with a corrected ambipolar-type diffusion. The simulation switches between the conventional and the averaging fluid model. Typically, the simulation runs from 10's to 100's of averaging fluid cycles before reentering the conventional fluid model for 10's of cycles. Speed increases of a factor of 100 are possible.
*This work was performed at Sandia National Laboratories and supported by the U.S. Department of Energy under contract No. DE-AC04-76DP00789.

BB-6 Modeling of RF Glow Discharges in SF_6 by RCT Model, N.NAKANO, N.SHIMURA, Z.Lj.PETROVIC* and T.MAKABE, Keio Univ. – Sulphur hexafluoride(SF_6) is used not only in the electrical power industry as an insulator but also in plasma etching for semiconductor. Three electron attachment processes to SF_6^-,SF_5^-, and F^- are considered, and the electron and four ions (SF_5^+, SF_6^-,SF_5^-,F^-) system are modeled. Numerical analysis is based on the relaxation continuum(RCT) model, previously developed considering the relaxation kinetics for momentum and energies of charged-particles. In this work, the energy relaxation time $\langle \tau_e \rangle$ is defined more exactly as a function of E/N. At 13.56 MHz, we confirm the typical electro-negative glow discharge structure, and positive and negative ion number densities are a few hundred times larger than electrons. Double layer is formed in front of the instantaneous anode. As a result, the electric field in a bulk plasma increases and the phase-shift between voltage and current becomes resistive and inductive. The results of RCT model is discussed and compared with those in spatiotemporal optical emission spectroscopy[1].
*Permanent address: Institute of Physics, Belgrade, Yugoslavia.
[1] Z.Lj. Petrović F.Tochikubo *et al.*,J.Appl.Phys.(submitted)

BB-7

Kinetic Modeling of the α To γ Transition in RF Discharges, W.N.G. Hitchon, **Department of Electrical and Computer Engineering and the Engineering Research Center for Plasma-Aided Manufacturing, University of Wisconsin,** G.J. Parker and J.E. Lawler, **Department of Physics, University of Wisconsin, Madison**– An accurate and comprehensive self-consistent kinetic model[1] has been applied to a helium rf discharge which in experiments[2] exhibits an "α to γ" transition. Agreement in most variables is to within a factor of two across the whole range, when plotted as a function of current or voltage, and typically better. The electron temperature agrees to the same accuracy when plotted as a function of the average electron velocity. Electron temperatures in the bulk plasma from theory and experiment also agree with tabulated transport data[3], at higher reduced fields. The remaining differences between theory and experiment are apparently due to the radial variation of density in the experiment.

1. T.J. Sommerer, W.N.G. Hitchon, R.E.P. Harvey and J.E. Lawler, *Phys. Rev. A* **43**, 4452 (1991).

2. V.A. Godyak, R.B. Piejak and B.M. Alexandrovich, *Phys. Rev. Lett.* **68**, 40 (1992).

3. J. Dutton, *J. of Phys. and Chem. Ref. Data*, vol. 4, no. 3, 577-856 (1975).

BB-8 Comparison of a 2D Hybrid Fluid-PIC Simulation to Experimental Results. H.M. PERSING, R.K. PORTEOUS, A.J. PERRY, B.A. NELSON*, R.W. BOSWELL, Plasma Research Laboratory , Australian National University, Canberra, Australia. A two dimensional hybrid fluid-PIC code has been written to simulate azimuthally symmetric inductively coupled plasma sources (see paper by Porteous this conference). It allows for a non-uniform magnetic field and a prescribed, spatially varying power deposition. The reactor may have separate source and diffusion regions and its walls may be locally insulating, grounded, or biased. The code is thus appropriate for simulating the helicon reactor used for both deposition and etching at the ANU. Spatial profiles (both radial and axial) of the floating and plasma potentials, electron temperature, ion energy and density, as functions of pressure in an argon plasma, are measured and compared to the model.

*Present Address: Department of Electrical Engineering, University of Washington-Seattle, Seattle, Washington.

Session CA

1:30 p.m. – 3:30 p.m.
Tuesday, October 27, 1992

Georgian Room

Electron Molecule Collisions

Chair
G. Victor, Harvard-Smithsonian Center for Astrophysics

CA-1 Low Energy Elastic Scattering from Molecular Ions*, A. E. Orel, University of California, Davis-The 'direct' mechanism of dissociative recombination requires the ground state of the molecular ion to be crossed by a dissociative state of the neutral. Such a state can be seen as a resonance in the low-energy elastic scattering from the molecular ion. We have carried out accurate calculations for range of nuclear configurations for H_3^+ and HCO^+. These calculations employed accurate multiconfiguration wave functions that contained enough flexibility to accurately describe both the target and resonance state. The implications of these results for the rate of dissociative recombination for these two molecules will be discussed.
*This work was supported by the National Science Foundation, grant No.PHY-90-14845, and performed under the auspices of the U.S. Department of Energy at Lawrence Livermore National Laboratory under contract number W-7405-Eng-48.

CA-2 Differential Cross Sections for Elastic Scattering of Electrons from N_2,* X. SHI, T.M. STEPHEN and P.D. BURROW, U. of Nebraska-Lincoln - Cross sections were measured at 0.55, 1.50 and 2.22 eV using the relative flow method and normalizing to He. At the two lower energies, our results are considerably larger than previous measurements but in close agreement with the calculations of Morrison et al.[1] At 1.5 eV we agree in magnitude with the recent data of Brennan et al.[2] but there are differences in the shapes of the angular distributions. We discuss several difficulties in making comparisons with both theory and experiment in the region of the temporary negative ion. We propose a protocol for making the measurements and presenting the data which overcomes these problems.

*Supported by NSF.

[1]M.A. Morrison, B.C. Saha and T.L. Gibson, Phys. Rev. A 36, 3682 (1987).

[2]M.J. Brennan, D.T. Alle, P. Euripides, S.J. Buckman and M.J. Brunger, J. Phys. B., in press.

CA-3 Electron Scattering from C_2H_2 Molecules in the Energy Range of 0.01–20 eV ♣: **Indira Khurana and Ashok Jain, Physics Department., FAMU, Tallahassee, Fl 32307**– The results for vibrationally and electronically elastic scattering of low–energy electrons with C_2H_2 molecules are presented by employing the close–coupling method under the fixed–nuclei approximation. The full e^-–C_2H_2 interaction is approximated parameter–free as a sum of static, polarization and exchange potentials. The final cross sections (differential, total and momentum transfer) are characterised by a minimum (around 0.2 eV), a maximum (around 2 eV, the well known Π_g shape resonance due to d–wave tunneling effect[1]) and a broad hump around 10 eV. All these features agree well with measurements. The scattering length for the e^-–C_2H_2 system is found to be −3.9 au. Details of Differential, integral and momentum transfer cross sections for rotationally elastic, inelastic and summed processes in the energy range of 0.01–20 eV will be reported.

♣ Work supported by Airforce Wright Aeronautical Laboratories

[1]Indira Khurana and Ashok Jain, J. Phys. **B25**, Lxxx (1992).

CA-4 Low-energy electron-H_2S Scattering*, B. H. Lengsfield III and T. N. Rescigno, Lawrence Livermore National Laboratory - The complex-Kohn method has recently been used to study low-energy electron scattering from a series of closed shell molecules (CH_4,SiH_4,C_2H_4,C_2H_6,NH_3 and H_2O). In these studies, an accurate description of target polarization was needed to obtain reliable cross sections below 3 eV. A compact polarized-SCF trial function which made use of polarized virtual orbitals was developed for this purpose. However, this model does not produce comparable results for H_2S as the polarizability computed from a polarized-SCF wave function is much too large In this work both polarized-SCF and polarized-MCSCF trial wave functions are employed in the scattering calculations and the results compared to the recent crossed beam experiments of Buckman.

*Work performed under the auspices of the U.S. Department of Energy at the Lawrence Livermore National Laboratory under contract W-7405-Eng-48.

CA-5 Relative Electron Excitation Efficicencies for Vibrations of O_3, CO_2, and N_2O,* K. HOLTZCLAW, K. L. CARLETON, B. L. UPSCHULTE, and B. D. GREEN, Physical Sciences Inc., S. LIPSON, and W. BLUMBERG, Phillips Laboratory Geophysics Directorate,--Low pressure gases were irradiated by 4 keV electrons in the cryogenic LABCEDE Facility. Experiments were performed with pure O_3, CO_2, and N_2O as well as with these species diluted in nitrogen and argon. The resulting fluorescence was resolved using a cryogenic CVF spectrometer. Emissions from the υ_3 vibrational modes were compared to obtain relative excitation rates. Emissions from diatomic fragments were also observed. The induced emissions were monitored with sufficient time resolution to isolate the roles of diffusion and sequential excitation processes. The excitation rates were determined from the rise of the initial slopes of the fluorescence over a wide range of pressures. Modeling shows that even at the low pressures secondary electron excitation dominates primary excitation. The observed rates for ozone are an order of magnitude greater than for CO_2 and N_2O. We will present excitation rates for the triatomics and their fragments.

* This work was supported by the Air Force Office of Scientific Research and the Defense Nuclear Agency.

CA-6 Generalized Oscillator Strengths of Valence and Carbon K Shell Excitations of Freons.* J.F. YING, C.P. MATHERS and K.T. LEUNG, Department of Physics and Department of Chemistry, University of Waterloo, Waterloo, Ontario N2L 3G1, Canada. Recently, there has been considerable interest in the electronic excitation of caged molecules, with particular reference to the so-called shape-resonance effect. Results from recent photoabsorption and small-angle electron energy loss studies have provided important information on the transition energies and dipole oscillator strengths of CF_nCl_{4-n} (n=0-4). Using angle-resolved electron energy loss spectroscopy at 2.5 keV impact energy, we obtained a complete measurement of the generalized oscillator strengths (GOS's) of both the valence and carbon K shells of these molecules. *New* dipole-forbidden transitions at ~7 and ~40 eV have been observed. The GOS's of these non-dipole states were found to have qualitatively different momentum-transfer dependence from that of the dipole-allowed states. This and other advantages of this simple electron scattering technique for electronic structural investigation will be discussed.

*Work supported by NSERC and CEMAID of Canada.

CA-7 Optical Pumping of the $b^4\Sigma^-$-$X^2\Pi$ Transition in NO, M. J. DYER, G. W. FARIS, P. C. COSBY, D. L. HUESTIS, and T. G. SLANGER, SRI International - The NO($b^4\Sigma^-$) state, in v = 2-5, has been excited from the $X^2\Pi$ ground state by optical pumping from 187 to 205 nm, and detected by $b^4\Sigma^-$-$a^4\Pi$ Ogawa band emission. This represents the first optical connection between the doublet and quartet systems and provides a foundation for investigations of the kinetics of the quartet states based on selective optical preparation. We have investigated the origin (contributions from perturbers of all potential symmetries: $^2\Sigma$, $^2\Pi$, $^2\Delta$, $^4\Sigma$, and $^4\Pi$) and strength ($A \sim 10^3$ s\-1) of the forbidden $b^4\Sigma^-$-$X^2\Pi$ transition; predissociation of $b^4\Sigma^-(v'=6)$ and high-J levels of b(5); and collisional production of $b^4\Sigma^-$ following optical excitation of the $A^2\Sigma^+$, $B^2\Pi$, and $D^2\Sigma^+$ states. As most of the NO(b) radiates to the NO($a^4\Pi$) state, this study also provides a means of preparing the low-v levels, principally v = 1,2, of the NO(a) state, whose kinetic importance has frequently been inferred, but for which no direct production scheme has been available.

CA-8 Valence Shell Electronic Structures of *Cis-*, *Trans-* and *Iso-*Butene by Symmetric Noncoplanar (e,2e) Spectroscopy and Synchrotron Radiation Photoelectron Spectroscopy.* C.P. MATHERS, J.F. YING, B.N. GOVER and K.T. LEUNG, Department of Physics and Department of Chemistry, University of Waterloo, Waterloo, Ontario N2L 3G1, Canada. The valence-shell ionization energy (IE) spectra of three butene isomers have been obtained by photoelectron spectroscopy (PES) at 100 eV photon energy. While the PES spectra of these isomers were found to be similar to one another, the electron momentum distributions (EMD) of the *frontier*-orbital states, obtained by noncoplanar symmetric (e,2e) spectroscopy, revealed rather different bonding topographies. Furthermore, ionization of the inner-valence (>18 eV) shell was found to be dominated by non-Koopmans-like behaviour. Some of the qualitative features of the many-body structures have been successfully predicted in recent multi-reference configuration-interaction calculations. Using EMD's measured at selected ionization energies and IE spectra measured at two electron momenta, we made an improved characterization of the nature and, in particular, orbital compositions of these many-body states.

*Work supported by NSERC and CEMAID of Canada.

Session CB

1:30 p.m. – 3:30 p.m.
Tuesday, October 27, 1992

Arlington Room

High Density Plasmas

Chair
J. Heidenreich, IBM-T.J. Watson Research Center

CB-1 Hollow Anode Discharge based High Efficiency RF Triode Reactor, **B.Singh, V. Patel, S. Sun, E. Whittaker, R. Kerns and J. Maher, NJ SEMATECH Center of Excellence for Plasma Etching, and Drytek, Inc.**- We report observations and characterization of a unique "hollow anode" effect, very similar to the hollow cathode effect, in the discharge of grid-based Drytek 384T triode etching reactor. The 384T reactor utilizes a screened grounded anode between the upper and lower electrodes of a parallel-plate triode to isolate plasma generation from the substrate environment. The hollow-anode effect is observed in the apertures of the grid. It produces an extremely high-density plasma with considerable increase in etchant specie due to charge exchange effects. This phenomena appears to be responsible for the very high etch rates observed at low powers and low substrate bias conditions. Measurements of both charged and neutral plasma species, using in-situ scanning Langmuir probes and FM infrared laser absorption spectroscopy are reported. The hollow anode phenomena appears to arise from the interaction of anode wall sheaths in a cavity geometry such as an aperture at ground potential in a RF discharge. The properties of the hollow-anode plasma (n_e, T_e and V_p) depend on the aperture diameter and length, reactor pressure, RF power and phase in triode systems. Data from probe mapping of the hollow-anode plasma show the existence of double-layer sheaths on either side of the apertures and a peak in plasma density at the aperture center. The hollow anode phenomena appears to provide unique approach to simultaneously intensifying and decoupling the plasma generation in etching reactors.

CB-2 RF Production of Dense Plasma Columns,* F.F. CHEN and G. CHEVALIER, UCLA — Long, uniform, quiescent plasma columns of density 10^{14} cm^{-3} and above have been produced by helicon wave ionization of argon at 27.12 MHz, with > 2 kW applied to a helical antenna and with > 1 kG of magnetic field. Care must be taken to feed enough gas. The central density, and even the total density, increase in a surprising way when a magnetic aperture limiter is created by flaring out the field lines near the antenna. Material aperture limiters also increase the density, but their placement is critical. Optimization and understanding of these effects, as well as the use of multiple antennas, will be discussed.

*Work supported by the National Science Foundation, Grant ECS-8901249.

CB-3 Comparison of Electrostatic Shielded and Unshielded Inductive Coupled Plasma Sources. WAYNE JOHNSON, Prototech Research, Inc. - Most inductive coupled plasmas also couple considerable power through capacitive coupling. The comparison of capacitive to inductive coupling depends upon pressure, gas species, and power level. By completely eliminating the capacitive coupling, independent control of ion bias energy and plasma density are realized. Pure inductive coupling constrains the unbiased, high density plasma volume to within the R. F. magnetic field. Applications are derived from the advantages of high density, low ion energy, limited plasma volume, and high pressure operation. The presentation will offer data of density and electron temperature as a function of power for ESRF [Electrostatic Shielded R.F.] plasma sources. Process results will include photo resist stripping and polysilicon RIE.

CB-4 RFInduction/Multipole Plasma for Etching, J. H. Keller, M. S. Barnes, J. C. Forster IBM E Fishkill Z/47A, Hopewell Jct., NY 12533, T. Wicker & R. Linquest Lam Research Corp, 4650 Cushing Parkway, Fremont, CA. In Low pressure high density plasmas, different processes require different ion energies and other optimizations. Etch data will be shown for highly selective oxide to polysilicon etching and poly silicon etching which is highly selective to oxide. At the same time rates of 7 KA/min and 4.5 KA/min respectively have been achieved. Sub .5 micron and aspect ratios of greater than 4 have been achieved for via etching in oxide films.

CB-5 Hybrid Models of Low Pressure Inductively Coupled Plasma Sources for Etching. Peter L. G. Ventzek and Mark J. Kushner, University of Illinois, Dept. Elect. & Comp. Engr., Urbana, IL 61801 * - There is renewed interest in Inductively Coupled Plasmas (ICPs) for low pressure (a few - 10s mTorr) etching for their high plasma densities and low ion energies. We have developed a 2-dimensional model for ICP reactors to investigate these devices for etching applications. The electromagnetic field is obtained for a series of conductivities, and are used in an electron Monte Carlo simulation. A hydrodynamic model is used to obtain charged particle and radical densities, and electrostatic potentials. An ion Monte Carlo simulation is used for ion energies and fluxes. The reactor is a magnetic "bucket" 5-10 cm tall and 20 cm in diameter with spiral coils placed on a dielectric roof. We will present results for plasma densities, temperatures, radical densities and ion flux distributions for ICPs in Ar, O_2, and CF_4. Comparisons will be made to experimental results for plasma potential and ion energies.[1] In Ar plasmas, the plasma potential is decreased by $\simeq$ 50% (25V to 13V at 10 mTorr) by using the magnetic bucket.

* Work supported by IBM, Lam Research, SRC, and NSF

[1] M. S. Barnes, J. H. Keller, J. O'Niell, unpublished.

CB-6 Inductive Low Pressure RF Discharges: Model and Experiment, R.B. PIEJAK, V.A. GODYAK and B.M. ALEXANDROVICH, GTE Laboratories Inc., Waltham MA - The electrical properties of an inductive rf discharge have been analyzed by considering the discharge to be a one-turn secondary of an air core transformer. Expressions for spatially averaged quantities of familiar discharge parameters such as voltage, current and electric field have been determined as functions of the measured electrical parameters of the primary circuit. Scaling laws for the discharge and the plasma parameters and the rf power distribution between the induction coil and the discharge are determined analytically. In the experimental part of this work the external electrical characteristics of a collisional dominated inductive discharge driven at 13.56 MHz were measured over a range of power in a mercury/noble gas mixture typical of a low pressure fluorescent lamp. Internal plasma parameters and power loss in the primary coil were inferred using analytical formulae. Extremely high power transfer efficiency was found along with good agreement between the effective electric field inferred for a collisional dominated rf inductive discharge and that calculated for a dc discharge under similar conditions. The approach developed here may be applied as a practical design and optimization tool for plasma processing reactors, ion sources, and light sources .

CB-7 Model Study of ECR Reactors, H.M. WU, D.B. GRAVES, R.K. PORTEOUS, and J.D. BUKOWSKI, University of California at Berkeley - A 2-D fluid electron - particle ion hybrid model of ECR discharges in argon has been applied to study the discharge structure and its dependence on discharge operating conditions. We examine an extended cylindrical source (14 cm. i.d., 50 cm. long) connected to a downstream region (20 cm. i.d., 50 cm long). The model predicts plasma density, electron temperature, ion average kinetic energy, ion flux and plasma potential profiles, in addition to ion velocity distributions at walls. Model predictions are shown to be in good agreement with experimental diagnostics[1].

[1]S.M. Gorbatkin et al., JVST A 8(3), 2893, (1990).

CB-8 Hybrid model of an ECR Etching System,* R. E. P. HARVEY, W. N. G. HITCHON, E. R. KEITER and K. M. KRAMER, Engineering Research Center for Plasma-Aided Manufacturing, U. of Wisconsin--Madison -- A two dimensional hybrid model of a CF_4 etching plasma is being developed. A fluid model describing the steady state densities of chemical species, charged species and the self-consistent potential is coupled with a kinetic model of the ionic species. Electron collisions with neutrals resulting in ionization or dissociation events are modeled by rates calculated from a convolution of the cross sections for ionization or dissociation with an experimentally measured bi-Maxwellian distribution. The kinetic description of the ions, moving in the self-consistent field, provides an estimate of "ion pumping" of neutrals and of ion energies at the sample surface. Effects of external parameters on neutral species densities are emphasized and compared to experiment.

* Work supported by NSF grant # ECD-8721545

Session D

3:30 p.m. – 5:30 p.m.
Tuesday, October 27, 1992

Castle

Posters

Heavy Particle Collisions
Diagnostics
Plasma Surface Interactions

Chair
H. Anderson, University of New Mexico

DA-1 Reflection of N_2 Metastables at the Boundary

S.SUZUKI, H.ITOH, H.SEKIZAWA and N.IKUTA*, Chiba Inst.Tech. Tokushima U*, Jpn.--- The loss processes of N_2 $A^3\Sigma_u^+$ metastable molecules have been investigated analysing in a one dimensional system with similar procedures as Molnar[1]. In the determination of lifetimes of active species, the boundary condition is important particularly in the low gas density. The assumption for the complete absorption at the boundary does not give consistent solution with experimental data. The reflection ratio at the surface of usual metals for metastables has been found to be unexpectedly high as well as for electrons. Boundary condition of the third kind as reported by Phelps[2] is necessarily requested for the lifetime analysis of metastables. The result has given quite consistent agreement with the experimental data. Values of diffusion coefficient at 0°C 1 Torr and the quenching rate coefficient of N_2 metastables in N_2 gas are 169 cm^2s^{-1} and 3.7×10^{-17} cm^3s^{-1} in relation with the reflection ratio at the boundaary of 0.3.

Results in N_2-CO mixtures will also be reported.

[1] J.P.Molnar, Phys.Rev.83,933(1951).
[2] A.V.Phelps, J.Research NIST,95,407(1990).

DA-2 Influence of Excited Oxygen Atoms (O^1D) to Wall Recombination Coefficient, S. WICKRAMANAYAKA, N. HOSOKAWA*and Y. HATANAKA, RIE, Shizuoka Uni. Japan— The relationship between the wall recombination coefficient (γ) of atomic oxygen on Pyrex glass and the $O(^1D)$ density in the downstream flow of a rf oxygen plasma was investigated. For the determination of excited states of oxygen atoms NO_2 chemiluminescent reactions[1] were applied. With the change of rf power from 200W to 800 W the $O(^1D)$ concentration in the downstream varies from 55% to 95% at 60 cm from the plasma. This $O(^1D)$ fraction drops to 90% with further increase of rf power up to 2500 W due to the production of O^+. γ is found to vary from 1.1×10^{-4} to 6.1×10^{-5} with the change of rf power from 200 W to 2500 W having a minimum of 5.1×10^{-5} at 800 W. The reduction of γ is considered due to the increase of $O(^1D)$ atoms which may have a lower probability for the recombination process. The slight increment of γ over 800 W is attributed to the production of ionic atomic oxygen.

*ANELVA Corporation, Yotsuya 5-8-1, Tokyo, Japan

[1] M. Break, J. Hinkle, J. Asmnsen, M. Haswley and R. Kerber, Plasma Chem. and Plasma Process 3, 63, (1983)

DA-3 Absorption Cross Section Measurements of Schumann-Runge Continuum of O_2 at 78 K and 295 K,* W.H. PARKINSON, J.R. ESMOND and K. YOSHINO, Harvard-Smithsonian CfA — We measured the photoabsorption cross sections of the S-R continuum at 78 K and 295 K in the wavelength region 130-175 nm. The 1-m Seya-Namioka vacuum spectrometer on the BL-12A beam line at the Photon Factory, KEK, Japan was used, in the first order, with synchrotron radiation as a background continuum. The measurements have been performed on a relative scale in scanning mode and also on the absolute scale at every 5 nm interval. These absolute cross sections measurements of O_2 have been used to put the relative cross sections on a firm absolute basis throughout the region 130-175 nm. Temperature effects on the cross sections of the S-R continuum are clearly seen and cross sections at 78 K are about 80% of those at 295 K. The observed cross sections at 78 K are limited to absorption originating from only the $v''=0$ level.

*This work is supported by NASA grant NAG5-484 to Smithsonian Astrophysical Observatory.

DA-4 EUV Absorption Spectroscopy of Supersonic-Jet-Cooled Molecules: CO Bands in the Wavelength Region Near 97 nm.* PETER L. SMITH, G. STARK, K. YOSHINO, K. ITO & J. R. ESMOND — Harvard-Smithsonian Center for Astrophysics — The FUV spectrum of CO at low temperatures is of interest in the study of photodissociation processes in interstellar clouds. Spectra obtained at 295 K show that many CO bands below 100 nm are both overlapped and perturbed. Extraction of reliable oscillator strengths from these spectra is problematic. In order to simplify and clarify such spectra for CO and other molecules, we have developed a supersonic jet expansion apparatus that is used for absorption spectroscopy with the 6.65-m vacuum spectrometer at the Photon Factory of KEK, Japan. The absorption spectrum of CO at ~25 K in the wavelength region near 97 nm has been investigated photoelectrically with this apparatus with $\lambda/\Delta\lambda \simeq 1.5\times10^5$. The measured spectrum is in reasonable agreement with some published modelled spectra for CO at low temperature, but our ratios of integrated band cross sections, i.e., ratios of band *f*-values, are somewhat different from those determined from low resolution spectra obtained at 295 K.

* This work is supported by NASA grant NAGW 1596.

DA-5 OH(v,N) Populations Determined from High-Resolution Spectra of the Airglow. Kinetic Model for State-to-State Dynamics,* J.A. DODD, Stewart Radiance Lab, W.A.M. BLUMBERG, S.J. LIPSON, J.R. LOWELL, P.S. ARMSTRONG, D.R. SMITH, R.M. NADILE, N.B. WHEELER, and E.R. HUPPI, Phillips Lab, Geophysics Directorate, S.M. ADLER-GOLDEN, Spectral Sciences, Inc., W.J. MARINELLI, K.W. HOLTZCLAW, and B.D. GREEN, Physical Sciences Inc.
-- Individual OH(v,N) rotational state population column densities have been derived from spectral analysis of CIRRIS 1A nighttime earthlimb airglow data. Both pure rotation and vibration-rotation fundamental spectra have been examined, providing unique information for highly excited rotational states of OH(v=0-5). Relative populations of the 1e, 1f, 2e, and 2f Λ-doublet states have also been determined, providing an important probe into OH dynamics. A kinetic analysis based on collision-induced transfer of vibrational to rotational energy produces good agreement with the data.

*Work supported by the Strategic Defense Initiative Organization, the Defense Nuclear Agency, and the Air Force Office of Scientific Research under Task 2303EP/PL007.

DA-6 ELECTRON THERMALIZATION PROCESSES IN AFTER GLOW PLASMA

Y.Sakai, S.Sawada and H.Tagashira, Department of Electrical Engineering, Hokkaido University, Sapporo 060 JAPAN.

Thermalization processes of electrons in after-glow plasma of rare gases and Penning gas mixtures has been analyzed using the time and energy dependent collision frequencies. The following collision processes were considered, i.e. elastic and excitation collisions and recombination for electrons, and generation of electrons from metastable atoms by Penning effect, ionization collision between two metastable atoms and stepwise ionization. The decay rate of the electron concentration in Xe gas was given to agree well with experimental values. During the thermalization the electron energy distribution showed peculiar structures. The thermalization process was discussed comparing with experimental data.

DA-7 Electron Attachment to Silicon Hydride and Silicon Fluoride Species*, H. H. Michels and R. H. Hobbs, UTRC ---- The thermochemistry of negatively charged species of silicon, hydrogen and fluorine is at present uncertain, owing to a sparsity of experimental data and the lack of a systematic theoretical study. Reliable heats of formation of SiH_n^- and SiF_n^- species are of considerable interest since theory may help to determine the role that such anions play in the deposition of amorphous silicon films and in the etching of silicon surfaces. In this study a systematic evaluation of the geometry and energetics of SiH_n^- and SiF_n^- anions, and their corresponding neutral parents, has been carried out using Møller-Plesset perturbation theory. Optimized geometries were calculated at the SCF and MP2 levels of theory using several basis sets. Correlation energy treatments included both MP4 and QCISD methods. The anion thermochemistry was calculated through several isogyric processes and compared with Pople's G1 and G2 method predictions. Good agreement with experimental affinities is found for the SiH_n^- anions. We find that all SiF_n^- anions (n = 0-3) are stable, with relative stabilities similar to that found for SiH_n^-.

*Supported in part by Air Force Wright Laboratory.

DA-8 Empirical Potentials for the Interaction of Electronically Excited Atoms, D. Hudson, Naval Surface Warfare Center/ White Oak Laboratory- Increasingly, a need is arising for including the interactions of electronically excited atoms in the study of electric discharges and other processes. Construction of such interaction potentials from first principles is not likely to become a common occurence due to the many interacting states involved. This paper reports attempts to use simple models such as the L-J and Exp-6 as well as more complicated and realistic analytic models such as those reported by Varandas and Brandao (1) to approximate these interactions. Results will be presented for He* + He* and for X* + X* where X is an alkali atom. The values from the model potentials will be compared with values from various wuantum calculations.

(1) Varandas, A.J.C. and J. Brandao, Mol. Phys., 45, 857 (1982)

DA-9 Single-particle Potential for Photo-excited States of Open-shell Atoms ,* J. J. BOYLE, ITAMP, Harvard-Smithsonian CfA - A single-particle potential for calculating photo-excited electron orbitals of open-shell atoms is introduced. This potential is defined to include exactly all the first order corrections appearing in the perturbation expansion of the dipole polarizability[1] with respect to the coulomb interaction, and which fall into the class of "potential correction" diagrams. It has been shown[2] that the angular coefficients associated with this potential can be written in the form of an average term plus a correction to the average which is dependent only upon the *initial state* coupling of the atom. The angular coefficients of this potential have been tabulated for all s^n, p^n, and d^n initial state *LS*-couplings to all dipole allowed final electron orbitals. This work modifies and extends a previous investigation by Qian *et. al.*[3]

* Work supported by a grant from the National Science Foundation.

[1] H. P. Kelly, Phys. Rev. **182**, 84 (1969).

[2] J. J. Boyle, Atomic Many-Body Theory Applied to Photoionization Processes in Complex Open-Shell Systems, Ph. D. Thesis, Univ. of Virginia (1992).

[3] Z. Qian, S. L. Carter, and H. P. Kelly, Phys. Rev. A, **33**, 1751 (1986).

DA-10 X-ray Double Ionization of Helium Isoelectronic Sequence : A. DALGARNO AND H. R. SADEGHPOUR, *Harvard-Smithsonian Center for Astrophysics, Cambridge, MA*, —A simple and accurate procedure for calculating the rate of double ionization of "two-electron" systems by X-ray photons is presented. Arguments are given to support the validity of the method used. In particular, we show that the many-body perturbation theory diagrams depend asymptotically on the choice of the gauge for the electric dipole operator. The ratio of double- to single-ionization is calculated to be 1.68% in agreement with the recent synchrotron measurements. For H^- and Li^+, we predict ratios of 1.51% and 0.89%, respectively.

*This work was supported by the U.S. Dept. of Energy, Division of Chemical Sciences, Office of Basic Energy Sciences, Office of Energy Research.

[1]A. Dalgarno and H. R. Sadeghpour, Phys. Rev. A, submitted.

DA-11 Model for Ion Trapping in Dusty Plasmas

J. Goree, *Dept. Physics, Univ. of Iowa, Iowa City, IA 52242*

A micron-size particulate in a plasma attains a large negative charge Q_D that can trap positive ions. Trapped ions are energetically bound to the grain in confined orbits, and like electrons bound in an atom, they shield the central charge from external fields. The number of trapped ions N_{trap} is a crucial parameter since it determines the level of shielding. Here a method of computing N_{trap} is reported. An untrapped ion passing the grain becomes trapped if it undergoes a collision that scatters its energy and angular momentum favorably. A later collision can detrap the ion. At steady-state N_{trap} is determined by balancing the collisional trapping and de-trapping rates. According to a single-particle Monte Carlo simulation of the process, the number of trapped ions in a lab plasma can be a very large fraction of Q_D/e everywhere except within an electrode sheath.

[1]J. Goree, Phys. Rev. Lett. 1992

DA-12 Effect of Ion-Neutral Collisions on the Perpendicular Ion Temperature in Argon.

R.K. PORTEOUS, S. DEFAUCONPRET, H.B. SMITH and R.W.BOSWELL, Plasma Research Laboratory, R.S.PhysS.E., The Australian National University. Perpendicular argon ion temperatures in low pressure ECR reactors have been measured[1,2], using laser-induced fluorescence techniques, to be 10 times greater than the neutral gas temperature. The most likely method of energy transfer into the perpendicular direction is through ions colliding with gas atoms. However, for ion energies greater than ~1eV the differential collision cross-section for collisions with atoms is expected to be highly anisotropic, with scattering angles close to 0° or 180° in the centre of mass frame, which results in negligible perpendicular heating. To investigate the effect of finite scattering angles, the collisions were modelled by fitting the interaction potentials for $Ar\text{-}Ar^+$ and then integrating classically to give the scattering angle as a function of energy and impact parameter. The resulting differential cross-sections were compared to experimental measurements. .A one dimensional Monte Carlo code was written to simulate argon ions travelling through a background of neutral argon gas; and the energy division between the parallel and perpendicular directions was investigated for various electric fields and gas pressures.

1. E.A.Den Hartog, H.Persing, and R.C.Woods, Appl.Phys.Lett 57,661 (1990).
2. N.Sadeghi, T.Nakano, D.J.Trevor, R.A.Gottscho, J.Appl.Phys.70, 2552 (1991).

DA-13 Quenching and Energy Transfer in $B^3\Pi$ State of N_2, * CHARLES SCRIPTER and JACEK BORYSOW, Physics Department, Michigan Tech. University - Quenching and electronic energy transfer in $B^3\Pi$ state of N_2 in the vicinity of crossing with the $A'^5\Sigma$ state have been studied using emission spectroscopy. The excited states ($v = 10, 9, 8$ of $B^3\Pi$) are formed in a pulsed positive column of N_2 and N_2/He discharges with ≈ 0.5 $Amp\ cm^{-2}$ current, ≈ 5 μs duration and pressures from 0.2 to 0.8 $Torr$. The initial production mechanism of $v = 10, 9, 8$ of $B^3\Pi$ state is an electron impact excitation. The apparent lifetime just after the discharge is in the range from 3 μs to 8 μs and becomes 80 to 160 $\mu s \approx 150 \mu s$ after the discharge depending on the pressure. Much longer lifetimes in the far afterglow are possibly due to an electronic energy transfer from $v = 0$ $A'^5\Sigma$ state. The measured build up transient of $v = 0$ $A'^5\Sigma$ state closely resembles population of $v = 10$ $B^3\Pi$ state.

* Supported by The National Science Foundation (ATM-9213854).

DA-14 Radiative association and inverse predissociation of oxygen atoms* J.F. BABB, A. DALGARNO, J. YEH, Inst. for Theoretical Atomic and Molecular Physics, Harvard-Smithsonian—The formation of oxygen molecules via radiative association $O + O(1\,^3\Pi_u) \rightarrow O_2(X\,^3\Sigma_g^-) + h\nu$ and inverse predissociation $O + O(1\,^3\Pi_u) \rightarrow O_2(B\,^3\Sigma_u^-) \rightarrow O_2(X\,^3\Sigma_g^-) + h\nu$ of $O(^3P)$ oxygen atoms is studied. Emission spectra for various initial energies of relative motion of the atoms and rate constants for various temperatures for the two processes are calculated. The associated spectra are compared to experimental results for oxygen plasmas at 3000K and 10 000K.

*Supported by the National Science Foundation

DA-15 Chemiluminescence in Suprathermal Reactive Collisions of O^+ and Ar^+ with Monomethylhydrazine, J. A. GARDNER, R. A. DRESSLER, R. H. SALTER, and E. MURAD, PhotoMetrics, Inc. and Phillips Lab, PL/WSSI–Chemiluminescence in gas phase ion-neutral reactive collisions is measured with a UV-enhanced charge coupled device (CCD) detector. Collision systems include O^+ and Ar^+ reacting with monomethylhydrazine (MMH = $N_2H_3CH_3$). Ultraviolet and visible emissions corresponding to NH $A \rightarrow X$ and CH $A \rightarrow X$ transitions are readily observed in high collision energy ($E_{c.m.} \approx 750$ eV) reactions between O^+ and MMH, and evidence is found for OH $A \rightarrow X$ emissions at low collision energies ($E_{c.m.} \approx 5$ eV) for these reactants. Also, NH and CH emissions have been observed in low energy collisions between Ar^+ and MMH. The energy dependence of these emissions will be presented and compared with previous emission measurements (using an intensified photodiode array) performed for reactions between these ions and hydrazine (N_2H_4).[1]

[1] J. A. Gardner, R. A. Dressler, R. H. Salter, and E. Murad, J. Phys. Chem. 96, 4210 (1992).

DA-16 Three-Body Conversion of He^{++} Ions in Helium* R.E. Tosh and R. Johnsen, U. of Pittsburgh- The formation of ionic rare-gas excimers, e.g. $(He_2^{++})^*$, is of interest for proposed tunable uv lasers[1]. Our earlier results[2] on the reactivity of doubly-charged ions were interpreted by assuming a three-body association reaction, e.g.

$$He^{++} + 2\,He \rightarrow He + (He_2^{++})^*$$

followed by emission of a photon in the so-called "third continuum". Using the drift-tube technique, we searched for other three-body reaction mechanisms. We observed He_2^+ ions as a reaction product indicating the existence of a competing channel that does not form the excimer:

$$He^{++} + 2\,He \rightarrow He^+ + (He_2^+)^*$$

The He_2^+ signal, however, was rather small and appeared to decrease with increasing He pressure (0.15 to 0.6 Torr). A similar reaction was found for Ne^{++} reacting in Ne.

[1] T. Griegel, H.W. Drottlef, J. W. Hammer, and K. Petkau, J.Chem. Phys. 93, 4581 (1990), see also references cited there.
2 R. Johnsen and M.A. Biondi, Phys. Rev. A 18, 996 (1978)

DA-17 Positive Ion Reactions in Perfluoroolefins. ROBERT A. MORRIS, A. A. VIGGIANO and JOHN F. PAULSON, Phillips Laboratory, Geophysics Directorate/GPID, Hanscom AFB - The gas phase reactions of CF^+, CF_2^+, CF_3^+, $C_2F_3^+$, $C_2F_4^+$, $C_3F_5^+$, and $C_3F_7^+$ with tetrafluoroethylene (C_2F_4) have been studied using a variable temperature-selected ion flow tube (VT-SIFT) instrument at 300 K and, for some of the reactions, at 496 K. In addition, reactions of CF_3^+ with the perfluorocarbons C_3F_6, 2-C_4F_8, and c-C_4F_8 have been studied at 300 and 496 K. Reaction rate constants and product branching fractions were measured. The reaction of CF^+ with C_2F_4 is fast and produces the ions CF_3^+, $C_3F_5^+$, and $C_2F_4^+$. The ion CF_2^+ reacts with C_2F_4 by non-dissociative charge transfer at the collisional rate. The reaction of CF_3^+ with C_2F_4 proceeds slowly by condensation. For the $C_2F_3^+ + C_2F_4$ reaction, which is fast, $C_3F_5^+$ and a small amount of $C_2F_4^+$ are produced. The reaction of $C_2F_4^+$ with C_2F_4 is slow and produces $C_3F_5^+$ which is itself unreactive with C_2F_4. $C_3F_7^+$ reacts slowly with C_2F_4 producing CF_3^+. While CF_3^+ does not detectably react with c-C_4F_8, CF_3^+ does react rapidly by F^- transfer with both C_3F_6 and 2-C_4F_8.

DA-18 A new theoretical study on the vibrational relaxation in N_2-N_2 collisions, M.CACCIATORE, G.D.BILLING and R.CAPORUSSO, Centro di Studio per la Chimica dei Plasmi, Dipartimento di Chimica, BARI (Italy) - Within a semiclassical "coupled states" method[1] and by using a refined intermolecular potential[2] we have computed a complete set of state-to-state rate constants for the vibration-to-vibration (V-V) and vibration-to-translation (V-T) energy exchanges in N_2-N_2 collisions. Compared to the well-known work of Billing and Fisher the present results exhibit substantial differences, our V-V rates being much smaller, particularly for N_2 in high v states and in the low temperature regime.

[1] M.Cacciatore and G.D.Billing J.Phys.Chem. 96 (1992) 217

[2] M.S.H.Ling and M.Rigby Mol.Phys. 51 (1984) 855; R.M.Berns and A.van der Avoird J.Chem.Phys 72 (1980) 6107

[3] G.D.Billing and E.R.Fisher Chem.Phys. 43 (1979) 395

DB-1 Temperature Dependence on Electron Degradation Spectra,* MINEO KIMURA, M. A. DILLON, and MITIO INOKUTI, Argonne National Laboratory, Argonne, IL 60439--Electron degradation has been studied extensively in the high-keV and subexcitation electron energy domains for a variety of atoms and molecules.[1] In these energy domains, the effect of electron energy gain on electron degradation in the surrounding molecules through superelastic and rovibrational deexcitation processes is negligible. However, as the energy approaches the thermal energy (<1 eV), the electron energy gain process plays a crucial role in the degradation, a role that should be properly accounted for in solving the kinetic equation. We have investigated the temperature dependence of the electron degradation of surrounding molecules by solving the Boltzmann equation. Our findings suggest that as temperature increases, electrons are more likely to gain energy, causing the time evolution to become slower and the distribution to become broader.

* Work supported in part by the U.S. Department of Energy, Office of Energy Research, Office of Health and Environmental Research, under Contract W-31-109-Eng-38.

[1] M. Kimura, M. A. Dillon, and M. Inokuti, unpublished results.

DB-2 Motion-compensated radiography using kinestatic charge detection. D.J. Wagenaar, R.A. Terwilliger, Brigham and Women's Hospital and Harvard Medical School, R.C. Lanza, Massachusetts Institute of Technology. --- Kinestatic charge detection relies upon the synchronization of cation drift velocity with the scan velocity of a parallel plate drift chamber to achieve a hundred-fold improvement in the utilization of x-ray tube output over line-beam radiographic imagers. Applications fall into two categories: 1) mammography, which uses x-rays of less than 40 keV and krypton at 10 atm, and 2) chest radiography, which uses x-rays up to 120 keV and xenon at 25 atm. Initial experiments demonstrated evidence of impurities, most likely H_2O. A new module has been constructed which employs an active getter, all-metal seals, and other high-purity features. Signal generation has included a Frisch grid, but there is evidence that the geometry of the cathode segments may allow "self-gridding" to be used to detect ions arriving at the cathode. Features of detector module design and data acquisition electronics will be presented.

Funding by the Whitaker Foundation is gratefully acknowledged.

DB-3 Diagnostic Techniques used in AVLIS*, G.M. Heestand and R.G. Beeler, Lawrence Livermore National Laboratory - This is the second part of a general overview talk on the atomic vapor laser isotope separation (AVLIS) process. In this presentation we will discuss the diagnostic techniques used to measure key parameters in our atomic vapor including densities, temperatures, velocities, charge exchange rates and background ionization levels. Although these techniques have been extensively applied to our uranium program they do have applicability to other systems. Relevant data demonstrating these techniques will be shown.

*This work was performed under the auspices of the U.S. Department of Energy by Lawrence Livermore National Laboratory under Contract No. W-7405-Eng-48.

DB-4 Comparisons of Capacitive Probe, Optical Emission and EEDF-Measurements in Low-Frequency RF Discharges* K. R. STALDER, SRI International and W. G. GRAHAM, Queen's University--We report on continuing measurements of rf parallel-plate plasma discharges in argon. The current series of experiments concentrated on understanding the differences between 100-kHz symmetric and asymmetric discharges and their effects on the spatial and temporal behavior of plasma potential, n_e, and EEDF's. Symmetric discharges were formed by driving the electrodes 180° out of phase; the grounded walls were far enough away not to influence the discharge. Asymmetric discharges were formed by grounding one plate. In asymmetric discharges, the plasma behaves closely to what we previously reported[1]. Symmetric discharges behave as expected, with the fluctuating plasma-potential and other plasma parameters varying at twice the rf frequency.

*Research supported, in part, by a NATO travel grant.

1. K.R. Stalder, C.A. Anderson, A.A. Mullan, and W.G. Graham, J. Appl. Phys. **72** (1992)

DB-5 Electron Energy Distribution Function Measurements in a Planar Inductive Oxygen RF Glow Discharge, Michael S. Barnes, John C. Forster and John H. Keller, IBM East Fishkill, Hopewell Junction, NY, A tuned, cylindrical Langmuir probe was used to measure current-voltage traces in a planar, inductive oxygen, rf glow discharge at several pressures ranging from 0.5 mT to 10 mT. By incorporating "good" probe design (according to V.A. Godyak's NATO Review Article) and tuning the probe so that it electrically "floats" with the rf-modulated plasma, the distortions encountered at the plasma and floating potential "knees" were minimized. The plasma potentials were determined from the zero-crossings of the trace second derivatives. Positive ion densities were evaluated using orbit motion limited probe theory; electron densities were estimated by integrating the area under the un-normalized distribution function. By applying the Druyvesteyn formula to the digitized probe traces, the electron energy distribution functions (EEDF) were obtained. The EEDF's range from Maxwellian at 0.5mT to almost Druyvesteyn-like at 10mT.

DB-6 Comparison of Measured and Simulated Electron Energy Distribution Functions (EEDFs) in a Low Pressure rf Discharge, M. M. TURNER and M. B. HOPKINS, Dublin City University, Ireland – The EEDF has been calculated in argon and nitrogen rf discharges at pressures up to 200 mTorr, using a one-dimensional PIC-MCC algorithm. These data are compared with the EEDFs measured by a tuned Langmuir probe with a technique described elsewhere[1]. We find good agreement between the experiments and the simulation in both gases. In nitrogen the EEDF has a distinctly seperate bulk and high energy tail at all pressures; the bulk electrons always have an effective temperature of $\approx$ 0.6 eV, but the density and mean energy of the tail electrons diminish as the pressure increases. In argon we observe a transition in the form of the EEDF qualitatively similar to that reported by Godyak and Piejak[2]. We will discuss the differences between the behaviour of electrons in nitrogen and argon.

[1]R. Doyle, M. B. Hopkins and M. M. Turner, this conference.

[2]V. A. Godyak and R. B. Piejak, Phys. Rev. Lett. **65**, 996 (1990).

DB-7 A Comparison of Thomson Scattering and Langmuir Probe Measurements of T_e and n_e in an ECR Discharge, M.D. BOWDEN, F. KIMURA, K. UCHINO, K. MUTA, K. MURAOKA and M. MAEDA, Kyushu U - Simultaneous measurements of electron temperature T_e and density n_e in the source region of an ECR discharge were made using Langmuir probes and incoherent Thomson scattering[1] of a high power pulsed YAG laser. Measurements were made in an argon discharge, at various pressures and with several different types of probes. It was found, for all discharge pressures and for each probe type, that there were significant differences, of up to a factor of 2, in the results of the two methods. Also, the Thomson scattered spectrum observed when a probe was present in the plasma was measurably different to the spectrum observed in the absence of a probe, indicating that the presence of the probe in the plasma was altering the electron velocity distribution. This effect appeared to become more significant at lower pressures.

[1]D.E. Evans and J. Katzenstein, Rep. Prog. Phys. 32, 207 (1969).

DB-8 Measurement of Low Pressure rf Plasma Parameters with a Tuned Langmuir Probe, R. DOYLE, M. B. HOPKINS and M. M. TURNER, Dublin City University, Ireland – A carefully designed tuned Langmuir probe has been used to measure plasma parameters, including the electron energy distribution function (EEDF), in argon and nitrogen rf discharges at 13.56 MHz. The data show that at low pressures ($\approx$ 20 mTorr) the EEDFs in both gases appear bi-Maxwellian, with bulk effective temperatures $<$ 1 eV. As the pressure is increased, the two-group EEDF vanishes in argon but persists in nitrogen up to the highest pressures investigated, although the "hot" group becomes very far from Maxwellian. This behaviour in argon has been observed previously; we find that that the results in nitrogen can be explained in terms of the structure of the electron impact cross sections of nitrogen.

DB-9 The Determining Method of Electron Temperature by Symmetric Triple Probe Covered with Dielectric Thin Film, DAISUKE OKANO, Kumamoto Inst. of Tech., Japan — For a nearly Maxwellian plasma - contaminated floating probe system biased at an low frequency voltage (V_{Tex}), a determining method of an electron temperature (T_e) with a symmetric triple probe (STP) covered with a dielectric material such as a polymer is numerically studied. When we obtain experimentally a ratio[1]-[2], $R_v=(V_2-V_1)/(V_3-V_2)$ at any instantaneous value of V_{Tex}, where V_2 is a floating potential for a probe P_2, and V_1 and V_3 are probe voltages for probes P_1 and P_3, respectively, with reference to a plasma space potential, R_v has a relation as follows at large $V_T=V_3-V_1$. $R_v=\alpha V_{Tex}/\ln(0.5+0.5\exp(\alpha V_{Tex}/T_e))/T_e-1$, where $V_T=\alpha V_{Tex}$, and α is an attenuation factor due to equally deposited thin films on STP. The value of α is obtained by a probe current ratio of clean and contaminated STP at same instantaneous voltage of V_{Tex}. From calculation results, it is found that T_e is uniquely determined by R_v, and at $V_T=20$ V, T_e is nearly proportional to R_v.

[1] *D. Okano: Jpn.J.Appl.Phys. 28, 1145 (1989).*
[2] *D. Okano: Jpn.J.Appl.Phys. 31, 383 (1992).*

DB-10 Mass Spectroscopy and Molecular-Beam Deposition from Hydrocarbon Arcjet Plasmas that Produce Diamond* W. HOMSI and K. R. STALDER, SRI International--Molecular beams originating from the stagnation point of hydrocarbon arcjet plasmas impinging on tantalum substrates are being studied. A two-stage differential pumping system with skimmers produces a beam that is analyzed by a quadrupole mass spectrometer, or is impinged upon a temperature-controlled silicon substrate and allowed to deposit a film. The mass spectroscopic measurements confirm that acetylene is the dominant species that is converted from the hydrogen-methane feedstock to the arcjet plasma. While diamond films, measured by ex-situ Raman spectroscopy, have been grown on silicon and tantalum substrates at the stagnation point for the high-pressure arcjet plasma, a limited number of concurrent molecular beam deposition experiments have yet to produce diamond films on heated silicon substrates in the high-vacuum region.

*Work supported by ARO Contract No. DAAL03-89-K-0157.

DB-11 Miniature Retarding Grid Ion Energy Analyzer, G.W. GIBSON, JR. and H.H. SAWIN, Massachusetts Institute of Technology - A retarding grid analyzer intended for use as a high-density (~10^12/cc) plasma diagnostic has been designed, built and tested. The analyzer's external dimensions are 0.125"x0.125"x0.050," which are smaller than macroscopic plasma scale lengths, thus allowing it to be stalk mounted and moved throughout the plasma. The grids are 2000 line/inch nickel mesh so that the linear dimension of grid open area is less than the debye length for plasmas with 10 eV electrons and 10^12/cc densities. Successive grids are separated by 0.01" in order to avoid space charge effects between grids and thus allow unprecedented energy resolution. Also, because the linear dimension normal to the grid is small compared to the ion mean free path in high pressure (>100 mTorr) discharges, it can be used without the differential pumping required of larger GEA's in such discharges. The analyzer has been tested on a plasma beam source (a modified ASTeX Compact ECR source) and on an ASTeX S1500 ECR source, and has been used as and edge diagnostic on the VERSATOR tokamak at M.I.T. Ion energy distribution functions as narrow as 5eV have been measured.

DB-12 The Diagnostics of RF Glow Discharges with Particulates by using Spatiotemporal Spectroscopy and Mie Scattering, S.KAKUTA, T.KAMATA, T.MAKABE, Keio Univ. – The influence of particulates on the structure of RF glow discharges in Ar has been investigated by spatiotemporal emission spectroscopy. In this study, carbon black, which is chemically nonreactive and conductive, is used as an impurity dust. We can discuss about the net-excitation rate of $Ar(3p_5)$, $\Lambda_j(z,t)$ during an RF cycle by the emission intensity of $ArI(3p_5 \rightarrow 1s_4)$. The spatiotemporal structure is quite different from that in pure Ar. That is, the profile of $\Lambda_j(z,t)$ in the first half cycle is similar to that of discharges with negative ions. The double layer is formed in front of the instantaneous anode, and the electric field in the bulk plasma is larger than that of electropositive gases. It is attributed to the negatively charged particles. In the latter half cycle, no evident excitation is observed. It strongly implies that the plasma potential is almost negative in the latter half cycle. This is a new plasma system composed mainly with negatively charged massive particles and positive ions. The growth of particles has been also observed by Mie scattering from He-Ne laser. The radius becomes up to $\sim 1\mu$m. The chemically nonreactive carbon black agglomerates by the electrostatic force.

DB-13 Artificial Neural Networks for Plasma Spectroscopy Analysis*, W.L. MORGAN, Kinema Research, Monument, CO, J.T. LARSEN, Cascade Applied Sciences, Boulder, CO, and W.H. Goldstein, LLNL, Livermore, CA - Artificial neural networks have been applied to a variety of signal processing and image recognition problems. Of the several common neural models the feed-forward, back-propagation network is well suited for the analysis of scientific laboratory data, which can be viewed as a pattern recognition problem. We present a discussion of the basic neural network concepts and illustrate its potential for analysis of experiments by applying it the spectra of laser produced plasmas in order to obtain estimates of electron temperatures and densities. Although these are high temperature and density plasmas, the neural network technique may be of interest in the analysis of the low temperature and density plasmas characteristic of experiments and devices in gasous electronics.

*Work supported by the Lawrence Livermore National Laboratory.

DB-14 Application of CARS to the Study of Surface Deactivation of Vibrationally Excited Homonuclear Diatomic Molecules. P. P. YANEY and K. A. RIMKUS,* U. of Dayton**; B. GANGULY, APPD, Wright Lab. -- Coherent anti-Stokes Raman Spectroscopy (CARS) provides an attractive optical probe technique for studying heterogeneous reactions between solid surfaces and N_2, O_2 or H_2 gases. The setup consists of a discharge device mounted on top of a probe chamber containing the surface. Vibrationally excited gas from the discharge device passes over the surface. The CARS beams are arranged to cross parallel to the surface. The chamber is mounted on a three-dimensional translation system to provide for spatially-resolved measurements. Measurements down to 10 Torr are currently possible. Population changes due to second gas can also be studied. Measurements will be reported on the population changes in the v = 0, 1 and 2 states of N_2 due to various surfaces.
* In partial fulfillment of the requirements for the M.S. degree in Electro-Optics.
** Supported by USAF Contract F33615-90-C-2036.

DB-15 Laser Induced-Fluorescence Measurement of Ion Velocity Distributions in a Pulsed Plasma Sheath,* M. J. GOECKNER, M. SHAMIM, R. A. BREUN, and J. R. CONRAD, - Engineering Research Center for Plasma-Aided Manufacturing, U. of Wisconsin

Laser induced-fluorescence (LIF) was used to measure both ion velocity distributions and densities in a 10-kV pulsed-plasma sheath of the plasma source ion implantation (PSII) device. In the PSII device, the substrate to be implanted is biased to a large negative voltage (V_{pulse} = 0 to -100 kV) for short periods of time (10 to 50 μs). Before the bias is applied to the substrate, there exists a Child's-law-like sheath having a width of several Debye lengths. When the bias is applied to the substrate, the electrons are 'blown off' and an ion-matrix-like sheath is formed temporarily. The sheath then expands to a Child's-law-like sheath that is consistent with the applied voltage. Such expansions of the sheath thickness have been observed by M. Shamim.[1] Ions that have been overrun by the expanding sheath edge are accelerated to the substrate surface and implanted. With these measurements, we have gained an understanding of the ion dynamics in a pulsed sheath. This knowledge should help us to optimize the operation of PSII. Experimental results will be shown and discussed.

* This work was supported by NSF Grant No. ECD-8721545.

1 Shamim, Ph.D. Thesis, University of Wisconsin - Madison, 1992.

DB-16 Laser Induced Fluorescence Measurements of the Sheath Thickness in a Magnetron Sputtering Discharge, M. BOWDEN, T. NAKAMURA, Y. YAMAGATA, B.W. JAMES, K. MURAOKA and M. MAEDA, Kyushu U., Kumamoto U. and U. of Sydney - The thickness of the sheath in a planar magnetron has been determined by a laser induced fluorescence technique[1]. The magnetron discharge was operated in BCl_3 at a pressure of 50mTorr and discharge current of 40mA. The presence of the discharge magnetic field affected the fluorescence intensities, making previous calibrations unsuitable. This meant that absolute values of the electric field could not be calculated. The sheath thickness, however, could be determined and for each of the magnetron discharge fields studied, was found to be approximately the same as the maximum displacement of a collisionless secondary electron fom the cathode surface. For these conditions at least, models based on the common assumptions of thin or thick sheaths would not be satisfactory.

[1]C.A. Moore, G.P. Davis and R.A. Gottscho, *Phys. Rev. Lett.* **52**, 538 (1984).

DB-17 Measurement of Magnetic Presheath in Collisional ECR Plasma.* G.-H. KIM and N. HERSHKOWITZ, University of Wisconsin-Madison — The first investigation of a magnetic presheath employing plasma potential measurements near a conducting plate in an outflowing electron cyclotron resonance (ECR) plasma is given. By measuring the characteristic lengths of presheaths in front of conducting plate which was grounded and titled with respect to DC magnetic field, the double structure of presheaths in collisional plasma was found for the first time. One, the charge exchange presheath, corresponded to the ion collision mean free path. The other one, the magnetic presheath, depended on the ion sound gyroradius as well as the sin Ψ, where Ψ is the angle between the magnetic field and the normal to a boundary, or the distance of the guiding center of an ion which first encounters the boundary. Potential measurements were carried out by using the inflection point emissive probe technique. Representative parameters are B = ~150 gauss, Te = 3~4 eV, N_2^+ plasma, n_e=1~3x10^{10} cm^{-3} and pressure = 0.75~2 mTorr.

*Work supported by NSF Grant No. ECD-8721545 for the Engineering Research Center for Plasma-Aided Manufacturing.

DB-18 Emission spectroscopy in dc C_3H_8-H_2 discharges generated in a plasma carburizing furnace,* G. SULTAN, G. BARAVIAN, LPGP (CNRS), U. of Paris-Sud, Orsay France, E. DENISSE, P. JACQUOT, INNOVATIQUE**, Chassieu France and G. DERVIEUX , BMI **, Lyon France - Optical emission spectroscopy was used as a diagnostic tool to characterize the discharge in a BMI plasma reactor for carburization of metallic parts. The discharge conditions were varied with the respective concentrations of the mixture propane-hydrogen. The current density was equal to about 1 mA/cm^2 , the total pressure 1 Torr, the gas temperature 730 K and the flow rate 5 l/mn. The study of the relative intensities of the CH line at 431.4 nm and the H_γ line at 434 nm shows that the excited H atoms would principally result from the dissociation of H_2 molecules rather than that of propane. This property is used for monitoring the process.

* Work supported in part by EDF and BMI.

** HIT Group France

DB-20 Detection of O and H atoms by Laser Induced Fluorescence and Stimulated Emission in a D.C. Glow Discharge.

J. AMORIM*, G. BARAVIAN, J. JOLLY, M. TOUZEAU,
LPGP(CNRS), University of Paris-Sud, 91405 - Orsay - France -

Stimulated Emission (SE) induced by two photon laser excitation, has been observed as an additional deexcitation pathway for the Laser Induced Fluorescence (LIF) diagnostics. The LIF signal was observed at right angle to the exciting laser beam, while the SE was probed in the forward direction, in order to measure the concentrations of O and H atoms in a O_2 and H_2 positive column of a dc glow discharge. For pressures ranging from 0.1 to 5.0 Torr and discharge current between 1 to 50 mA, the threshold and the evolution of SE were observed both, for a given atomic density as a function of laser energy and as function of the atomic density for a fixed laser energy. A set of rate equations was solved in order to account for time density evolutions of the involved atomic levels, and to relate LIF and SE signal intensities to the fundamental level concentrations of O and H atoms.

* partially supported by CNPq/MAer - Brazil.

DB-21 Laser and Spectroscopic Studies of RF-Excited Hydrogen Discharges -- A. T. YOUNG, P. CHEN, K. N. LEUNG, L. C. PAN, AND D. M. PONCE, Lawrence Berkeley Laboratory, University of California, Berkeley, CA 94720, and H. F. DÖBELE, Insititut für Laser-und Plasmaphysik, Universität Gesamthochschule Essen, D-4300, Essen, Germany, -- RF-excited plasmas have found use in a wide variety of applications, such as ion sources or as the plasma environments for semiconductor processing. Using rf excitation has several advantages when compared with filament-driven discharges, including the production of plasmas free from cathode material and operation unencumbered by limited filament lifetime. The chemical physics occurring in these plasmas, however, is not well understood. In order to better understand these processes, laser and spectroscopic measurements of rf-driven hydrogen discharges have been performed. A variety of techniques has been used: visible and vacuum ultraviolet emission spectroscopy, multiphoton laser induced fluorescence and ionization, and vacuum ultraviolet laser absorption spectroscopy. Populations of the atomic and molecular hydrogen have been measured. Both inductively and capacitively-coupled discharges have been studied. Comparisons and contrasts between these discharges and filament-driven discharges will be made.

* This work has been supported by AFOSR, a NATO Collaborative Research Grant, and the US DOE under contract No. DE-AC03-76SF00098.

DB-22 Pressure Dependence of CF_3 Radical Density in RF Discharge CHF_3 Plasma, K. MARUYAMA, K. TAKAHASHI and T. GOTO, Nagoya Univ. - In this work, we measured the CF_3 radical density using infrared diode laser absorption spectroscopy (IRLAS). The RF plasma chamber had parallel circular plane electrodes of 20 cm diameter and 3 cm separation. CHF_3 plasma was excited by an on-off modulated RF power with on-period of 40 ms and off-period of 80 ms applied to the upper electrode. The measurement of CF_3 radical was carried out at 1.5 cm above the lower (grounded) electrode using ${}^rR_{18}(18)$ line of ν_3 band. The CF_3 radical density was measured at a CHF_3 pressure of $30 \sim 120$ mTorr, a flow rate of 45 sccm and an on-period RF power density of $0.48\,W/cm^2$. The radical density increased with an increase in gas pressure. However, it showed a tendency to be saturated at a gas pressure above 50 mTorr. The CF_3 radical density and the decay time were estimated to be $2 \times 10^{14}\,cm^{-3}$ and 13 ms at a gas pressure of 50 mTorr, respectively. In contrast, the intensity of the laser beam passed through the plasma decreased all over the wavelengths with an increase in gas pressure.

DB-23 Glow discharges electric field measurement using Stark spectroscopy of Hydrogen, J.P. BOOTH, J. DEROUARD, M. FADLALLAH and N. SADEGHI, Labo. de Spectrométrie Physique, Université J. Fourier Grenoble I, FRANCE--We have tried different methods based on Stark spectroscopy of H atoms to measure the electric field in discharges. Using plasma induced emission spectroscopy[1], we have observed the sheath oscillations in 30 kHz discharges. Optogalvanic laser spectroscopy of Balmer n=2-n=7 transitions showed some Stark structure but quantitative measurement was not successful because of line shape distortion due to laser saturation effects and to the noise due to discharge current instabilities. Finally we shall present results concerning the laser excitation spectrum of ground state H atoms to the 7P level using two step, two colour (243 nm and 397 nm) laser excitation, detected by the induced fluorescence, which opens the way to a new diagnostic method with high sensitivity and high 3D spatial resolution

[1]J.P. Booth, J. Derouard and N. Sadeghi, contribution to the 44th GEC

DB-24 *In Situ* Diode Laser Diagnostics of a Plasma Etching Reactor, DANIEL B. OH and ALAN C. STANTON, Southwest Sciences, Inc., MICHAEL P. SPLICHAL and HAROLD M. ANDERSON, Center for High Technology Materials, University of New Mexico - A major objective of the microelectronics industry is to perfect methods for controlling dimensional accuracy during plasma etching of submicron features in wafer substrates. Optical sensors as monitors of gas phase etch chemistry are attractive because they offer the potential of nonintrusive *in situ* measurements for use as real time inputs to process control. In this study, lead salt infrared diode lasers were used to measure CF_4 feed gas dissociation, neutral CF_2 reactive intermediates, and CF_2O etch products in fluorocarbon -based plasmas used for etching of silicon and silicon dioxide. These measurements were conducted *in situ* in a GEC Reference Cell Reactor, using high frequency diode laser wavelength modulation techniques and a single-pass optical configuration. Correlations between measured species concentrations and process characteristics such as etch rates, end point, and selectivity were identified. For example, diode laser measurement of CF_2 concentration was found to be useful as an indicator of etch selectivity. End point detection by diode laser monitoring of CF_2O during etching of SiO_2 was also demonstrated. Further research and development based on these results is expected to lead to new process control strategies for improved reliability and product yield in plasma etching.

DB-25 Long Range Tunable Diode Laser for Plasma Diagnostics, * SERGUEI FILIMONOV and JACEK BORYSOW, Physics Department, Michigan Tech. University - We have developed new simple tuning mechanism for single mode, pseudo-external cavity diode lasers. Our model calculations predict that lasers can be tuned continuously as much as 600 GHz without locking to an external cavity. Experimentally, the continuous tuning range is about 120 GHz at constant current and temperature; this is about 5 times more than previously reported [1]. The laser is based upon a commercial chip and a diffraction grating is used for feedback. A rotating wedge inside the laser cavity is used as the only tuning element. By proper selection of the wedge angle and wedge thickness, changes in cavity length and the angle of the feedback grating may be achieved simultaneously. The laser was used for measuring densities of metastable states of Ar in a GEC reference cell.

1. Carl E. Wieman and Leo Hollberg, *Rev. Sci. Instrum.* **62**, 1 (1991).

* Supported by The State of Michigan Research Excellence Fund

DB-26 Optogalvanic Measurement of Electric Fields in Neon Hollow Cathode Discharges, Y. MATSUDA, F. AMAZAKI and H. FUJIYAMA, Fac. of Eng., Nagasaki Univ.- Optogalvanic spectroscopy using two-step laser excitation[1] was applied to measure the local electric field in the cathode fall region of a neon hollow cathode glow discharge (6Torr, discharge voltage:156.4V, cathode inner diameter:3mm). Laser beams were focused and coaxially incident into the plasma, with a spatial resolution of 0.1mm. Electric field intensity was evaluated from experimental Stark splitted spectra. The measured electric fields did not decrease linearly with the distance from cathode surface, while their integral value (experimental cathode fall potential) was in good agreement with the discharge voltage. In addition, ratio of ion to electron current at the cathode surface was evaluated to be 2.4. These results indicate the importance of not only geometrical effect due to the cylindrical structure, but also enhanced ionization in the cathode fall due to the efficient confinement of electrons, metastable atoms, and VUV photons.

[1]D.K.Doughty,S.Salih and J.E.Lawler,Phys.Lett.,103A,41(1984).

DB-27 Measurement of Electron Energy Distribution by Biased Optical Probe, H. TOYODA, K. NAKANO and H. SUGAI, Dept. Electrical Eng., Nagoya U., Japan Electron Energy Distribution Function (EEDF) in a plasma was measured by a Biased Optical Probe(BOP), which is a new high-sensitivity technique based on combination of optical emission spectroscopy and electrostatic retarding bias. The BOP is consist of a thin mesh cylinder whose bias voltage is variable. The energy of electrons entering the cylinder is decreased by a negative potential applied to the cylinder. Electrons collide with neutrals and the light emitted in the cylinder is collected and detected by a monochromator and photomultiplier. From the measured emission intensity as a function of bias voltage, the EEDF is reconstructed by a numerical calculation using emission cross section data. It was found that the high energy part of EEDF in a dc glow discharge deviate upward from a Maxwellian distribution because of a good confinement of high energy electrons. On the other hand, the EEDF of an inductive rf plasma coincides with a single Maxwellian distribution.

DB-28 **Reconciliation of density measurements using Stark Broadening of the Hydrogen Balmer and Neutral Helium Lines in a High Pressure, Low Electron Temperature Helium Plasma,** L. W. Downes, Miami University, Oxford, OH and J. Stevefelt, GREMI, Université d'Orléans, France. In our ongoing studies of high-pressure (50 - 5000 Torr), electron-beam-pumped (900 ns, 10 A/cm^2, 250 keV) helium plasmas, the use of Stark-broadened linewidths as a measure of electron density gives as much as two orders of magnitude difference depending on whether hydrogen or helium lines are used. Using the quasi-static approximation[2], the Stark-broadened linewidths of the neutral helium lines at 388.9 nm, 587.6 nm and 706.5 nm in the triplet and 501.5 nm and 728.1 nm in the singlet indicate electron densities of the order 10^{16} cm^{-3}. In both emission and absorption, the line at 388.9 nm in helium gives the same density. Similar measurements of the hydrogen Balmer-α (656.3 nm) and -β (486.1 nm) lines give a density of only 10^{14} cm^{-3} for the same pressure. The latter value is more reasonable and is in excellent agreement with calculation[1]. Since such measurements based on the H-β linewidth are known to be relatively insensitive to electron temperature[2] (in the 5000 K range and greater) and the helium lines should also be close (~30%)[2] in value, our results suggest a more significant electron temperature effect (in the 300 K range) for the other studied lines than previously known.

[1]"Estimation of Electron Densities in ^{3}He Dominated Plasmas," by B.D. Depaola, S.D. Marcum, H.K. Wrench, B.L. Whitten and W.E. Wells in *Proceedings of the First International Symposium on Nuclear Induced Plasmas and Nuclear Pumped LASERs*, M. Fitaire, ed., Les Editions de Physique, 91402 Orsay, France, 1978.
[2]*Spectral Line Broadening by Plasmas*, H.R. Griem, Academic Press, New York, 1974

DB-29 A Fast Alternative to Ray Tracing for Calculating the Collection Efficiency in Optical Emission Spectroscopy,* M. J. COLGAN, Physics Dept., Rutgers University, Newark, NJ 07102—Knowledge of the collection efficiency of an optical system is required for absolute calibration of emission intensities and for deconvolution of position-dependent emission data. Previously, extensive ray tracing has been necessary to estimate collection efficiency.[1,2] In this work, an alternative to ray tracing has been developed with application to nearly-ideal optical systems. The simple geometric algorithm is several orders of magnitude faster than ray tracing. Sample calculations show excellent agreement with ray tracing over a wide range of system parameters.

*Work supported in part by the USARO.

[1]P. B. Farnsworth, B. W. Smith, and N. Omenetto, *Spectrochim. Acta.* **45B**, 1151 (1990).
[2]F. Tochikubo and T. Makabe, *Meas. Sci. Technol.* **2**, 1133 (1991).

DB-30

Saturation Broadning of the $5s'^4D_{5/2}$ Cu Autoionization Level by the optogalvanic effect. M. Hakham Itzhaq and R. Shuker Department of Physics Ben Gurion University of the Negev Beer-Sheva , Israel Use of the optogalvanic technique to study the line profile of the Cu $5s'\ ^4D_{5/2}$ autoionization level is demonstrated .The degree of saturation broadning as a function of laser intensities on the $4p'\ ^4F^o_{7/2}$ - $5s'\ ^4D_{5/2}$ autoionization transition at 458.7 nm is measured. The experiment pointed out that the growth of the autoionization level breadth follows the square root increase in the laser intensity, in agreement with the well known saturation broadning equation $\Gamma=\Gamma_0[1+I/I_S]^{1/2}$. We measured the natural breadth of the Cu $5s'\ ^4D_{5/2}$ autoionization level Γ_0 which is in our case [7.1±0.8] cm^{-1} and the laser saturation intensity I_S which is [0.35±0.11] MW/cm^2. Saturated line width of up to 18.3 cm^{-1} was measured at laser intensity of 2 MW/cm^2.

DB-31 Ground State Cu Atom Density Measurements in Laser-Ablated Copper Plumes Using Hook Spectroscopy, A. Sappey and T. Gamble, Los Alamos National Laboratory - The Rozhdestvenskii Hook method has been implemented to measure atomic number density in a laser ablated plasma for the first time. The technique combines a Mach-Zehnder interferometer, a broad band light source, and a stigmatic spectrograph to record wavelength dependent changes in phase caused by the region of anomolous dispersion around electronic transitions in atoms. Our plumes are produced by laser ablation of a copper target into a He buffer gas with ablation fluences of approximately 1 GW/cm^2. The helium backing gas (typically 10-100 torr) serves to translationally cool the hot atomic vapor and maintains high atomic densities for times sufficiently long to foster condensation of the vapor into macroscopic particulate, a process which we are studying in detail. With 25 torr of He, the Cu ground state densities range from 1.5×10^{15} cm^{-3}, 200 μsec after the ablation event to 4.4×10^{13} cm^{-3}, 5 msec after ablation. The Hook method is very useful for density measurement in high density, high temperature environments where other commonly used techniques such as absorption fail due to pressure and opacity line broadening processes.

DC-1 Glow Discharge Characterization of Plasma Source Ion Implantation*, M. M. SHAMIM, P. FETHERSTON, K. SRIDHRAN and J. R. CONRAD, Engineering Research Center Univ. of Wisc., Madison, WI 53706.

In Plasma Source Ion Implantation (PSII)[1] a target is immersed in a plasma and pulse biased to a high negative voltage (~50kV). Originally the plasma has been generated in the PSII vacuum chamber using energetic electron impact technique. We have also applied glow discharge plasma to implant various substrate materials using nitrogen and carbon ions. Diamond-like-carbon films have been successfully produced using acetylene and methane plasma. A Langmuir probe has been used to detect gas breakdown during the applied pulse.[2] Glow discharge analyses of nitrogen, argon and methane at various pressures have been performed. Analysis of these results will be presented.

* This work supported by NSF Grants ECS-8314488 and DMC-8712461, US Army Grant DAAL03-89-K-0048 and by a number of industrial grants.

1 J. R. Conrad et al.,J. Appl. Phys.**62**, 4951 (1987).

2 M. Shamim et al., J. Appl. Phys. **69(6)**, 2904 (1991).

DC-2 **Modeling of Microwave Plasmas for Applications to CVD of Thin Diamond Films.**, B. Lane, *Plasma Dynamics*, Belmont, MA 02178, E. Hyman, K. Tsang and A. Drobot, *Science Applications International Corporation*, McLean, VA 22102, and Richard Post, *ASTeX, Inc.*, Woburn, MA.01801. We report on results from modelling of microwave plasmas in the 1-100 torr regime. Such modelling requires the treatment of (a) the microscopic coupling of electromagnetic energy to electrons and thence to the neutral gas, (b) the local gas phase neutral chemistry of hydrogen, hydrocarbons and oxygen molecules and their various radicals, (c) the macroscopic flow, neutral density and temperature patterns, and (d) the macroscopic electromagnetic field pattern within realistic cavity geometries. These aspects are tightly coupled: (i) the flow pattern and neutral density profiles depend on the heat deposition pattern which depends on the microwave coupling which in turn depends on the neutral density profile; (ii) the plasma density pattern depends on the electromagnetic field pattern which in turn is strongly influenced by the plasma. The problem thus requires a simulataneous, self consistent solution of each of the above aspects. We present the results of the simulation to date: (a) a 1 point, self-consistent time dependent integration of the Boltzmann equation together with evolution equations for hydrogenic and hydrocarbon species, (b) 2D (R-Z) simulations of the fluid flow and electromagnetic field patterns for fixed spatial heat input sources and plasma profiles, (c) a 1D fully self-consistent simulation coupling the fluid flow and multispecies diffusion, the neutral density dependence of the microwave coupling and the self-consistent electromagnetic field shape and magnitude in the presence of plasma generated by that field.

DC-3 Characterization of Thin Film-Diamond and DLC Producing Discharges.* R.C. CHESHIRE, M.J. HIGGINS, T. MORROW and W.G. GRAHAM. Physics Department, Queen's University, Belfast, Northern Ireland. Plasma deposition provides a convenient method for industrial production of both diamond and diamond-like carbon films. The atomic and molecular species in the discharge play an important role in determining the film quality. A 2+1 multiphoton laser induced fluorescence technique is being developed to detect H atoms in both rf and microwave driven discharges. Electrons play a dominant role in sustaining the discharge and are very important in the plasma chemistry. We are currently using an electrostatic probe technique to measure the basic plasma parameters i.e. electron density, electron energy distribution function and plasma potential. The results of these LIF and electrostatic probe measurements will be correlated with the DLC film quality. In particular we hope to establish the exact role of H atoms in diamond film deposition and its main production mechanisms in the discharge.
*Supported by EC/BRITE/EURAM.

DC-4 Thin Film Ceramics for Improved Performance of Repetitively-Pulsed High-Power Microwave Sources,* C. B. FLEDDERMANN, E. SCHAMILOGLU, J. GAHL, D. SHIFFLER, B. WROBLEWSKI, L. MORELAND, and T. CAVAZOS, Dept. of Electrical and Computer Engineering, U. of New Mexico- The use of both resistive and ferroelectric ceramic thin films is being investigated in a repetitively-pulsed high-power microwave source. Resistive ceramics such as titanium oxide and titanium nitride are used as coatings for metallic and insulating surfaces to reduce the breakdown in a relativistic backward-wave oscillator (BWO). We will report on the effects of film properties such as thickness and composition on the breakdown characteristics.

The use of ferroelectrics such as PLZT on cathodes has been suggested as a means to increase electron emission[1], and thus provide high brightness electron sources. The high electron emission is attributed to a rapid phase transformation when the cathode is pulsed. In our experiments, a thin film ferroelectric cathode is pulsed using a 30kV, 1 kHz pulser. We will present data characterizing the performance of these cathodes.

1. H. Gundel et al., Nucl. Inst. and Methods in Phys. Res. A280, 1 (1989).
* Work supported by AFOSR.

DC-5 Secondary Electron Emission from Electrode Surface Covered with Hydrogenated Amorphous Silicon, Y. MATSUDA, H. KAWASAKI, S. YANG and H. FUJIYAMA, Fac. of Eng., Nagasaki Univ.– In order to investigate the reproducibility in reactive silane (SiH_4(10%)/Ar) plasmas, temporal variations of discharge characteristics have been observed during the deposition of hydrogenated amorphous silicon (a-Si:H) thin films. From the variations of discharge currents and optical emissions, it was confirmed that plasma density rapidly decreased as the deposition started, then completely saturated after the deposition time of one hour. This temporal variation of the plasmas is possiblly due to the decrease in the number of γ electrons which are ejected from the cathode surface. Therefore, we investigated the γ coefficients of a-Si:H thin films doposited at the various deposition time by the breakdown characteristics (Paschen's curves) in pure Ar. Estimated γ coefficient for virgin Al electrode was about 0.1. On the other hand, γ coefficient for Al completely covered with a-Si:H thin films was estimated to be 7×10^{-3}.

DC-6 SiO_2 Deposition by TEOS and Selected Oxygen Atoms. S. WICKRAMANAYAKA, A. MATSUMOTO, Y. NAKANISHI and Y. HATANAKA, RIE, Shizuoka Uni.,Japan— Thin SiO_2 films were deposited at 300° C by the reaction of tetraethoxysilane (TEOS) with selected oxygen atoms in an oxygen plasma downstream at 1.0 Torr pressure. The $O(^1D)$ fraction at 60 cm from the plasma exit is 95 % for 800 W plasma and this ratio gradually decreases to 45% with the decrease of rf power to 100 W. SiO_2 films deposited with higher $O(^1D)$ densities yield better quality films. However, for the film growth rate the state of the oxygen atom dose not affect but the total oxygen atom concentration. The activation energy for the film growth was found to vary from 0 to -0.29 eV with the changing rf power applied to produce the plasma. This variation can be attributed to the change of oxygen atom concentration at the deposition site. The minimum ratio of oxygen atoms to TEOS in order to maintain the equilibrium of absorption/ desorption reaction at the growing film surface, which causes to yield a negative activation energy is estimated as $\sim$0.4 at which the lowest activation energy is yielded. The film quality goes up for higher ratios and drops for lower ratios.

DC-7 Spectroscopic and actinometric investigation of SiO_2 etching chemistry in the helicon reactor. H. PERSING, A.J. PERRY and R.W.BOSWELL. , Plasma Research Laboratory, Research School of Physical Sciences and Engineering. The Australian National University.

— A helicon reactor has been used to etch, anisotropically, planar waveguide structures in thick (20μm) layers of SiO_2 deposited in a separate helicon reactor. Etch rates of over 1μm/min are easily obtained in CHF_3 plasmas at 1500W with surface quality high enough for optical quality SiO_2 to be deposited over the etched structures. We are interested in determining the chemical species that are responsible for the etching (e.g. compare ref 1,2) of the SiO_2 under these conditions and here report the results of experiments in which the etch rate was measured as a function of the concentrations of F and CF_2 in the plasma.

1. R. d'Agostino, F. Cramarossa, S. De Benedictis and G. Ferraro., J. Appl. Phys. **52**, 1259 (1981)
2. M. Kitamura, H. Akiya and T. Urisu., J. Vac. Sci. Technol. **B7**, 14 (1989)

DC-8 **Molecular Dynamics Simulations of Fluorine Etching Silicon in the Presence of Ion Bombardment**

M.E. BARONE, T. SCHOOLCRAFT*, B. GARRISON**, and D. B. GRAVES, University of California,Berkeley -

A molecular dynamics simulation of fluorine etching silicon has been performed in the presence of bombardment by a non-reactive energetic species. We assume that all exposed silicon dangling bonds are fully saturated with fluorine on a time scale rapid with respect to the rate of energetic species bombardment. Results from these simulations are compared to previous MD simulation results of fluorine etching silicon without dangling bond saturation or non-reactive energetic species bombardment.[1] In addition, simulation results are compared to experimental studies of fluorine etching silicon under simulated plasma conditions in high vacuum.

* Department of Chemistry, Gettysburg College, Gettysburg , PA 17325
** Department of Chemistry, The Pennsylvania State University, PA 16802

1 T. A. Schoolcraft and B.J. Garrison, *J. Am. Chem. Soc.*, 113 (1991).

DC-9 Above-surface neutralization of multicharged ions incident on a cesiated Au target,* F.W. MEYER, I.G. HUGHES, S.H. OVERBURY, D.M. ZEHNER, and P.A. ZEIJLMANS VAN EMMICHOVEN, ORNL--The critical distance above the surface at which conduction band electrons can start to neutralize incident multicharged projectiles by classical overbarrier transitions is inversely proportional to the metal work function. By varying the amount of Cs coverage on a Au single crystal target between 0 and 1 monolayers, we have been able to verify an up to 3.3 eV decrease of the surface work function, corresponding to more than a factor of two decrease relative to that tabulated for clean Au. This change should result in more than doubling the above-surface interaction time. At larger above-surface distances, however, the electron capture most likely occurs into higher principal quantum numbers of the projectile. The subsequent de-excitation cascade by which inner shells of the projectiles are populated may thus require more time. We have investigated the overall effect that lowering the work function has on the above-surface component of projectile K-Auger electron emission for grazing incidence N^{6+} ions interacting with cesiated Au single crystals. We will present results showing that an enhancement of this component is indeed observed, and that it is strongly dependent on incidence angle.

*Funded by the Office of Basic Energy Sciences, USDOE, under contract DE-AC05-84OR21400 with Martin Marietta Energy Systems, Inc.

DC-10 An Industrial-scale Plasma Source Ion Implantation Facility*, J.T. SCHEUER, B.P. WOOD, W.A. REASS, R.H. OLSHER, M.A. NASTASI, D.J. REJ, Los Alamos National Lab-Plasma source ion implantation (PSII) is a non-line-of-sight method of surface modification in which a target is immersed in a plasma and repetitively biased to high, negative voltage. Previously reported PSII experiments have demonstrated improvements in surface hardness, and wear and corrosion resistances with acceptable surface uniformity on a small scale (in volumes less than 1 m^3). We have designed and are constructing a PSII facility encompassing a 1.5 m diameter, 5 m long, cylindrical vacuum chamber and a pulse modulator capable of dose rates an order of magnitude larger than previous work. This presentation will concentrate on the experimental facility and its associated diagnostics, the plasma source, the pulse modulator design, the response of the plasma to high pulse rates, and the required x-ray shielding.

*This work performed under the auspices of the US Department of Energy.

DC-11 Fabrication and Characterisation of Schottky Diodes Obtained by Deposition of TiN on Si Substrates

K.F. Al-Assadi, M. Boudiaf and N.M.D. Brown
The Joint Ceramics Research Centre, Dept. of Applied Physical Sciences, University of Ulster, Coleraine BT52 1SA

Titanium nitride (TiN) is being deposited of n- and p- type Si substrates using RF magneton sputtering techniques. The ohmic contact on the p- type boron doped silicon wafer with a carrier concentration of 10^{13} cm^{-3} was tested and a negligible added resistance to the bulk silicon is found. The surface resistivity of TiN coating, measured by the four probe method was $50\mu\Omega.cm^2$. Schottky diodes fabricated by evaporating aluminium dots of 1mm diameter, using TiN as an ohmic contact, show a barrier height of 3.31, 2.82 and 2.78 eV at the measurement temperatures of -83, 20, 70 °C, respectively. Schottky diodes fabricated on n-type silicon, of carrier concentration 2 x 10^{13} cm^{-3}, by depositing TiN dots as Schottky contacts while the ohmic contact was made by evaporating aluminium. The barrier height of these devices was found to increase, i.e. 1.55, 1.58 and 1.60 eV at temperatures of -83, 20 and 70 °C, respectively. These devices show no hysteresis over a wide range of temperatures as measured by a Boonton capacitance meter with a sensing frequency of 1 MHz.

Acknowledgements: The authors wish to thank Dr. C. Stevenson for his collaboration .

DC-12 Volume and Surface Effects upon Oxygen Addition to YBaCuO Thin Film Producing Discharges.

B.F. BURNS and W.G. GRAHAM.
Physics Department, Queen's University, Belfast Northern Ireland.

The addition of oxygen to discharges used to sputter deposit YBaCuO thin films is critical for "in situ" production. Using laser induced fluorescence, plasma induced emission and for electrostatic probe techniques we have demonstrated that in DC driven magnetrons the addition of oxygen to the AR source gas perturbs the discharge. We also infer that there is a considerable effect on the target surface. These changes cause a significant reduction in the deposition rate of the thin films. In this particular system an apparently related phenomena is observed when heating the substrate.

DC-13 Trapped Dust in Rare Gas Plasmas, Biswa Ganguly, Alan Garscadden, and Peter Haaland, Wright Laboratory, Wright Patterson Air Force Base, OH 45433-6563 - Carbon particles are formed in direct current and audio frequency (10-50 kHz) discharges of helium and argon with vertical graphite electrodes. The particles, which are observed in situ by laser light scattering and ex situ by field emission scanning electron microscopy, form more rapidly and in greater quantities with helium than with argon gas fills. The discharge impedance changes as dust concentrations increase, leading to a self-trapping region between the electrodes. Competition between the ambipolar electrostatic and gravitational fields influences the distribution of particles in the plasma.

DC-14 A Self-consistent Study of the Plasma-Particulate Interface in Dusty Glow Discharges. Seung J. Choi and Mark J. Kushner, University of Illinois, Dept. of Elect. & Comp. Engr., Urbana, IL 61801 * - Contamination due to particulates or "dust" (100s nm to 10s μm in size) is a major concern in the plasma processing of microelectronics. The transport of particulates depends on electrostatic and "ion-drag" forces, both of which depend on details of the plasma shielding of the dust. We have developed a microscopic model consisting of a Particle-in-Cell/Monte Carlo simulation for electron and ion transport near a dust particle, and solution of the electric field based on the free charge density in the plasma and surface charge density on the dust. Results provide the shielding characteristics and forces on the dust. In low pressure plasmas ($10^9 < [e] < 10^{11}$ cm^{-3}) the shielding length around the dust is approximately the ion Debye length. The ion density near the dust can increase an order of magnitude compared to the plasma, resulting in ion-ion collisions which, together with charge exchange collisions, drop ions into orbits around the particle. The dust potential is sensitive to the size of the dust, falling by half between 5 μm and 1 μm.

* Work supported by NSF, SRC, IBM E. Fishkill and the U. of Wisconsin ERC.

DC-15 Particulate Transport in ECR Discharges, M.D.KILGORE, J.E.DAUGHERTY, R.K.PORTEOUS, H.M.WU and D.B.GRAVES, U.C. Berkeley - The transport behavior of particulates in ECR discharges is examined. A detailed model of the forces on charged particulates in discharges has been developed. Forces arising from the discharge electric field and ion momentum transfer as well as gravitational, thermophoretic, and convective forces determine the location of particulates in the discharge. This particulate transport model is coupled with a 2-D, hybrid fluid-particle model of the ECR discharge with realistic geometries.

Session EA

8:00 a.m. – 10:00 a.m.
Wednesday, October 28, 1992

Georgian Room

Electronic and Atomic Collision Processes

Chair
K. Becker, City College of New York

EA-1 Electron-Atom Scattering Using Atomic Recoil,* B. BEDERSON, New York University-This talk will review electron-atom scattering experiments using recoil techniques, wherein observation of the collision process is made on the recoil-scattered atom rather than on the electron. Using this technique it is possible to obtain absolute cross sections without normalization or knowledge of the atom density in the interaction region; atomic state selection and analysis is also more readily performed. Comparisons with theory and with other crossed beam experiments, including those using polarized electrons, will be made. Details of ongoing experiments are presented in companion papers at this Conference[1]. A discussion of how laser cooling, and velocity and spatial compression can be employed to improve dramatically spatial and energy resolution and sensitivity will be presented.

*Supported by the National Science Foundation.

1. L. Vuskovic, paper in focus session on electron-atom collisions; C. H. Ying, et al., poster paper, this Conference.

EA-2 Collisional Deexcitation of Excited Rare Gas Atoms by Molecules Containing Group IV Elements, Y.HATANO, Dept. of Chem., Tokyo Inst. of Tech.-Absolute cross sections for the deexcitation of He(2^3S, 2^1S, 2^1P), Ne($^3P_2$, $^3P_1$, $^3P_0$), and Ar($^1P_1$, $^3P_2$, $^3P_1$, $^3P_0$) by CH_4, SiH_4, GeH_4, C_2H_6, Si_2H_6, CF_4, and SiF_4 have been measured using a pulse radiolysis method combined with time-resolved spectroscopy and compared with cross sections for observed product formation as well as with theories of deexcitation processes.[1,2]

1)Y.Hatano, Proc. of 19th ICPIG, Belgrade, 1989, ed., V.J.Zigman, Univ. Belgrade Press (1989), p.242; Y.Hatano, "Pulse Radiolysis", ed., Y.Tabata, CRC Press, Boca Raton (1991); M.Ukai and Y.Hatano, "Gaseous Electronics and Its Applications", ed., R.W.Crompton, M.Hayashi, D.E.Boyd, and T.Makabe, KTK Sci. Publ., Tokyo (1991), p.51, and references cited therein.

2)See, e.g., H.Yoshida, H.Kawamura, M.Ukai, N.Kouchi, and Y.Hatano J. Chem. Phys., 96, 4372(1992).

EA-3 The Production and Extraction of Polarized Electrons from an Optically Pumped Helium Discharge,* R.J. Vandiver, L.D. Schearer, and T.J. Gay, Univ. of MO at Rolla - Polarized electrons are produced from interactions involving nearly 100% polarized helium 2^3S_1 metastable atoms in a weak electrical discharge. The high metastable polarizations are obtained through the use of recently developed, high-power lasers tunable to the relevant helium transitions near 1083 nm and the development of a crossed beam pumping technique. The dominant interactions involving the 2^3S_1 atoms and electrons are spin preserving; hence the electrons of the discharge attain a high polarization. We have extracted a well collimated electron beam with over 20 μA of current from the discharge. An optical polarimeter will be used to determine the polarization of the extracted electrons.

*This work supported in part by NSF-PHY-9201289 and Texas Instruments Inc.

EA-4 Electron Drift in Alkali-metal Vapors.* I.I.FABRIKANT, Univ. of Nebraska-Lincoln— Electron drift velocities in sodium, potassium, rubidium, and cesium vapors are calculated using theoretical momentum-transfer cross sections for electron–atom scattering. The results strongly disagree with experimental data for saturated vapors at low values of E/N (ratio of electric field to the vapor number density). We show, using the case of sodium as an example, that the disagreement could be explained by the presence of alkali dimers in saturated vapors which lead to the processes of electron-impact vibrational excitation and deexcitation, and dissociative attachment. These processes strongly affect the electron energy distribution function and reduce drift velocities. Results of model calculations show that inclusion of inelastic processes involving the dimers lead to a better agreement with the experiment.

*Supported by the National Science Foundation

EA-5 First-Order Distorted-Wave Calculation for the Excitation of Hydrogen using Stark States*, J.L. PEACHER and D.H. MADISON, University of Missouri-Rolla; K. TAULBJERG, University of Aarhus - The first-order distorted-wave approximation has proved to be one of the most successful approaches for the theoretical calculation of electron-atom scattering. In a recent paper Madison, Bartschat, and Peacher [1] presented the first-order distorted-wave formalism for nonspherical potentials. They investigated the effects of quadrupole distortion for electron-impact excitation of the 2p state of hydrogen and found that for practical purposes it could be neglected. To investigate the effect of polarization on the excitation of the 2p state of hydrogen we have considered the first-order distorted-wave approximation using the Stark states to represent the excited atomic states. This leads to a nonspherical dipole distortion in the final-state potential. First-order distorted-wave results will be given for a range of energies from threshold to intermediate energies.

1. D.H. Madison, K. Bartschat, and J.L. Peacher, Phys. Rev. A 44, 304 (1991).

*Work supported by the National Science Foundation.

EA-6 Application of the Complex Kohn Method to the Calculation of Photoionization Cross Sections*, T. N. Rescigno, B. Elza, B. H. Lengsfield III, Lawrence Livermore National Laboratory, A. E. Orel, Department of Applied Science, U.C. Davis The complex Kohn variational method, which has been very successful in treating the scattering of electrons from molecular ions, can also be used to calculate photoionization cross-sections for neutral polyatomic molecules. We will discuss our modification of this method to obtain the new matrix elements needed for photoionization, in particular when an *ab initio* optical potential is used in the scattering calculation. We will illustrate this method on the photoionization of CO.

*Work performed under the auspices of the U.S. Department of Energy at the Lawrence Livermore National Laboratory under contract W-7405-Eng-48.

Session EB

8:00 a.m. – 10:00 a.m.
Wednesday, October 28, 1992

Arlington Room

Radiation, Metastables, and Lasers

Chair
J.T. Dakin, GE Lighting

EB-1 Ionization Balance in the Negative Glow of a Hg-Ar Hot Cathode Discharge, R. C. WAMSLEY, K. MITSUHASHI, J. E. LAWLER, University of Wisconsin--Measurements of the absolute density of excited Ar atoms in the negative glow region of a Hg-Ar glow discharge have led to a quantitative understanding of the ionization balance of the negative glow. We find that Penning ionization of ground state Hg atoms by Ar atoms in the $3p^5 4s$ configuration is the dominant ionization process. The excited Ar is initially produced very near the cathode, (< 2 mm), and then resonance radiation transport produces excited Ar throughout the negative glow. A Monte Carlo simulation is used to model the radiation transport of the excited Ar. A radial Green's function solution of the ambipolar diffusion equation is used to calculate the Hg^+ density using the Hg^+ production distribution obtained from the Monte Carlo simulation. The model is compared to absolute measurements of the excited Ar and ground state Hg^+ densities.

*Work supported by the General Electric Co.

EB-2 A Monte Carlo simulation of resonance radiation transport in a rare-gas–mercury positive column TIMOTHY J. SOMMERER *General Electric Corporate Research and Development, P. O. Box 8, Schenectady, New York 12301*—A Monte Carlo simulation of resonance radiation transport in a fluorescent lamp-like discharge has been developed. The absorption lineshape is presumed to be dominated by natural, Doppler, and Lorentz broadening. Photons transport through an absorbing medium with constant density and gas temperature. Excitation transfer among the various mercury isotopes is considered, as is nonresonant quenching of excited mercury atoms. Predicted exit spectra and relative photon lifetimes (as a function of the ^{196}Hg mole fraction) are in general agreement with Anderson, *et al.*[1] Exit spectra and relative photon escape probabilities are calculated as a function of i) ^{196}Hg mole fraction, ii) variations in the mole fraction of the abundant mercury isotopes, iii) cold spot temperature (mercury atom density), and iv) magnetic field strength (Zeeman splitting).

[1]J. B. Anderson, J. Maya, M. W. Grossman, R. Lagushenko, and J. F. Waymouth, Phys. Rev. A **31** 2968 (1985).

EB-3 Behavior of Excited Atoms in High Density Plasma, K.KADOTA, A.MIYATA, T.FUJIMOTO, T.NI-IMI and Y.HARA, Nagoya Univ. - Processes of production and decay of excited atoms in high density plasmas, have been studied. Rare gas and reactive plasmas of the order of 10^{12}-10^{13} cm^{-3} are produced by exciting helicon wave. Metastable atoms of rare gas and radical are detected by laser-induced fluorescence. Emission spectroscopy is also used for detection of excited atoms. The behavior of metastable atoms in rare gas plasmas is investigated in two phases of plasma and afterglow. In the plasma phase, excitation and de-excitation by electron impact are dominant processes of production and decay, respectively. The decay rate of metastable Ar atoms by electron collision is estimated. On the other hand, recombination is dominant one in afterglow. For metastable F atoms in reactive CF_4 plasma, it has been observed that they have considerably high temperature and short lifetime compared with those for the Ar atoms.

EB-4 Are Metastable Ions in High Density Glow Discharges Significant?, K. P. Giapis[&], R. A. Gottscho, N. Sadeghi[#], J. Margot[*], and T. C. Lee, AT&T Bell Labs, 600 Mountain Ave, Murray Hill, NJ 07974— Critical to implementing new high density plasma sources in plasma etching and deposition, is the ability to control ion flux and energy. However, this may be more difficult than originally anticipated, due to the generation of significant densities of excited, metastable ions, which can bombard wafers with high translational and internal energy. We measure absolute metastable ion densities by self-absorption, and their corresponding velocity distributions and density scaling with pressure and electron density by laser-induced fluorescence. For a low pressure, helicon-wave excited plasma, the metastable ion density is at least 20% of the total ion flux to the wafer. Metastable ion density is found to scale with the reciprocal of the pressure, owing to quenching collisions with neutrals, and the square of the electron density, suggesting two-step electron impact formation. Therefore, metastables are more prevalent in low pressure, high charge density plasmas.

& Current address: California Institute of Technology, Pasadena CA

* University of Montreal, Montreal, Canada

\# Laboratoire de Spectrometrie Physique, Universite Joseph Fourier and CNRS, Grenoble, France

EB-5 Influence of Metastables on the Discharge Structure in Ar, F.TOCHIKUBO*, T.KAMATA and T.MAKABE, Dep't of Electrical Engineering, Keio University, Japan - Spatiotemporal optical emission spectroscopy of ArI($3p_5 \rightarrow 1s_4$), second positive band of N_2(2nd P.B.) and first negative band of N_2^+(1st N.B.) have been performed in the rf glow discharge with the parallel plate electrodes in Ar/N_2(0.1%). Absolute density and the spatial profile of Ar metastables are determined from the absolute emission intensity[1] of 2nd P.B., which results from the energy transfer collision from Ar metastables to N_2 molecules. The measured density is about $4 \times 10^{10}cm^{-3}$ at 1.0 Torr, 13.56 MHz, and 50 V of the voltage amplitude. The spatial density profile of the metastables is mainly subjected to the electron quenching. There exists two kind of discharge structures in Ar at the same applied voltage[2], which is caused by the metastable density. The emission of 1st N.B. has a large intensity with no time-variation, and we suppose that it reflects plasma density.
*Dep't of Electrical Engineering, Tokyo Metropolitan University
[1] F.Tochikubo and T.Makabe, Meas.Sci.Technol. 2, 1133(1991)
[2] F.Tochikubo, T.Makabe *et al.*, J.Phys.D 23, 1184(1990)

EB-6 Parametric Studies of the Neon Recombination Laser at 585 nm using Electron Beam Pumping*, R.L. RHOADES, L. LITTLE and J.T. VERDEYEN, U of Illinois. We have observed lasing on the 585.2 nm transition of neon in various He/Ne/Ar mixtures when the gas mixtures[1,2] were excited in a coaxial diode driven by a Febetron 706 pulse forming line. Parametric studies show that a maximum peak power is obtained with a mix of approximately 10:2:1 at a total system pressure of 2-3 atmospheres. The resulting laser pulse has a duration of about 75 nsec and a peak power of nearly 5 watts. As will be demonstrated by the experiments, the role of helium in such mixtures is to relax the electron energy so as to promote the dissociative recombination leading to the upper state.
[1]N. G. Basov,et al, Sov. Tech. Phys. Lett., 11(4), 181, (1985)
[2]G. A. Hebner and G. N. Hays, Appl. Phys. Lett. 57(21), 2175, (1990)
* Work supported by Sandia National Laboratory.

EB-7 Modeling of the Atomic Ne Laser in He/Ne/Ar Gas Mixtures. Jong W. Shon and Mark J. Kushner, University of Illinois, Department of Electrical and Computer Engineering, Urbana, IL 61801 * - The high pressure atomic Ne laser operates on 4 visible transitions between the 3p and 3s manifolds. There has been renewed interest in this laser due to demonstrated high efficiency lasing at 585 nm in e-beam and fission fragment excited plasmas. A comprehensive computer model for the Ne laser in He/Ne/Ar mixtures has been developed to examine excitation mechanisms. We found that direct excitation of the 3p manifold by dissociative recombination of Ne_2^+ is the likely pumping mechanism, while state-selective Penning reactions dominantly relax the lower levels. Comparisons to experiments performed on a short pulsed e-beam excited laser[1] showed that the electron temperature in the afterglow is determined by a slow relaxation of excited states in Ar. Oscillation does not occur until these manifolds are depleted, and the electron temperature falls. Scaling laws for the Ne laser at low pump powers, as obtained using fission fragment excitation, will be discussed.

* Work supported by Sandia National Labs and NSF.

[1] R. Rhodes and J. T. Verdeyen, unpublished.

EB-8 **The Ar-Xe Laser: Efficiency as a Function of Xe Partial Pressure and Energy Loading**, S.F. Fulghum, T.T. Perkins, R.L. Watterson and J.H. Jacob, *Science Research Laboratory, Inc.*– Ar-Xe laser efficiency measurements as a function of Xe and Ar concentrations at total cell pressures between 1/2 and 2 atmospheres have been performed. From these data one obtains insight into the laser kinetics as a function of Ar, Xe and electron densities. In addition, effects of high specific energy loading on an atomic Xe laser have also been performed by pumping with a 180 μsec long, constant power electron-beam-controlled discharge. A 200 keV, thermionic cathode, electron beam controlled a transverse discharge. Multiple, lumped element transmission lines matched to the discharge impedance were employed to supply up 40 J of discharge energy into the active volume. The effects of high energy loading can be studied by comparing purely electron beam pumped laser performance immediately before and after the discharge.

This work was sponsored by Sandia National Laboratory under Document #56-5433

Session F

10:30 a.m. – 11:30 a.m.
Wednesday, October 28, 1992

Georgian Room

Plenary Lecture

Chair
L.W. Anderson, University of Wisconsin

F-1 Laser Spectroscopy on the Cathode Fall and Negative Glow, J. E. LAWLER, University of Wisconsin. - A research program using laser diagnostics on the cathode region of a clean, cold cathode He glow discharge will be reviewed. These laser diagnostics now enable us to map: the space charge fields, the densities of ions and excited atoms, the current balance at the cathode, the gas temperature, the locations of field reversals, the density and temperature of the cold trapped electrons, and other quantities in the cathode region.[1,2] A comparison of these accurate, absolute spatial maps in clean helium discharges to kinetic theory simulations has yielded a detailed ionization balance and power balance of the cathode region. It has also enabled us to construct more realistic models of the cathode region. Fully self-consistent kinetic models of discharge plasmas have the potential to provide greatly improved predictive capability.[3]

[1]E. A. Den Hartog et. al., Phys. Rev. A 38, 2471 (1988).
[2]J. E. Lawler et. al., Phys. Rev. A 43, 4427 (1991).
[3]T. J. Sommerer et. al., Phys. Rev. A 39, 6356 (1989).

Session HA

1:30 p.m. – 3:00 p.m.
Wednesday, October 28, 1992

Georgian Room

Surface Interactions

Chair
L. Christophorou, Oak Ridge National Laboratory

HA-1 The Physics and Chemistry of Large Carbon Clusters*
R. N. COMPTON and R. L. HETTICH, ORNL— The generation, separation, physics, and chemistry of large carbon clusters (fullerenes) and many of their exohedral (e.g. $C_{60}H_{36}$, $C_{60}F_{48}$) and endohedral (e.g. $Ce@C_{60}$) derivatives will be reviewed. Electronic and ionic properties of these species are studied using resonantly enhanced multiphoton ionization spectroscopy and mass spectroscopy (FTMS). Gas and surface phase reactions will be discussed. The production of $C_{60}^{=}$ via laser desorption from a surface is of particular interest.[1] Exposure of a surface of C_{60} (buckyball) to a hydrogen plasma results in coalescence of a large fraction of these clusters into C_{120}, C_{180}, C_{240}, etc. (buckytubes or geodesic domes?).

*Work supported by the Directors R&D Fund at Oak Ridge National Laboratory, U.S. Department of Energy under contract DE-AC05-84OR21400 with Martin Marietta Energy Systems, Inc.

[1]R. L. Hettich *et al.*, *Phys. Rev. Lett.* **67**, 1242 (1991).

HA-2 **Interaction Dynamics of Hydrogen at a Cu(111) Surface,**
D.J. AUERBACH, C.T. RETTNER, and H.A. MICHELSEN*, IBM Almaden Research Center - **We have used molecular beam and laser detection techniques to study the dynamics of adsorption and desorption of H_2 and D_2 at a Cu(111) surface. We have determined the adsorption probability for beams with kinetic energies up to 0.85 eV, vibrational temperatures up to 2100 K, and incidence angles from 0° to 60°. A detailed analysis provides adsorption probability functions for molecules in individual vibrational states. We have also studied the internal state distribution of molecules scattered from the surface. These measurements provide state-resolved information on both adsorption and vibrational excitation. This work has been complemented by studies of the desorption dynamics. Angular distributions for desorption have been measured for a range of surface temperatures. These distributions are found to be strongly peaked and symmetric about the surface normal. We will also report on progress towards measuring the velocity distributions molecules desorbing in specific quantum states. Results will be discussed in terms of the principle of detailed balance and compared to recent theoretical calculations on the hydrogen/Cu system.**

***Dept. of Chemistry, Stanford University, Stanford CA 94305, USA**

HA-3 Real Time, *In Situ* Monitoring of Surface Reactions During Plasma Processing E. S. AYDIL, Z. H. ZHOU, K. P. GIAPIS, R. A. GOTTSCHO, V. M. DONNELLY, Y. CHABAL, and J. A. GREGUS, AT&T Bell Labs, Murray Hill, NJ 07974 - There is a need for *in situ*, real-time surface diagnostics to probe heterogeneous kinetics during plasma processing from which mechanistic insight into the surface reactions can be gained. To this end, we have used, *in situ* and in real time, photoluminescence (PL) and Attenuated Total Reflection Fourier Transform Infrared Spectroscopy (ATR-FTIR) to monitor hydrogen-atom based (NH_3, H_2) downstream microwave (2.45 GHz) plasma passivation of native oxide contaminated GaAs surfaces. Using PL, ATR-FTIR in conjunction with *ex situ* X-Ray photoelectron spectroscopy (XPS) we show that surface modification occurs on two different time scales. First, H atoms, produced in the plasma, reduce the surface state density by removing As and As_2O_3 during the first ~1-10 seconds of plasma exposure. This fast reaction is followed by formation of gallium oxide which takes place on a longer time scale (10-15 minutes). The PL data indicate that the gallium oxide formation is assisted by H atoms and does not occur in absence of plasma. With insight gained from the surface diagnostics, a possible reaction mechanism is proposed and a simple kinetic model of the process is found to be consistent with the salient features of the measured PL as a function of time. In addition, the *in situ*, real time surface diagnostics enabled us to rapidly optimize the passivation process and to evaluate the effect of plasma operating parameters such as pressure, power, plasma excitation method (RF parallel plate or downstream microwave), flow rate and flow configuration.

HA-4 Spatially and Temporally Resolved Detection of H atoms in RF Plasmas,*A.D TSEREPI, and T.A. MILLER, The Ohio State University- Two-photon absorption laser-induced fluorescence has been used to obtain the spatial distribution of H atoms in the interelectrode space of a parallel plate rf reactor. Continuous and pulsed operation of the discharge allows the monitoring of H atoms, which are produced at the sheath boundary and lost on the confining surfaces, at rates that depend on the conditions of the discharge and the nature of the surfaces. A variety of metallic and semiconducting surfaces have been loaded on the ground electrode resulting in H concentration decay rates in the range 300-1000 s^{-1} (in 3 Torr H_2 plasma), and concentration gradients, characteristic of the surface, ranging from nearly reflecting to significantly absorbing. A simple analytical model that simulates spatial and temporal profiles, provides a way to measure surface loss coefficients γ in the range $0.02\% < \gamma < 20\%$ for H atoms interacting with surfaces. Finally, we demonstrate the sensitivity of the method in probing changes on surfaces *in-situ*, by employing it in a low pressure and high power H_2/Ar discharge, where an increase of the loss coefficient on a Si wafer is attributed to metallic atoms sputtered on its surface.

*Work supported by Air Force Wright Research and Development Center.

Session HB

1:30 p.m. – 3:30 p.m.
Wednesday, October 28, 1992

Arlington Room

Novel Plasma Applications

Chair
R. Piejak, GTE Laboratories Incorporated

HB-1 Uranium Atomic Vapor Laser Isotope Separation (AVLIS)*, R.G. Beeler and G.M. Heestand, Lawrence Livermore National Laboratory - The high cost associated with gaseous diffusion technology has fostered world-wide competition in the uranium enrichment market. Enrichment costs based on AVLIS technology are projected to be a factor of about three to five times lower. Full scale AVLIS equipment has been built and its performance is being demonstrated now at LLNL. An overview of the AVLIS process will be discussed and key process parameters will be identified. Application of AVLIS technologies to non-uranium systems will also be highlighted. Finally, the vaporization process along with some key parameters will be discussed.

*This work was performed under the auspices of the U.S. Department of Energy by Lawrence Livermore National Laboratory under Contract No. W-7405-Eng-48.

HB-2 Plasmolysis of Ammonia.[1] G.P. MILLER AND J.K. BAIRD, Department of Chemistry, University of Alabama in Huntsville, Huntsville, AL 35899. --- We report the results of experiments on the plasma destruction (plasmolysis) of ammonia vapor in a low pressure, inductively coupled, glow discharge operated over a wide range of conditions of pressure, flow rate, and electric power. In analogy with the radiolysis of ammonia, we state our yields in terms of the G-value, which is defined as the number of molecules decomposed per 100 eV of energy absorbed. For our inductively coupled discharge, the range of G-values is 6-32; while for a capacitatively coupled discharge under similar conditions,[2] the range is 6-20; as compared to radiolysis, where it is 2.7-10. Assuming a reaction mechanism, we give a theory that links G for the plasmolysis or radiolysis of ammonia to the quantum yield for its photolysis.[3]

1. Research sponsored by NASA Marshall Space Flight Center, under Contract No. NAS8-37195.
2. J.K. Baird, G.P. Miller and N. Li, J. Appl. Phys. 68, 3661 (1990).
3. J.K. Baird and G.P. Miller, Trends in Chemical Physics, 1, 119 (1991).

HB-3 Plasma Remediation of Gas Streams Contaminated by Trichloroethylene. Dianne Evans and Mark J. Kushner University of Illinois, Dept. Elect. & Comp. Engr., Urbana, IL 61801; Louis A. Rosocha, Graydon K. Anderson, and John J. Coogan, Los Alamos National Laboratory, Los Alamos New Mexico 87545 * - There is increasing interest in using plasmas to cleanse gas streams of toxic gases and for toxic waste remediation. Silent discharges (or dielectric barrier discharges) are attractive in this regard because they operate stably at high power deposition and atmospheric pressure. We have experimentally and computationally investigated the removal of trichloroethylene (C_2HCl_3) or TCE from $Ar/O_2/H_2O$ gas streams using a silent discharge. Experimental results will be discussed where TCE is removed from the gas stream (1000 ppm reduced to < 1 ppm) with moderate energy deposition (10s $mJ-cm^{-3}$). The desired reaction products are CO_2 and HCl. The plasma removal of TCE, however, directly produces undesirable products such as CHOCl and $COCl_2$ (phosgene). These products can also be oxidized and removed from the gas stream by further increasing power deposition beyond that required for removal of TCE. Reaction mechanisms will be discussed with results from a plasma chemistry computer model.

* Work supported by Los Alamos National Lab. and NSF.

HB-4 Optical diagnostics of corona discharges as envisaged for NO_x removal from flue gas. T.H. TEICH, Swiss Federal Institute of Technology, Zürich. Light emission from corona can give information on local gas composition (including some radicals) and reactions in or near the discharge. Knowledge of the early processes is required as initial condition data for the prediction of results of subsequent reactions by conventional chemical kinetics analysis. NO manifests itself by NO_γ emission, N_2O by NO_β, OH (from H_2O and important for onward reactions for NO removal) by OH(A-X). Attempts to confirm the role of $O(^1S)$ as the reactant responsible for formation of NO(B) from N_2O by way of excimer formation [1,2] have so far failed to demonstrate the relevant emission. - The time history of particular emissions from a Trichel pulse discharge was recorded by time correlated single photon counting, thus giving hints to *direct* or *indirect* formation of the excited states and data on their destruction rates. The rapid disappearance of OH emission in moist gas together with substantial reduction of NO_β emissions may indicate the high reaction rate at least of OH(A) with some oxides of nitrogen; in moist N_2O, the emission from $N_2O^+(^2\Sigma\text{-}^2\Pi)$ is not significantly affected by water vapour and may thus continue to be used as a measure of electron density in dependence upon time.

[1]K. Yuasa, 44th Annual Gaseous Electronics Conference, Albuquerque, Paper PB-4 (1991)

[2]L.R. Leclair, J.J. Corr, J.W. McConkey, ibid., Paper HB-6 (1991)

HB-5 Emission of UV to Visible Radiation Produced by Pulsed RF Excitation of Ionizing Radiation Particle Tracks in a Gas,* S.R.HUNTER and W.A.GIBSON, Pellissippi International Inc. - Time dependent excitation and fluorescence studies have been performed on ionizing radiation particle tracks in Ne, Ar and Xe-N_2 gas mixtures over the N_2 concentration range 1-10% (total gas pressure = 200-700 torr), using pulsed RF field excitation (f = 27.125 MHz, duration $\approx$ 1-5 μsec, $E/N_{av} = 10^{-16}$ - 10^{-15} V cm^2). The motivation for this work is the development of a detector to image the ionization tracks in a gas produced by various types ionizing radiation (α, β, neutrons, etc)[1]. The UV to visible radiation (220 - 600 nm) produced in the excitation of the particle tracks was imaged by an intensified CCD digital camera (512 x 512 pixels) with single photon sensitivity. Exposure times were controllable from 5 nsec to 1 millisecond. Spatial resolution measurements of the particle tracks (primarily governed by drift and diffusion of the electrons in the particle track before and during RF field excitation) and relative optical emission efficiencies will be reported as a function of the RF pulse duration and magnitude, and camera exposure time.

*Work supported by the National Cancer Institute, NIH, under grant No. CA45869-03

[1]S.R.Hunter, Nucl. Instr. Meth. A260, 469 (1987).

HB-6 Modeling and Temperature Measurement of a dc Plasma Torch Discharging into Air, A.B. MURPHY, CSIRO Division of Applied Physics, Sydney, Australia — A numerical model of a dc plasma torch[1] has been extended to treat mixing of the plasma gas with a different ambient gas. The model takes into account the electromagnetic, heat flow, and laminar and turbulent fluid flow phenomena, both in the arc and plume regions. The predictions of the model are compared with temperature distributions in the plume of the torch measured by a laser-scattering technique,[2,3] for the case in which the plasma gas is argon and the ambient gas is air. Good agreement is found for a wide range of torch operating conditions. Turbulent effects are shown to cause strong mixing of the air with the plume, which is rapidly cooled through transfer of energy to the dissociation of oxygen and nitrogen molecules.

[1]D.A. Scott, P. Kovitya, and G.N. Haddad, J. Appl. Phys. 66, 5232 (1989).

[2]A.B. Murphy, A.J.D. Farmer, and J. Haidar, Appl. Phys. Lett. 60, 1304 (1992).

[3]A.B. Murphy and A.J.D. Farmer, J. Phys. D 25, 634 (1992).

Session J

3:30 p.m. – 5:30 p.m.
Wednesday, October 28, 1992

Castle

Posters

Glow Discharges
Electron Transport
Ion Transport
Laser Kinetics
Lamps and Switching Arcs
Electron Collisions: Theory
Breakdown

Chair
J.T. Verdeyen, University of Illinois

JA-1 Cathode Fall Development in Low-Pressure Hydrogen Discharges.* B. M. JELENKOVIĆ** and A. V. PHELPS, JILA, U. of Colorado and NIST. - Measurements are reported of the temporal and spatial development of discharges in H_2 that are dominated by the cathode fall. Current, voltage, and optical emission transients and absolute excitation coefficients versus position are measured. Starting with a base current of $\approx$ 20 μA, 1 to 3 μs are required to reach final currents of $\leq$ 50 mA over 50 cm^2. The discharge pulses last $\approx$ 100 μs. The ion space charge causes electric field changes ranging from small to fully developed cathode falls. For pressure x electrode separations of 0.5 to 3 Torr-cm, the cathode fall thickness (0.5 - 1 Torr-cm) varies from greater than to less than the electrode separation of 1 cm at voltages of 350 to 730 V. Spatial scans of Hα and near uv continuum emission are dominated by H atom excitation of H_2 near the cathode and electron excitation of H_2 near the anode or the start of the negative glow. High energy electrons are monitored by adding 2% N_2 to the H_2 and observing N_2^+ emission at 391.4 nm. Steady-state data and models are compared.

* Work supported in part by Air Force Wright Laboratories.
** Present address: Institute of Physics, Belgrade, Yugoslavia.

JA-2 A Model of the Cathode Spot Glow Discharge for a Cathode with Inclusions of Low Work Function Material, L. PEKKER, U. of Minnesota - A model is presented which describes the self-maintained glow discharge for a composite cathode in which cathode spots are formed on low work function material inclusions. Based on this model we obtain expressions for the radius of the spot, the cathode voltage, and the spot current as functions of *pd* (where *p* is the gas pressure and *d* is the thickness of cathode layer), the parameters of the inclusions, and the basic material matrix. Numerical results for the case of a glow discharge in 10 Torr nitrogen gas with a copper cathode matrix and inclusions of LaB_6 (average radius of inclusions equals O.05 mm) are presented.

Conditions under which the glow discharge migrates from the inclusions and begins to spread onto the surface of the basic matrix, are obtained. The transition of the glow discharge into an arc discharge, depending on the structure of the composite material, is also considered.

JA-3 Frequency Dependent Effects in Parallel-Plate Argon rf Discharges, M. J. COLGAN, Y. LI and D. E. MURNICK, Physics Dept., Rutgers University, Newark, NJ 07102–At frequencies higher than 13.6 MHz, capacitively coupled rf systems may be competitive with ECR and magnetron systems for high flux, low damage, anisotropic etching.[1] Scaling laws for various discharge parameters will help determine optimum operating conditions. Data will be presented from rf discharges in argon at frequencies between 2 and 100 MHz. Measurements are made on a *symmetrical* system with 7.6 cm diameter aluminum electrodes separated by 2.0 cm. Preliminary data taken at 1.0 Torr, 5 sccm, constant rf voltage (200 V peak-to-peak) and at frequencies f from 2.5 to 25 MHz show that both rf current and emission intensity at 750.4 nm scale as $f^{1.4}$. Electron-impact excitation rates derived from time and space resolved emission at 750.4 nm will also be presented.

[1]M. Surendra and D. B. Graves, *Appl. Phys. Lett.* **59**, 2091 (1991).

JA-4 **Characterization of Strange Attractor in Electrical Discharges in N_2 at 30 to 800 Pa.** T. AKITSU, E. OGAWA, and H. MATSUZAWA, Dept. of Electrical Engineering and Computer Science, Yamanashi Univ., In electrical discharges in capillary, the 2^n bifurcation and strange attractor were observed in N_2 at 600 Pa. The fractal dimension was estimated with modified Malraison's algorithm, when the discharge current gradually approached to the chaotic region. The fractal dimension was 1.09 for a single periodic state, 1.47 for the 2 periodic state and 1.70 for 2^2 periodic state. The fractal dimension for the multi-periodic state saturated at 1.90. The present result indicated non-integer dimension smaller than the fractal dimensions for the white noise (> 8) and Rayleigh - Bernard convection (2.8 ± 0.1) [Ref. 1]

1 B. Malraison et al., J. Physique - Letters 44 (1983) L-897

JA-5 Suppression of Oscillations in Low Current Hydrogen Discharges.* Z. Lj. PETROVIĆ** and A. V. PHELPS, JILA, U. of Colorado and NIST. - Previous measurements of negative differential resistance Rd of discharges in the Townsend regime were made in a current range limited by the onset of oscillations.[1] Based on predictions of a model of low-current, low-pressure discharges[2] we suppressed the oscillations in hydrogen for pd = 0.5 Torr cm by adding adjecent to one electrode a resistor that is larger in magnitude than Rd. Measurements in the region between 30 μA and 50 mA (50 cm^2 electrodes) show that Rd increases gradually from 3 kΩ to 4 kΩ at 22 mA, where a sharp voltage drop of 10-15 V occurs. Since Rd is proportional to the change in potential due to space charge it is expected that Rd will deviate from a constant at higher currents as the cathode fall begins to develop.

* Work supported in part by Air Force Wright Laboratories.
** Permanent address: Institute of Physics, Belgrade, Yugoslavia.

[1] R.S. Sigmond, Proc. IV ICPIG (North Holland, Amsterdam, 1962) p 234.
[2] A.V.Phelps, Z.Lj. Petrović and B.M. Jelenković (this conference).

JB-1 Electron Drift Velocities in Hydrogen-Argon Gas Mixtures.* by D. L. MOSTELLER, and J. D. CLARK, Physics Department, Wright State University and A. GARSCADDEN, Plasma Research Group, Wright Laboratory. - A pulsed-Townsend technique was used to measure drift velocities in several mixtures ranging from 0.1% to 5% hydrogen in argon which extended the range of previous investigations. The drift velocities were measured in the 0.005 to 15 Td E/N range, and comparisons with the more limited previous measurements have shown good agreement. Monte Carlo simulations have been performed for these gas mixtures using theoretical, crossed beam derived, and swarm derived hydrogen and argon cross sections. A compatible set of cross sections has been determined.

* Supported by Aero Propulsion and Power Directorate through the Southeastern Center for Electrical Engineering Education.

JB-2 Electron Drift Velocities in Boron Trichloride in Argon and Helium Gas Mixtures.* by D. L. MOSTELLER, and J. D. CLARK, Physics Department, Wright State University and A. GARSCADDEN, Plasma Research Group, Wright Laboratory. - Recent studies of Argon-Boron Trichloride gas mixtures stem from its commercial application in boron doping, plasma deposition of boron, and plasma etching of aluminum and other III-IV compounds. Electron drift velocities were determined for several gas mixtures ranging from 10 ppm to 1% BCl_3 in Argon and 0.54% BCl_3 in Helium. It was shown that over a wide range, the electron mobility increased as the E/N (electric field to gas density ratio) decreased. Analysis of the drift velocity in these gas mixtures at the higher concentrations of BCl_3 was complicated by anode current waveform changes and small signals due to the presence of negative ions formed by attachment. Consequently a method of analysis was used which measured the swarm drift times differs from the traditional approach by identifying the time position of greatest electron flux from the derivative of the current signal.

* Supported by Aero Propulsion and Power Directorate through the Southeastern Center for Electrical Engineering Education.

JB-3 Electron Transport in Gases at High Densities,* E. E. Kunhardt, Stevens Institute of Technology.-- A switch technology is emerging that makes use of gases at very high densities ($N \sim 10^{21}$ cm^{-3}) as the switching medium. Switching speeds in the 10's of picosecond have been obtained for biasing Electric fields (E) in the 10^5 V/cm range. In this paper, model for the kinetics of electron in high density gases is presented. It is then used in the Monte Carlo simulation of the behavior of an assembly of electrons in Argon and Zenon subjected to high Electric fields. To implement this simulation, a set of scattering rates for electrons at high densities have been obtained. Electron energy distribution, transport parameters, and ionization rates have been calculated and compared to those obtained at lower densities for the same values of E/N.

*Work supported by the Office of Naval Research

JB-4 Monte Carlo Simulation of Electrons Including e-e Collisions,* M. Chung and E. E. Kunhardt, Polytechnic University.-- Two technics for including e-e collisions in Monte Carlo simulation of electron kinetics in ionized gases are presented and the results compared. The first method is an extension of that presented by Weng and Kushner[1], in which electrons are treated as an energy resolved fluid and a time-varying null-collision method is used to incorporate e-e scattering. In this approach, the vector information of the colliding particles is lost. A second approach is discussed which incorporates the vector information by comparing each incoming particle velocity with that of an average particle in the target grid. The results indicate that neglecting this velocity information leads to an overestimation of the e-e scattering rates, which increases with electron mean energy. This phenomena is investigated further in the context of a streamer discharge.

*Work supported by SDIO/DNA

[1]Y. Weng and M.J. Kushner, Phys. Rev. 42, 6192 (1990).

JB-5 Relating Scattering Crossections to Swarm Data.* E. E. Kunhardt. Stevens Institute of Technology.-- A reduced formulation for the inverse scattering problem of electron kinetics, namely, that of obtaining the electron-atom scattering crossections from swarm data, is presented. An equation for the electron density is obtained using a modal expansion of the electron velocity distribution function in terms of eigenfunctions of an extended collision operator. From an asymptotic analysis of this equation, the conditions that lead to a relationship between the experimental data and the scattering crossetions are obtained. From an analysis of this relationship, the conditions that permit the evaluation of the crossection are discussed.

*Work supported by the Office of Naval Research

JB-6 Comparative Study of Positron and Electron Transport in Neon,* P.J. DRALLOS and J.M WADEHRA, Department of Physics and Astronomy, Wayne State University -- We are investigating the transport of positrons and electrons in neon for a variety of E/N values. The study is accomplished by directly solving the space-independent Boltzmann equation using an exact numerical technique[1]. Our preliminary results (for E/N between 0 and 12 Td) suggest some systematic differences between the positron and electron transport data. For instance, we find electrons to have drift velocities which are approximately 3.5 times smaller than corresponding positron drift velocities. Ratios of other transport parameters show similar but somewhat more complex behavior. We are also making an effort to extend the energy range of our positron cross section sets which have, thus far, limited our comparisons to low E/N values.

*This work is supported by the National Science Foundation under Grant Number PHY91-11870.

1. P.J. Drallos and J.M. Wadehra, Phys Rev. A 40, 1967 (1989).

JB-7 Transport of Electrons in Hydrocarbon Gases at High E/N* A. A Sebastian, P.J. Drallos and J. M. Wadehra, Wayne State University.--- In a recent paper by Nishimura and Tawara[1], the total cross sections for scattering of electrons by several gaseous hydrocarbons were reported to be well described by a constant collision frequency. We have developed an *exact* analytical method describing the time-dependent behavior of electron swarm parameters (utilizing the time dependent, spatially homogeneous Boltzmann equation) for the case where the total elastic cross section is of such a form. Our solution requires *no* expansion of the electron velocity distribution function (EVDF) in Legendre polynomials which has been the traditional approach. Additionally, we present results obtained from our computer algorithm which also makes no approximations to the EVDF. A comparison of some recent experimentally derived swarm parameters of electrons in hydrocarbons by Schmidt and Roncossek[2] is made with both our analytical and numerical results over a wide range of E/N.

*Support of the AFOSR (F49620-92-J-0027) is gratefully acknowledged.

1. Nishimura H. and Tawara H., *J. Phys. B.* **24** (1991) L363-66
2. Schmidt B. and Roncossek M., *Aust. J. Phys.* to be published (1992)

JB-8 RF Electron Swarm Transport in Ar and HCl by Direct Numerical Method of the Boltzmann Equation. K.MAEDA and T.MAKABE, Keio Univ. — Driving frequency is one of key parameters in order to study the excitation efficiency of molecules in an RF range of discharge plasmas. The electron transport in a spatially uniform and temporally varying field is of great importance on the occasion that bulk plasma properties control the process, such as RF excited-CO_2 laser. In this work, RF electron swarm transport is investigated over $1M \leq f(Hz) \leq 1G$, by the direct numerical analysis of the Boltzmann equation in Ar and HCl. The temporal structure of $f(\boldsymbol{v}, t)$ is discussed in terms of cross sectional behaviors of collisions. It is noted that DC component of excitation rate or mean energy has a maximum as a function of f at constant E_R/N. Time variation of the transport is discussed over a wide range of E/N. It is concluded that the optimum frequency in the bulk plasma process subject to a direct electronic excitation is situated in VHF. The number of peaks of the rates for the electron attachment and vibrational excitations, respectively, changes to $1 \rightarrow 2 \rightarrow 1$ with increasing E_R/N at constant frequency in a time modulating mode of the rates. Each peak at both low and high E_R/N appears at different phase of the applied field.

JB-9 Characteristic Energy of Electrons in NO at Moderate E/N,* W.ROZNERSKI and J.MECHLIŃSKA-DREWKO, Dept. Tech. Phys. and Appl. Math., Tech. Univ. Gdańsk, Poland and Z.LJ.PETROVIĆ, Inst. Phys., Belgrade, Yugoslavia - Characteristic energy of electrons in NO over the reduced electric field: 12≤E/N≤280Td at ambient temperature has been determined by means of a numerical procedure described previously[1]. All our results lie lower than those of Bailey and Sommerville[2] as well as Skinker and White[3] and the difference between our data and the results of both latter works increases from about 6 percent at 50Td up to about 40 percent at 12Td. At 280Td the result of our work agrees fairly-well with that of Lakshminarasimha et al[4].

*Work supported in part by Komitet Badań Naukowych - project PB 1777/2/91

[1]W.Roznerski, J.Mechlińska-Drewko and K.Leja, ICPIG XX, 1991, p.432.
[2]V.A.Bailey and J.M.Sommerville, Phil. Mag. 17, 1169 (1934).
[3]M.F.Skinker and J.V.White, Phil. Mag. 46, 630 (1923).
[4]C.S.Lakshminarasimha and J.J.Lucas, J.Phys.D 10, 313 (1977).

JB-10 Nonequilibrium Kinetics of Nitrogen Under Plasma Conditions: an Improvement, C. GORSE, M. CAPITELLI, University of Bari and Centro Studio Chimica Plasmi (CNR) Italy - The nonequilibrium vibrational distribution (N_v), the kinetics of some of the electronic states (N*), the dissociation kinetics and the electron energy distribution function (eedf) in both discharge and post-discharge conditions have been numerically obtained from a self consistent model coupling the vibrational master equations for N_v and N*, the dissociation kinetics and the Boltzmann equation for eedf. Comparing with our earlier work[1] the most significant improvement in the model consists in using a new complete set of V-T (vibration-translation) deactivation rates of vibrationally excited molecules by nitrogen atoms. The results show that created nitrogen atoms are able to deactivate the high lying vibrational levels (v>25) of N_v with strong consequences on the pure vibrational mechanism discussed by our group in the last years. We also present some comparisons with experimental results for eedf and population densities of electronic states.

[1]C. Gorse, M. Cacciatore, M. Capitelli, S. De Benedictis, G. Dilecce, Chem. Phys. 119, 63 (1988).

JC-1 Accurate Analysis of Transport Property of Ions by FTI Method for Isotropic Scattering in CM Frame

E.NISHI E.HOLCOMB and N.IKUTA, Tokushima U.Jpn.--- Using the FTI method[1], transport properties of ions in model gas of equal mass are accurately analysed assuming isotropic scattering in the center of mass (CM) frame. The velocity dispersion functions $S(V_0', V')$ for gas of temperature T_g are used with $H(V', V_0)$ to determine the normalized starting rate distribution $\Psi_s(V_0)$. $\Psi_s(V_0)$ which has a forward velocity moment is determined by relaxative procedures of the four loops L_{00}, L_{01}, L_{10} and L_{11}. Inconsistent assumptions adopted in previous analyses[2], that is, isotropic scattering in both the CM and the Lab frames are removed, and excellent balance in energy and momenta is obtained. Depending on the gas temperature, the thermal region appears in the low E/N range and extends smoothly to the E/N dependent region. Although the transport coefficients generally have larger values than those of previous analysis[2], the ion transport properties obtained in this analysis are basically the the same as the previous results.

1 M.Fukutoku and N.Ikuta, J.Phys.Soc.Jpn.59 2727 (1990).

2 N.Ikuta and E.Nishi,J.Phys.Soc.Jpn. 61 1132 (1992).

JC-2 Mobility curves of gaseous ions with a hump

E.NISHI, and N.IKUTA, Tokushima U.Jpn.-- In the mobility curves for E/N of alkali ions in rare gases, a hump is usually observed at the right side of a flat region. Such mobility curves with a hump have been believed to be caused by the sum of potentials due to an induced polarization and of repulsive, for example, $V(r) = C_1 r^{-6} - C_2 r^{-4}$. In which, the potential well between these two and the atraction potential are said to cause a hump and a region of constant mobility[1]. However, the constant mobility in the low E/N region was found being given by the thermal motion of ambient gas atoms[2]. Therefore, we consider that the hump can be obtained by assuming only repulsive potentials. Test analysis has been carried out assuming the cross sections of the form $q(v_r) = A/v_r^2 + q_0$. The result clearly shows that a hump appears at the right side of the flat thermal region when the gas temperature is low. The mobility in the thermal region rises to the top of the hump with the rise of gas temperature. Further increase of gas temperature makes the flat thermal mobility lower with an expanded E/N range over the hump region. Similar changes are observed in the experimental mobility curves.

1. G.H.Wannier, Bell Sys.Tech.J. 343 (1970).
2. N.Ikuta and E.Nishi,J.Phys.Soc.Jpn. 61 1132 (1992).

JC-3 Constant Mobilities of Gaseous Ions in Low Field
N.IKUTA and E.NISHI, Tokushima U.Jpn.--- Transport properties of ions in model gases are analysed by the flight time integral (FTI) method[1] over a wide range of reduced electric fields (E/N) taking into account the thermal motion of gas. The ohmic region of constant mobility K_0 is observed in the low E/N range regardless of the existence of humps. Ohmic regions have been thought to be due the to induced polarization potential. However, the variation of the ohmic region in length and hight with gas temperatures suggests that the constant mobility might be caused by the thermal motion of gas atoms. The results of FTI analyses have shown large influences of gas temperature on the mobility in vanishingly low E/N; the zero field mobility $K_0(0)$. As the measured values of $K_0(0)$ change with gas temperatures in similar manner, we think that the collision cross sections no longer need to be inversely proportional to the relative speed v_r to give a constant mobility in the low field region at a given gas temperature. In order to obtain accurate data for the collision cross sections, it is hoped that the mobility curves for a wide range of E/N will be measured varying gas temperatures over wider range than those so far reported.

1. N.Ikuta and E.Nishi,J.Phys.Soc.Jpn. 61 1132 (1992).

JC-4 The Influence of Charge Transfer on Plasma Balance. T.E. GIST, W.F. BAILEY, Air Force Institute of Technology, and A. GARSCADDEN, Wright Laboratory, WPAFP, OH -- A multi-ion ambipolar diffusion model is developed and initially employed in the analysis of hydrogen contaminated nitrogen discharge. Electron temperature, species profiles and fluxes are calculated for two ion models of the discharge: an N_2^+ - N_4^+ system and N_2^+ - HN_2^+ system. The results are compared to the experimental data of Schmidt[1]. Charge transfer leads to a sensitive dependence of the electron temperature and ion fluxes on the degree of hydrogen contamination. For 0.1% hydrogen contamination, the electron temperature increases by 15% and the dominant ion, 95%, is HN_2^+. Neglecting recombination, analytic solutions are then obtained for the ion ratios and a plasma balance equation, including charge transfer, results. The combined equations are parameterized in terms of the ratio of ionization frequency to charge transfer frequency and the ratio of the ion diffusion coefficients. The parameterization suggests that discharge conditions may be adjusted by judicious addition of a minority species.

[1]M. Schmidt, Beit. der Plasmaphysik, 11, 147 (1965).

JC-5 Combined Diffusion Coefficients in a Partially-ionized Binary Gas Mixture, A.B. MURPHY, CSIRO Division of Applied Physics, Sydney, Australia — An improved method of describing diffusion in a partially-ionized binary gas mixture is presented. The method applies to mixtures containing species derived from two homonuclear non-reacting gases, for example, argon and nitrogen. It is shown that diffusion can be fully described by three combined diffusion coefficients, quantifying respectively diffusion driven by concentration, pressure, and temperature gradients. The method is an extension of previous treatments based on the Chapman–Enskog method,[1] which require $n^2 - n$ ordinary diffusion coefficients and $n - 1$ thermal diffusion coefficients to describe diffusion in a gas containing n species. The method dramatically simplifies the treatment of many important phenomena, such as vaporization of a particle in a plasma, and demixing in arcs.

[1]J.O. Hirschfelder, C.F. Curtiss, and R.B. Bird, 'Molecular Theory of Gases and Liquids', Wiley, New York, 1964.

JC-6 Direct Experimental Observation of Velocity Component Correlations and Transport Properties of Ba^+ Drifting in Ar, * M. J. BASTIAN, V. M. BIERBAUM and S. R. LEONE, JILA, U. of Colorado and NIST- Velocity distributions of Ba^+ ions drifting in Ar are measured by laser probing of the Doppler profiles. Measurements at 0°, 45° and 90° with respect to the applied electric field are presented as a function of field strength up to E/N values of 200 Td. The results show a positive velocity component correlation between the velocity components parallel and perpendicular to the electric field. A simple model with an assumed form of correlation is presented which qualitatively reproduces the experimental observations. Maxima are observed in both the reduced mobility, $2.38 \pm .04$ cm^2/V s at 160 Td, and in the skewness, $0.95 \pm .01$ at 119 Td, which will facilitate fits to obtain the Ba^+/Ar interaction potential. The parallel and perpendicular translational temperatures agree well with those predicted by a parametrized version of the three temperature theory developed by Waldman and Mason.

*Work supported by the AFOSR with additional equipment provided by the NSF.

JC-7 Ne_2^+ Dissociative Recombination Products in Metastable Ne Effusing from a Ne Gas Discharge
A.Barrios,W.Chism,J.Li,J.W.Sheldon and K.A. Hardy
Florida International University and J.R. Peterson
SRI International

We have observed a superthermal component in a metastable neon beam issuing from a neon discharge which we believe results from Ne_2^+ dissociative recombination (DR) reactions in the discharge. Preliminary data show the velocity of this peak to be $2.8 \pm .5$ km/sec while the velocity of the thermal peak is about 875 m/sec. The velocity of the superthermal peak is in good agreement with the velocity of $2.7 \pm .1$ km/sec predicted for the DR of Ne_2^+ to the 3p states of neon, indicating that the main products are the 3p states in contrast to the (n+1)s states found in Ar and Kr.[1] There is however, also some evidence of direct DR to the $2p^5 3s$ J=2 and J=0 metastable states.

1. A. Barrios, J.W. Sheldon, K.A. Hardy, and J.R. Peterson (To be published.)

JC-8 Mobility of $C_2H_5^+$ in Methane*, J. de URQUIJO, I.ALVAREZ, C.CISNEROS and H.MARTINEZ, Instituto de Fisica, UNAM, México - Using a drift tube-mass spectrometer, the mobility of $C_2H_5^+$ in CH_4 has been measured over a wide range of the reduced-field strength, E/N, from 15 to 480 Td ($1Td = 10^{-17}$ V cm^2). The mobility curve shows a broad maximum between 150 and 240 Td. The zero-field reduced mobility yields a value of 2.33 cm^2 V^{-1} s^{-1}, which is in good agreement with the values obtained by Polley et al[1] and by Ridge and Beauchamp[2], who used different techniques. However, our data disagree with those of Saporoshenko[3] by about 10-20% up to 240 Td.

*Work supported by DGAPA, IN-10-4889

[1]G.W. Polley, A.J. Illies and G.C.Meisels, Anal.Chem. 52 1797 (1980)
[2]D.P.Ridge and J.L.Beauchamp, J.Chem.Phys., 64, 2735 (1976)
[3]M.Saporoshenko, Int.J.Mass Spectrom.Ion Phys., 42, 285 (1982)

JC-9 Kinetic Energy Distributions of Ions from Low Current, Diffuse Discharges in Argon and Nitrogen at High E/N, S. B. RADOVANOV, B. M. JELENKOVIC, S. B. VRHOVAC, *Inst. of Physics, Belgrade*, J. K. OLTHOFF, R. J. VAN BRUNT, *NIST*, — The kinetic-energy distributions of ions impinging on the cathode of parallel-plate Townsend discharges in argon and nitrogen have been measured for electric field-to-gas density ratios (E/N) in the range of 600 to 12000 Td (1 Td $\equiv 10^{-21}$ Vm^2). The measurements were made by sampling ions through a small aperture in the electrode using a quadrupole mass spectrometer equipped with a cylindrical mirror type ion energy selector. Distributions were recorded for the ions Ar^+, Ar^{++}, N^+, and N_2^+. Except for E/N above 10 kTd, the distributions do not deviate significantly from Maxwellian distributions thus allowing one to define an ion temperature. In the case of Ar^+, the measured ion temperature is proportional to $E/N\sigma_{ct}$ (σ_{ct} = charge transfer cross section) as predicted using the Boltzmann transport equation assuming a predominance of resonant charge-transfer collisions. The results are also consistent with retarding potential analysis measurements.

JD-1 Laser Oscillation in Cylindrical Hollow Cathode Magnetron Discharge,* L. LI, K. ROZSA, Z. YU, AND G. J. COLLINS, Colorado State University - Copper ion laser oscillation in a cylindrical hollow cathode magnetron discharge has been demonstrated for the first time. The magnetron discharge creates the ambient metal vapor pressure in the laser medium at room temperature cold cathode operation via cathode sputtering. The cylindrical magnetron discharge employs eight internal axial anode rods to raise the electron temperature in the discharge plasma via enhanced electron collection at the anode. The dependence of IR CuII laser output and oscillation current threshold on operating parameters, such as rare gas pressure and longitudinal magnetic field, will be presented.

*Work supported by National Science Foundation, Grant #ECS-8815051.

JD-2 Scaling Laws for the Atomic Xe Laser in Ne/Ar/Xe and He/Ar/Xe Gas Mixtures. Matthew S. Vogel, Jong W. Shon and Mark J. Kushner, University of Illinois, Department of Electrical and Computer Engineering, Urbana, IL 61801 * - The atomic Xe laser oscillates on 6 transitions (1.73 μm - 3.7 μm) between the 5d and 6p manifolds. Ar/Xe gas mixtures usually produce the highest laser efficiencies at 1.73 μm, however gas heating from energy loading can reduce or terminate laser output due to an increase in the electron density. One is therefore motivated to increase the gas pressure by adding a lighter rare gas (He or Ne). The scaling of the atomic Xe laser using Ne/Ar/Xe and He/Ar/Xe gas mixtures have been investigated using a computer model. Addition of Ne significantly alters the kinetic pathways leading to increased pumping of the 6p manifold by dissociative recombination of Xe_2^+ thereby decreasing laser power. Increasing the heat capacity of the mixture by adding Ne can regain some of this loss at high energy loading. He addition is less disruptive with respect to the ion chemistry, but preferential quenching of the lower laser levels causes osciallation to be dominantly at 2.03 μm.

* Work supported by Los Alamos National Lab, Sandia National Lab and NSF.

JD-3 Laser Parameters of the 1.73 μm Atomic Xenon Transition at Very High He/Ar Buffer Gas Ratios,* G. A. Hebner and G. N. Hays, Sandia National Laboratories, Albuquerque NM, 87185--Fission-fragment excitation can potentially be used to efficiently pump high power gas lasers with long run times. However, high energy loading of the laser gas mixture results in gas heating and degraded laser performance of the atmospheric pressure Ar/Xe laser. Addition of helium, which is efficiently excited by fission-fragments, has been shown to significantly improve the 1.73 μm atomic xenon laser performance. Using a narrow band dielectric laser cavity to suppress the 2.03 μm atomic xenon transition, the 1.73 μm laser power efficiency varied between 2 and 3 percent for a total pressure of 780 Torr, He/Ar ratios of 3/1 to 16/1 and pump rates of 5 to 40 W/cc. For a constant energy loading, the FWHM of the laser pulse with respect to the pump pulse for some gas mixtures increased by a factor of 2.5 when argon is replaced by helium. Probed small signal gain measurements indicate that the gain varies between 0.2 and 0.8 %/cm for the previous experimental conditions. In addition, replacing argon with helium eliminates the strong absorption observed in Ar/Xe gas mixtures under some operating conditions. Possible explanations for the improvement in laser performance will be discussed.

*This work was performed at Sandia National Laboratories and supported by the U.S. Department of Energy under DE-AC04-76DP00789.

JD-4 Neutral Particle Flow Patterns in the DC Positive Column of He-Ne Mixtures, D. W. ERNIE and L. PEKKER, U. of Minnesota - The model previously reported[1] for the axial neutral particle pressure gradients and flow patterns in the DC positive column of a monatomic gas has been extended to the case of binary gas mixtures. Analytical expressions are derived for these neutral particle properties for binary gas discharges in which only a single ion species is predominate. Numerical results for He-Ne mixtures are presented for by-pass discharge tube configurations as a function of discharge current, gas mixture and pressure, and tube radii. These results are compared with previous modeling efforts[1,2] and available experimental data. While quantitatively different than the monatomic case, this model also yields a cathode directed flow for one (or both) neutral species for small discharge current densities. This flow direction is opposite that predicted by other studies[2].

[1]D. Ernie and L. Pekker, 44th GEC, **JB-14**, (1991).

[2]J. H. Ingold and H. J. Oskam, Phys. Fluids **27**, 214 (1984).

JE-1 Discharge Dynamics in an Electrostatic Plasma Injection Switch (EPIS),* E. E. Kunhardt and M. Chung, Polytechnic University.-- A low pressure gas discharge switch has been developed that uses transmission line techniques to generate a voltage distribution on a multi-section electrode to electrostatically inject a triggering plasma into the inter-electrode (anode-cathode) space. Subsequently, a hollow cathode discharge is established between the main electrodes. This switch operates in a similar pressure regime as the Thyratron and the Pseudospark switches. Experiments have been carried out to determine the dynamics of plasma generation, injection, and discharge initiation in the EPIS. Results from this investigation will be presented. These results indicate that plasma transfers faster than predicted by lumped circuit analysis have been observed, indicating that the transfer mechanism may involve displacement currents and collective acceleration.

*Work supported by SDIO/DNA

JE-2 Study of Mercury Transport in Hg-Argon D.C. Discharges, M.W. Grossman, GTE Electrical Products, Danvers, MA Transport of mercury with resulting effects on Hg vapor distribution has important applications in mercury rare gas glow discharges used for light generation. Related work on density gradients in dc discharges has assumed uniform temperature[1] or assumed temperature non-uniformities to be of no importance[2]. However, uniform temperature is far from conditions found in glow discharge light sources with regard to mercury vapor distribution. Three aspects of mercury transport have been considered in this work: mobility, diffusion, and temperature non-uniformity effects. Reference experimental results to be presented are as follows: utilizing typical fluorescent lamp closed cylindrical discharges, but with discrete and controlled temperature zones, mercury transport in the range of mercury doses of 2mg to 10mg with transport times of 50 to 150 minutes through 1.1 meters have been observed. Over a restricted range of temperature, the transport rate is proportional to the mercury density. Time dependence of average light output at the anode or discharge voltage indicates specific states of mercury distribution in the discharge. This time characteristic, permits a straightforward method of measuring transport rates. Use of an auxiliary rf discharge to effect Hg transport relative to the reference type of discharge will also be discussed.

[1] J.H. Ingold and H.J. Oskam, Phys. Fluids 27, 214 (1984)
[2] C. Kenty, J. Appl. Phys., 38, 4517 (1967)

JE-3 A Simple Procedure for Integrating the Elenbaas-Heller Equation.: John F. Waymouth, 16 Bennett Rd. Marblehead MA 01945- A simple stepwise integration routine is described for solving the Elenbaas-Heller Equation for an LTE arc to determine the radial temperature profile. It expresses the differential equation as a difference equation, and stepwise integrates the temperature from the wall inward towards the axis. The independent variables are the wall temperature and the heat conduction loss to the wall. The electric field is a characteristic value of the problem, and is adjusted until the integration of temperature reaches the axis with $dT/dr = 0$. This technique has been implemented using a spread-sheet program on the Macintosh LC computer (4 Meg RAM). I have also extended the methodology to an optically-thick case in which radiation absorption figures strongly in the energy balance. I assume two hemispherical fluxes, one ingoing, the other outgoing, with a radiation transport equation for each. Absorption of radiation from both fluxes appears in the net emission coefficient of the Elenbaas-Heller equation. The Elenbaas-Heller equation and the two radiation-transport equations are integrated stepwise simultaneously from the wall inward. The outward flux at the wall is an additional characteristic value to be determined, to match inbound and outbound fluxes at the axis, but the poorly-converging iterative solutions of the T-profile hitherto employed for this type of problem are unnecessary.

JE-4 On the application of Similarity Formalism to Hg-Kr and Hg-Ne Discharge Lamps. G.ZISSIS, N.BASHLOV*, C.P.A.Toulouse.-- The operating conditions of the Hg-rare gas low pressure discharge lamps depend closely on several external parameters such as tube shape and radius, power supply mode, Hg and rare gas partial pressures as well as rare gas nature. A full simulation of such discharges taking into account collisional and radiative processes necessitates a large number of atomic data and consumes important computer time. Another approach of the problem is based on the fact that some discharges could be considered as similar. In the case of steady-sate dc discharges in binary mixtures it has been shown[1] that "family" characterisation can be carried out using two reduced parameters only. Furthermore, having experimental data for one member of the family it is possible enable us to obtain valuable information for the rest of the family through this formalism. In Hg-rare gas low pressure discharges the validity of this approach, is demonstrated by comparing experimental values of electric field strength obtained in our laboratory in the case of Hg-Kr and Hg-Ne lamps with our calculations. These discharges have been established in narrow rubes (0.08cm<R<0.3cm) with a rare gas pressure of 15 Torr and a discharge current fixed between 18 and 26 mA. The mercury partial pressure was controlled by fixing the cold spot temperature at 40°C. The comparison between data and calculations has shown that differences in electric field are of the order of 12% in the case of Kr and about 8% in the case of Ne. These results confirm the applicability of the similarity formalism in the case of Hg-rare gas low-pressure discharges.

*Laboratory of Plasma Physics, St Petersburg State University, Russia.

[1]V.P. Kalanov, V.M. Milenin, et al Phys. Lett. **A126**, 336-340 (1988).

JE-5 Excited Mercury Density Measurements in a Hg-Kr Inductively Coupled Discharge, D. MICHAEL, GE Lighting. The axial and radial density distributions of the excited Hg ($6\ ^3P_1$) state existing in a 2.5 MHz Hg-Kr Inductively Coupled Discharge (0.5 Torr) is measured using the Near-Resonance Electronic Raman-Scattering (NRERS) method [1]. The discharge is created within a cylindrical glass container with a coaxial inner wall (76mm OD, 23mm ID and 103mm length). RF power is transferred to the discharge via a Ferrite core ($\mu = 14$) centrally located within the inner tube. The pump laser beam is directed axially through the discharge and the NRERS signal detected perpendicular to the pump beam. The density distributions are obtained for various input power levels to the Ferrite (12-20W) at a fixed Hg vapor pressure. By calibrating the Raman signal with a known amount of H_2, one can obtain absolute Hg ($6\ ^3P_1$) densities. These are then compared with measured excited Hg densities in standard Fluorescent lamps. Discussion of the magnitude of the experimental errors involved in the measurement is also presented.

[1]L.Bigio and D.Johnson, "Near-Resonance Electronic Raman-Scattering Measurements of Hg ($6\ ^3P_1$) in a low pressure Hg-Ar discharge", J. of Opt. Soc. Am. B, Vol.8 No.3, 525-530 (1991)

JE-6 Convection in an Inductively-Excited, Electrodeless, High-Pressure Hg Discharge, J.T. Dakin and M.E. Duffy, GE Lighting, Cleveland, OH 44112 – A 2-D axisymmetric model is used in conjunction with experimental observations to investigate the role of convection in an inductively-excited high-pressure Hg discharge. In a typical configuration, a cylindrical quartz arctube is 20 mm high, 30 mm in diameter, and dosed with Hg. An induction coil around the midplane of the arctube is excited at 13.56 MHz. Power in the 200-500 W range is inductively coupled into the annular discharge, which operates at a Hg pressure of approximately 1 atm. The model, which assumes local thermodynamic equilibrium in solving the coupled energy, momentum, electromagnetics, and radiation transport equations for the discharge fluid, is an extension of earlier work on electroded arctubes.[1] In the present electrodeless arctubes, the gravitational buoyancy force is overwhelmed by the $\mathbf{J} \times \mathbf{B}$ force. In the ensuing $\mathbf{J} \times \mathbf{B}$ convection, fluid flows radially inward in the arctube midplane, and radially outward at the ends. The impact of this flow on the energy balance is investigated.

[1]J.T. Dakin et al., J. Appl. Phys. 66, 4074 (1989).

JF-1 **Positron Scattering from C_2H_2 Molecules below Positronium Formation Threshold: Indira Khurana and Ashok Jain, Physics Department, Florida A& M University, Tallahassee, Fl 32307** – Total cross sections for positron–C_2H_2 scattering are reported in the 0.1–E_{Ps} range, where E_{Ps} is the energy of Positronium threshold for the C_2H_2 molecule. We employ the close–coupling method under the fixed–nuclei approximation. The full positron–C_2H_2 interaction is approximated as a sum of static and polarization potentials. The polarization force is included parameter free under the positron correlaion potential (PCOP) model recently proposed by one of the authors [1]. The calculated total cross sections are compared with the measurements [2]. We will also present our numbers on the differential and momentum transfer cross sections in the present energy region. A comparison with the corresponding electron cross sections will also be reported.

[1] Ashok Jain, Phys. Rev. **A41**, 2437 (1990); J. Phys. **B23**, 863 (1990).

[2] O Sueoka and S Mori, J. Phys. **B22**, 963 (1989).

JF-2 Differential Electron-Impact Excitation and Quenching Cross Sections for Ba(...6s6p ^{1}P) and Ba(...6s5d ^{1}D) Atoms*, R.E.H. Clark, J. Abdallah, Jr., G. Csanak, Los Alamos National Laboratory and S. Trajmar, Jet Propulsion Laboratory, California Institute of Technology - Theoretical results based on the uniterized distorted wave approximation (UDWA) will be presented and compared with experimental results[1] for electron collisions corresponding to excitation of nine higher lying levels from the 6s6p ^{1}P level and two higher lying levels from the 6s5d ^{1}D level. Several deexcitation differential cross sections will also be presented. Calculations have been carried out at impact energies ranging from 5 to 100 eV. In general, good order of magnitude agreement is found between theory and experiment at 30 eV and in several cases the agreement is very good both in magnitude and shape of the DCS.

*Work supported by DOE and NSF.

[1]D. F. Register, S. Trajmar, S. W. Jensen and R. T. Poe, Phys. Rev. Lett. 41, 749 (1978).

JF-3 Calculation of Electron Impact Excitation Cross Sections for CO, F_2, and CH_4, C. WINSTEAD, Q. SUN, and V. McKOY, Caltech—We report electron impact excitation cross sections for the valence states of CO and F_2 and for low-lying Rydberg states of CH_4. These cross sections were obtained using the Schwinger multichannel variational method as implemented on distributed-memory parallel computers. Agreement with experimental data, where available, is generally good, although some discrepancies exist. We also present estimates, based on the present calculations, of the total excitation cross sections for CO and F_2 in the low energy range and of dissociation cross sections for CH_4.

JF-4 Angular Scattering in Vibrational Excitation from Low Energy Electron Impact on Polyatomic Molecules, G. GALLUP, Chem. Dept. U. of Nebraska--We derive equations giving the differential cross section for excitation of vibrations by resonant electron impact in polyatomic molecules. We apply the theory to methyl chloride, CH_3Cl, and compare the results with the experiments of Shi and Burrow.[1] Fano-Feshbach theory is used to determine the qausi bound states corresponding to the $^2A_1$ and ^2E resonances and their spherical harmonic expansions. These same states give the forces acting upon the nuclei during the time the resonant state exists. These physical processes operate in the impulse regime, and we show why the harmonic approximation for the oscillations is satisfactory in this case. We discuss the influence of the phases of the scattering amplitude matrix on the angular scattering in vibrational excitation. In particular, we find that the linear Jahn-Teller effect together with mixing appropriate partial waves is predicted to result in scattering more back than forward for doubly degenerate resonance and degenerate vibrational modes for the $\nu = 0$ to $\nu = 1$ excitation.

[1] X. Shi, Ph. D. Thesis, University of Nebraska, 1992

JF-5

Excitation from the Metastable States of Helium by Electron-Impact*, D. C. CARTWRIGHT and G. CSANAK, Los Alamos National Laboratory---Differential and Integral cross sections for excitation from the 2-3-S and 2-1-S states in He have been calculated using both First Order Many Body Theory and the Distorted Wave approximation to evaluate the importance of incident channel distortion. Both sets of cross sections agree very well with the limited experimental data and differ from each other only at low energy and larger scattering angles. As known previously, the integral cross sections are two-to-three orders of magnitude larger than corresponding processes from the ground state. These cross sections obtained by Born and Eikonal-type approximations are orders of magnitude too small at intermediate and large scattering angles because of the neglect of exchange. The new cross sections will be compared to results from R-matrix and related theories.

*Supported by NSF/OIP, the DOE, and Univ. of California/Los Alamos Collaboration (CALCOR)

JF-6 Low-Energy e - N_2^+ Collisions Using the Finite-Element Method. W. M. HUO and J. A. SHEEHY* NASA Ames Research Center – In a previous study,[1] we showed that it requires a highly correlated target wave function to determine the potential energy curves for the e - N_2^+ dissociative recombination process. Here we investigate the use of target wave functions with different levels of correlation in the calculation of e - N_2^+ elastic scattering. A finite-element method, in prolate spheroidal coordinates, is used to solve the close coupling equations.

* NRC/NASA Research Associate.

[1] J. A. Sheehy and W. M. Huo, Bull. Am. Phys. 35, 1147 (1990).

JF-7 Theoretical Determination of Electron-Impact Ionization Cross Sections for Molecular Radicals. H. DEUTSCH, Universität Greifswald, Germany, C. CORNELISSEN, L. CESPIVA and V. BONACIC-KOUTECKY, Freie Universität Berlin, Germany and D. MARGREITER and T.D. MÄRK, Universität Innsbruck, Austria – The recently proposed semi-classical DM approach[1] was used to calculate absolute cross sections for the single electron ionization of molecular radicals including CH_n, SiF_n and CF_n (n=1-3). The necessary atomic properties (such as binding energy, atomic orbital identification, etc.) were obtained from a Mulliken analysis involving ab-initio SCF calculations employing the standard split-valence 6-31G* AO basis set. The present results confirm (1) a previously noted anomaly in the ordering of the SiF_n cross sections, i.e. $\sigma(SiF) > \sigma(SiF_2) > \sigma(SiF_3)$ and (2) the failure of the simple additivity rule.

[1] H. Deutsch and T.D. Märk, Int. J. Mass. Spectr. Ion Proc., 79, R1,(1987)

JF-8 Electron collision Cross sections for H_2

H.WADA, H.ITOH and N.IKUTA*, Chiba Inst.Tech., Tokushima U*Jpn.--- There still remain various problems in the analyses of electron transport property. The discrepancy between the transport coefficients calculated using cross sections derived from the electron swarm data and those theoretically derived is the representative case[1]. The problem is serious due to the fact that the discrepancies exist even for the familiar H_2 molecules. The key point, however, is that the discrepancy appears with frequent inelastic collisions. Precise analyses are being made between 0.01 and 10 Td of reduced field E/N by FTI method in pure H_2 and in H_2-Ne mixtures. Errors of several percent still remain between the calculated and experimental values of drift velocity W and of characteristic energy D_T/μ in H_2 around 0.3 Td where the vibrational excitation is not frequent yet. In the E/N range above 1 Td, another discrepancy increases due to joining of the vibrational excitation. These facts suggest that some deficit in the two term analysis has caused such discrepancies due to large anisotropy in relation with the description of transport coefficients.

[1]M.A.Morrison, R.W.Crompton, Bidhan C.Saha and Z.Lj. Petrović, Aust.J.Phys.40,239(1987).

JF-9 Low Energy Cross Sections for Hydrogen Obtained from Electron Swarm Data Using a Numerical Optimization Algorithm, W.L. MORGAN, Kinema Research, Monument, CO - Low energy momentum transfer, j = 0 -> 2 rotational, and v = 0 -> 1 vibrational cross sections have been determined from measured electron swarm data for parahydrogen. The downhill simplex numerical optimization algorithm[1 2 3] is used to find cross sections that represent the best numerical fit to the measured electron drift velocity and characteristic energy over a large range of E/N. The two-term approximation to Boltzmann's equation is used in the analysis and, beyond demanding that they be smooth functions of energy, no external constraints are applied to the cross sections. The resulting cross sections are in excellent agreement with published cross sections[4] derived using traditional swarm analysis techniques. These results further demonstrate the potential of such computational devices for reducing the labor involved in fitting cross sections to transport data.

[1]W.H. Press, et al., Numerical Recipes (Cambridge U. Press, 1986).
[2]W.L. Morgan, Phys. Rev. A 44, 1677 (1991).
[3]W.L. Morgan, submitted to J. Phys. B.
[4]J.P. England, et al., Aust. J. Phys. 41, 573 (1988).

JF-10 Analysis of Transport Coefficients for RF Discharge Fluid Models,* Fongray Young and Chwan-Hwa Wu, Dept. of Electrical Engineering, Auburn University - Correct transport coefficients are critical to the fluid models for rf discharges. An analysis is performed for transport coefficients for fluid models of rf discharges in CF_4. A hysteresis loop in the transport coefficients and the state variable of fluid model[1] space is observed. This analysis is based on the new cross section set provided by Bonham.

*This work is supported by NSF under ECS-9009395.

[1] E.E.Kunhardt, C.Wu, B.Penetrante, Phys. Rev. A 37, 1654 (1988)

JF-11 Recommended Set of Cross Sections For Modeling of RF discharges in Argon: Excited State Kinetics* Z. Lj. PETROVIĆ**, J.JOVANOVIĆ**, S.VRHOVAC** and J.T.BROAD, JILA, U. of Colorado and NIST. - This work is part of an ongoing project to evaluate avalable data needed for theoretical models of RF discharges in the GEC reference RF cell. Here we compare the available cross sections for excitation or ionization from excited states. Energy gain of electrons in superelastic collisions and losses in inelastic collisions, collisional coupling between metastable and resonant levels, excitation of higher levels and ionization from metastable levels were included in calculations of rate coefficients with metastable densities typical for RF discharges. Electron-induced quenching of metastable levels for low mean energies typical of the bulk electrons (1 eV) proceeds through excitation of 4p level[1] and higher levels and by collisional coupling with resonant levels.[2]

** Permanent address: Institute of Physics, Belgrade, Yugoslavia.

[1]J.F.Behnke, H.Deutch and H.Scheibner, Beitr. Plasmaphys. 25, 41 (1985).
[2]E.A.Andreev and A.E.Bodrov, Chem.Phys. Lett. 109, 450 (1984).

JF-12 Electron Driven Chemistry for the CF_4 Chemical System as a Function of Electron Temperature,* R. E. P. HARVEY Engineering Research Center for Plasma-Aided Manufacturing, U. of Wisconsin--Madison -- Electron cross sections have been compiled and convoluted with Maxwellian distributions over temperatures from 0.5 to 50 eV to produce reaction rates for electrons with neutrals. Reaction rates are in the form cm^3/s. Electron processes include ionization, attachment, dissociation and excitation for the CF_4 system. Some charge exchange processes have also been calculated for ion temperatures from 0.1 to 50 eV. The neutral gas temperature is assumed to be 300 K. The electron collision rates are in a form which can be easily implemented when the electron temperature and density are known, but when the full electron distribution function is not.

* Work supported by NSF grant # ECD-8721545

JF-13 Mechanisms, Cross Sections and Rates for Dissociative Recombination,* STEVEN L. GUBERMAN, Institute for Scientific Research- We have studied the dissociative recombination (DR) of OH^+, N_2^+, and HeH^+ using a theoretical approach. Large scale wave functions have been used to identify the dissociative routes. Electron capture widths have been determined from high principal quantum number Rydberg states and rates and cross sections have been calculated from multichannel quantum defect theory. For each molecular ion, DR from the lowest vibrational level is dominated by a single dissociative electronic state symmetry. For N_2^+, we show that electron-ion continuum-continuum mixing is important for the DR cross sections and rates of vibrationally excited ion levels. Also for N_2^+, we find that Rydberg levels with low n and high v play an important role in determining the resonance structure in the cross section.

* Research supported by NASA and NSF.

JF-14 **Collisional excitation of $O(^1D)$ via the $O_2(^1\Pi_g)$ state** *. Y.SUN, A.DALGARNO, **Harvard-Smithsonian Center for Astrophysics**—We studied the collisional process $O(^3P) + O(^3P) \rightarrow O_2(^1\Pi_g) \rightarrow O(^1D) + O(^1D)$ by numerically solving the two-channel coupled Shrödinger equations. Our calculated cross sections suggest that the collision process is an important source of the 6300$\AA$ red line emission in the day and night glow.

*This work is supported by the National Science Foundation

JF-15 Dissociative Recombination of Electrons with $ArXe^+$ A. P. HICKMAN, D. L. HUESTIS, and R. P. SAXON, SRI International--We have recently reported calculations for low-lying excited state potential curves of XeAr [J. Chem. Phys. **96**, 2099 (1992)], and we have used these potential curves for coupled channel scattering calculations of inelastic scattering of Xe. A typical process is $Xe^* + Ar \rightarrow Xe^{**} + Ar$. Dissociative recombination (DR) corresponds to different arrangements of the same particles. DR may be written $ArXe^+ + e \rightarrow Xe^* + Ar$. Because the same Hamiltonian describes inelastic scattering and DR, much of our earlier work can be extended to provide the potential curves and coupling matrix elements necessary to treat DR. Part of the task is to determine the energies of very highly excited states of Xe^*Ar; this can be done by using Multichannel Quantum Defect Theory (MQDT) to extrapolate our earlier results. Preliminary results will be reported.

*Work supported by Sandia National Laboratories.

JF-16 Monte Carlo Calculation of Illustrative Electron Trajectory Patterns in a Hollow Cathode Cylindrical Magnetron Discharge, *B.Shi, Z.Yu, L.Li and G.J.Collins, Colorado State University - Monte Carlo calculations in an obstructed hollow cathode discharge provide fundamental electron trajectory patterns at various discharge conditions. Eight coaxial anode rods are placed inside the cathode cylinder forming an obstructed cathode glow. We can calculate the critical longitudinal magnetic field for the experimentally observed transition from a high impedance operation mode to a low impedance discharge mode. We calculated the ionization rate in both hydrogen and helium under varying, applied voltage, and magnetic field. It was found that the experimental discharge sustaining voltage versus magnetic field (V-B) plot and the theoretical V-B both display a critical magnetic field at about 700 Gauss where a transition from a high impedance discharge to a low impedance discharge occurs.

*Work supported by NSF Grants #INT-8913426, #INT-90079031, and #DDM-9108531.

JF-17 Effective Radiative Recombination Coefficients of Atomic Oxygen, V. ESCALANTE and G.A. VICTOR, UNAM, Mexico and ITAMP, Harvard-Smithsonian CFA- Effective radiative recombination coefficients are calculated for atomic oxygen using an atomic model potential to obtain accurate non-hydrogenic transition probabilities of singly-excited states. Results are presented for many lines for temperatures up to 3000°K. Simple analytic fits are given which are accurate for most lines.

JF-18 Rates for electron collisional excitation of OII.

BRENDAN M. MCLAUGHLIN* AND KENNETH L BELL† *ITAMP, *Harvard-Smithsonian CfA, 60 Garden Street, Cambridge, MA 02138* †*The Queens University of Belfast, Belfast BT7 1NN, N. Ireland* —

One of the most important classes of atomic data needed for the analyses of Far Ultra Violet (FUV) and Extreme Ultra Violet (EUV) spectra is electron collisional excitation cross sections. Eleven state O^+ target configuration interaction wavefunctions are used with the R-matrix method to calculate electron collisional excitation strengths Ω, in $LS\pi$ coupling, from which we obtain effective collision strengths and rate coefficients for temperatures in the range $5\times10^3 \rightarrow 10^6$ K. The singly ionized atomic oxygen is excited from the $1s^22s^22p^3$ ($^4S^o$) ground state configuration, primarily to the $1s^22s^22p^3$ ($^2D^o$, $^2P^o$) and to the higher lying $1s^22s2p^4$ ($^4P^e$, $^2D^e$, $^2P^e$, $^2S^e$) and $1s^22s^22p^23s$ ($^4P^e$, $^2D^e$, $^2P^e$, $^2S^e$) states. Fine structure calculations are also being performed to obtain cross sections and transition rates. Further details will be presented at the meeting.

*ITAMP is supported by a grant from the National Science Foundation

JF-19 Collisional Rates and Cooling within Atomic Hydrogen Plasmas.

T.T.Scholz, ITAMP, Harvard–Smithsonian Center for Astrophysics –

Accurate collision rates for electron impact excitation and ionization of atomic hydrogen have been evaluated[1]. The $n = 2$ excitation rates were based upon cross sections obtained from an extensive series of calculations using the intermediate energy R–matrix theory[2]. The peak at a plasma temperature of 10^6K was found to lie about 20% either above or below the results from previous calculations. Ionization rate coefficients were derived from the experimental cross sections of Shah et al.[3]. Nearly all reported theoretical results lie above this experimentally based rate over most of the temperature range considered. Both the excitation and ionization rate coefficients have been calculated for plasma temperatures ranging from 2×10^3 K to 1×10^8 K and fitted to easy to use analytic formula.

[1] T.T.Scholz and H.R.J.Walters, Astrophys.Jour. 380, 302 (1991).

[2] M.P.Scott, T.T.Scholz, H.R.J.Walters and P.G.Burke, J.Phys.B: At.Mol.Opt.Phys 22, 3055 (1989).

[3] M.B.Shah, B.Elliott and H.B.Gilbody, J.Phys.B 20, 3501 (1987)

JF-20

Angle-differential and momentum-transfer cross sections for low-energy electron-Cs scattering U. THUMM* and D. W. NORCROSS JILA, Univ.of Colorado and National Institute of Standards and Technology, Boulder, CO 80309-0440 — Based on a previous Dirac R-matrix calculation [1] we have derived elastic and inelastic angle-differential and elastic momentum-transfer cross sections for slow electrons ($E_{\rm kin} \leq 2.8$ eV) colliding with neutral Cs atoms [2]. Our results for the angle-differential cross sections are in good agreement with scaled experimental data and, depending on the incident electron energy, in qualitative or fair quantitative agreement with previously published theoretical work. The inelastic angle-differential cross sections for $6p_{1/2}$ and $6p_{3/2}$ excitation differ by more than a statistical branching ratio due to relativistic effects. For the momentum-transfer cross sections, we hope to resolve existing discrepancies in the literature and to provide more reliable input for transport calculations [2].

* Present address: Dept. of Physics, Cardwell Hall, Kansas State University, Manhattan, KS 66506-2601.

[1] U. Thumm and D. W. Norcross, Phys. Rev. A **45**, 6349 (1992).
[2] U. Thumm and D. W. Norcross, Phys. Rev. A, to be published.

JG-1 Observation of the breakdown in a planar hollow cathode discharge, M.P. ALBERTA and J. DEROUARD, Laboratoire de Spectrométrie Physique, Université J. Fourier Grenoble I, FRANCE--We have performed space and time resolved plasma induced optical emission and electric field measurements to study the initiation phase of the breakdown in a hollow cathode. The discharge was operated in a pulsed, repetitive mode (at about 1 Khz). A delay is observed between the voltage application and the breakdown, which depends on the pressure and the repetition rate. The discharge then starts abrubtly with a large and short (80 ns) current spike. This corresponds to the formation of the space charge field inside the hollow cathode volume. At the same time we observe an intense flash of plasma induced optical emission on the axis of the device, which demonstrates that a concentrated beam of energetic electrons is formed.

JG-2 Low Density Breakdown Characteristics in the Presence of Magnetic Field. * S. POPOVIC and E. KUNNHARDT, Stevens Inst. of Technology, Hoboken, N. J. - We measured the density dependence of the electrical breakdown characteristics of cylindrical and spherical cathodes in the presence of axial magnetic field at low pressure. There is a simple relationship between density, magnetic field and electrical breakdown voltage. This empirical relation is valid for the relatively wide range of densities and discharge regimes, from noncollisional to the intermediate, "Bohm" regime. Its validity was tested for densities between 10^{16} m^{-3} and 10^{20} m^{-3}, and for the magnetic field strengths between 0.2 and 5 Ga. The formula describes accurately the sensitivity of electrical breakdown voltage to the changes of geomagnetic field. It reflects the ballistic properties of charge particle motion in the superimposed electric and magnetic fields, rather than kinetic properties of the rarefied ionized gas medium.

* Work supported by SDIO/ DNA

JG-3 The Morphology of Streamer Coronas,* P. A. Vitello, B. M. Penetrante, and J. N. Bardsley, LLNL – Streamer coronas are of interest due to their application to pollution control devices. A streamer coronal discharge produces energetic electrons which, through dissociation and ionization processes, generate active radicals that in turn react with toxic molecules. The morphology of streamer coronas determines the energy distribution of the electrons produced. Streamers propagate due to a highly non-linear space charge driven ionization wave. Because of the complexity of the equations describing streamer dynamics, most of the numerical simulations have been restricted to one (longitudinal) spatial dimension. Some low resolution 2-D simulations have been previously performed, but so far have been restricted to plane-parallel electrode configurations. We have developed multi-dimensional streamer models that can be applied to arbitrarily shaped electrode structures. Our models have generated the first multi-dimensional fully resolved streamers which form self-consistent radial structure. We have applied these codes to study some of the issues related to finding the optimum working conditions for streamer corona reactors. Our results show that the radial components of the electron flow and the space charge field are very important in providing an accurate picture of the streamer morphology, especially near the highly stressed electrode.

*This work was performed at LLNL under the auspices of the U. S. DOE under Contract Number W-7405- ENG-48.

Session KA

8:00 a.m. – 10:00 a.m.
Thursday, October 29, 1992

Georgian Room

Collisions of Laser Cooled Atoms

Chair
P.L. Gould, University of Connecticut

KA-1 Optical manipulation of Ultracold Atomic Collisions, P. S. JULIENNE, NIST- Excited state collisions of laser cooled atoms exhibit novel effects due to the long time and distance scales associated with collisions of the very slowly moving atoms. These collisions are controlled by a quasimolecular excitation/survival process by which reaction during a close collision of two atoms is only possible if the atoms are excited when they are within an optical wavelength of each other and then come together on an excited state potential without undergoing spontaneous decay. Such collisions are subject to optical manipulation by varying laser detuning and power. We have developed optical Bloch equation methods for treating ultracold collisions in a light field with spontaneous decay, and have applied these to fine structure changing collisions[1] and to associative and Penning ionization collisions.[2] Examples will be given to illustrate the unique features of ultracold collision physics.

[1]Y. Band and P. Julienne, Phys. Rev. A 46, July, 1992.

[2]C. Williams, P. Julienne, and Y. Band, unpublished, 1992.

KA-2 "Bright Beams" of Ne* Metastable Atoms, H.C.W. BEIJERINCK, H.J.L. MEGENS, M.P. SCHUWER, M.D. HOOGERLAND and K.A.H. VAN LEEUWEN, Dept. of Physics, Eindhoven University of Technology, The Netherlands– Because laser cooling is a dissipative process, its application to the transverse velocity component of an atomic beam beats Liouville and results in phase space compression with a corresponding increase in brightness. Starting out with a LN_2 cooled discharge source for metastable Ne* atoms, the design consists of three stages: a transverse cooling stage with a 100 mrad half–width capture angle resulting in a 30 mm diameter parallel beam, a magneto–optical lens (f = 600 mm) and a final cooling stage with an output beam diameter and divergence of 1 mm and 0.5 mrad, respectively. The required laser power is 240 mW, with 70% used for the lens. The brightness then is $5\ 10^{18}$ sr^{-1} mm^{-2}, an increase by a factor 10^4 ! Test measurements on the effectively curved wavefront, near–parallel mirror transverse cooling stage have been completed. The modularly built beam–line will be operational in the fall of 1992. Its first application will be in a four–vector correlation experiment on intramultiplet mixing in the Ne**(3p) + He system, where the increase in collision–induced fluorescence from 100 counts s^{-1} to approximately 10^6 counts s^{-1} is of crucial importance.

KA-3 Collisions of Trapped Atoms, Thad Walker*, U. of Wisconsin-Madison – Spontaneous-force optical traps provide samples of atoms cooled to temperatures of 100 μK and below at densities of $> 10^{10}$ cm^{-3}. Collisions between trapped atoms can be observed by measuring the rates at which the atoms are ejected from the trap. Excited-state collisions are of particular interest since the low energies and velocities involved mean that collision times become comparable to spontaneous emission times. Thus the collision dynamics are very different for these cold collisions as compared to collisions at higher temperatures. The novel dynamical features that result from spontaneous emission during collisions are best studied by measuring collision rates as a function of the frequency of the light used to excite the atoms. Our observations[1] of different frequency dependences for ^{85}Rb and ^{87}Rb reveal that hyperfine interactions also strongly affect the dynamics of these collisions. Both modification of the dynamics by spontaneous emission and hyperfine interactions are necessary to understand our data.

[1] D. Hoffmann, P. Feng, R. Williamson, and T. Walker, to be published.

KA-4 Ultracold Collisions by Velocity Selection in an Atomic Beam, *J. Weiner, Y. Wang, and D. Laman, Chem. Dept. U. of Maryland, College Park–We have carried out a series of experiments studying associative ionization (AI) between excited sodium atoms, $Na^*(3p) + Na^*(3p) \rightarrow Na_2^+ + e$, in which a monomode laser selects a narrow velocity class of atoms from an atomic beam. The relative collision energy arising from velocity dispersion within the selected velocity class reaches equivalent temperatures ($T = \hbar/k$) of about 18 mK. We present measurements of the distribution function (cross section vs velocity) over an energy range from 18 mK to 1000 K as a function of optical polarization and intensity. This technique permits detailed state preparation (alignment and orientation) prior to collision in the conventional collision regime and systematic study of the active role played by the optical field in the "ultracold" collision regime, where the time of collision becomes long compared to the characteristic radiative lifetime.

*Work supported in part by the National Science Foundation and the Donors of the Petroleum Research Fund under grant ACS-PRF# 24190-AC5

Session KB

8:00 a.m. – 10:00 a.m.
Thursday, October 29, 1992

Arlington Room

Sheaths and Cathodes

Chair
W. Byszewski, GTE Laboratories Incorporated

KB-1 Ion and atom temperatures in a pulsed vacuum arc, I.S. FALCONER, A.J. STUDER, B.W.JAMES and D.R. McKENZIE, School of Physics, U. of Sydney, Australia - Time-resolved measurements of the ion and atom temperatures in the cathode spot of a pulsed vacuum arc have been made using a combination of a Fizeau interferometer and a gated Optical Multichannel Analyser. These confirm earlier experimental measurements[1] which suggested that both the ions and atoms have a remarkably high temperature. The temperatures do not vary during the 400 μs pulse length to the extent that do the electron temperature and charge state distribution.[2] Attempts to look for a shift in the wavelength of the spectral lines, which would not be inconsistent with the potential hump model[3] of vacuum arcs, will be reported.

1 P.J. Martin *et al.* J. Vac. Sci. Technol. **A5** 22-8 (1987)
2 I. S. Falconer *et al.* Bull. Am. Phys. Soc. **36** 192 (1991)
3 W.D. Davis and H.C. Miller, J.Appl. Phys. **40** 2212 (1969)

KB-2 Measurement of the electric field in the cathode fall region of a hollow-cathode discharge from the intensity of forbidden spectral transitions, I.S. FALCONER, L.Y.MONTUNO and B.W.JAMES, School of Physics, U. of Sydney, Australia - Mixing of energy levels in a multiplet due to Stark perturbation will enhance the intensity of normally-forbidden transitions. Thus the measurement of the ratio of the intensities of forbidden to allowed transitions with common upper levels (or upper levels in the same multiplet) can be used to determine the intense electric field in the cathode region of gas discharges. We report here the application of this technique to the measurement of the electric field in the cathode fall region of a hollow cathode discharge in helium by measurement of the ratio of the intensity of the forbidden 4^1F - 2^1P transition to the allowed 4^1D-2^1P transition. Measurements of the electrical field distribution as a function of pressure and current density will be reported.

KB-3 Kinetics and Dynamics of Non-Equilibrium Cathode Heating, W.L. MORGAN*, Kinema Research, Monument, CO USA, L.C. PITCHFORD and S. BOISSEAU, CNRS, Centre de Physique Atomique, Toulouse France - Issues of cathode temperature and electron emission in pseudo-spark discharges[1] [2] have led us to investigate the atomic processes involved in cathode heating; specifically the heating of Mo or W metal surfaces by the impact of 100-500 eV protons. Because of the mass difference, the ion kinetic energy is transferred primarily to the conduction electrons in the metal, which are heated transiently to very high temperature due to their small heat capacity and diminished thermal conductivity. Thus the electron gas acts as a reservoir of energy which is slowly transferred to the lattice over the $\mathcal{O}$(0.5-1ps) electron-phonon coupling time.[3] [4] This results in higher surface temperatures due to ion impact than one would compute using a model based on direct heating of the lattice by ion impact. We have used 3-dimensional finite difference solutions of the coupled heat equations and atomic scale molecular dynamics methods in studying these processes.

*Visiting Scientist, CNRS Centre de Physique Atomique, 1991-92.

[1]W. Hartmann & M.A. Gundersen,Phys. Rev. Lett. 60,2371 (1988).
[2]W. Hartmann, et al., J. Appl. Phys. 65, 4388 (1989).
[3]J.G. Fujimoto, et al., Phys. Rev. Lett. 53, 1837 (1984).
[4]W.S. Fann, et al., Phys. Rev. Lett. 68, 2834 (1992).

KB-4 Sheath and Presheath in Plasmas of Coaxial and Concentric Geometries*

H.-B. VALENTINI, IPHT e.V., Jena, Germany

Using a two-fluid model and simple geometries, for a low pressure plasma the thickness of sheath and presheath, i.e., of the region from where electrons and ions flow to walls or probes are calculated. Generation of charge carriers, elastic and charge exchange collisions, external electric fields and electric currents are included. The positive column with an internal wall, single and double probes are treated [1,2]. An eigen value problem with a free boundary is solved. Results are given for the number densities , the drift velocities, the electric potential and the characteristics of probes. It is shown that the floating potential can depend on the geometry and the distances to walls. For electrons and ions the dimensions of the regions of particle collection can become very different if external fields act.

* Work supported by Deutsche Forschungsgemeinschaft.

[1]I.M. Cohen, Phys.Fluids 8,2097(1965). [2]H.-B. Valentini, Contrib.Plasma Phys. 31,211(1991)

KB-5 **Monte-Carlo Simulation of Pulsating Dielectric Barrier Discharges-Stochastic Analysis**, R. J. VAN BRUNT, E. W. CERNYAR, *NIST*, and P. VON GLAHN, *Villanova Univ.* — A description is given of a Monte-Carlo simulator of pulsating partial discharges generated in a dielectric barrier gap by applying an alternating voltage. The basic assumptions include: 1) initiation by a surface field emission mechanism, 2) a Gaussian distributed discharge pulse magnitude resulting in a mean local electric field reduction slightly above zero, and 3) negligible rate of dielectric surface charge decay. The phase-correlated sequence of discharge pulses generated by the simulator are subjected to a stochastic analysis and shown to exhibit the same significant effects of phase-to-phase memory propogation that have been observed experimentally for point-dielectric gaps.[1] It is argued that a stochastic analysis involving determinations of a set of unconditional and conditional pulse-amplitude, integrated-charge, and phase-of-occurrence distributions is an essential test of the discharge model.

1. R. J. Van Brunt and E. W. Cernyar, *Appl. Phys. Lett.* **58**, 2628 (1991).

KB-6 Nonequilibrium Ion Transport in a Collisional Sheath. JOHN INGOLD, GE Lighting, Cleveland, OH 44112—The five-moment method[1] is used to predict ion transport in a collisional sheath. Poisson's equation is used to calculate electric field consistent with ion density. The model gives total ion energy at the wall for variable amount of collisional interaction with neutrals. Theoretical results are shown to be in semi-quantitative agreement with published Monte Carlo calculations for the same physical problem.[2]

KB-7 A Unified Theory of Arc-Electrode Systems,* P.ZHU**, J.J.LOWKE & R.MORROW, CSIRO, Div. of Appl. Phys. and **U.of Sydney- A theoretical method of predicting properties of free burning arcs and their electrodes is presented in a unified treatment. By introducing four internal boundaries, the method combines a 1-D model[1] of a non-equilibrium plasma sheath adjacent to both the cathode and anode with a 2-D model[2] for the arc column and the solid electrodes. The internal boundary conditions are self adjusted during the calculation using the equations for energy conservation and electric current continuity. No assumptions are made as to the distribution of current density and temperature at the cathode surface and the properties of the arc and its electrodes are predicted in a unified treatment. Calculated temperatures of the arc column and electrodes are in good agreement with experimental data. The threshold current for anode melting is predicted for a water cooled anode made of copper as a function of its thickness.

*Work supported by GIRD and BHP in Australia

[1]R.Morrow and J.J.Lowke, submitted to J.Phys.D

[2]J.J.Lowke, P.Kovitya and H-P Schmidt, submitted to J.Phys.D

KB-8 Investigation of Arc Spot Development on Cold Cathodes,* J.SCHEIN, R.BAYER and J.MENTEL, AEEO, Ruhr-Universität Bochum, FRG- The column of a high current arc is magnetically blown against a cathode positioned perpendicularly to the arc axis[1]. By a small aperture in front of the cathode surface a small plasma jet is formed directly aiming towards the cathode surface. The arc spot ignition taking place within the contact area is investigated by high speed photography (HSP) and later on by S.E.M. micrographs. The HSPs show a bright sheat covering the cathode surface and a plasma channel which connects the surface with the arc plasma. Craters are formed at the cathode surface within the base of the channel. Their shape depends on the material and the surface properties.

*Supported by DFG, grant SFB 191, A3

[1]K.P.Nachtigall, J.Mentel IEEE Trans. Plasma Sci., Vol. 19, No. 5, pp. 942-953, 1991

Session L

10:15 a.m. – 12:15 p.m.
Thursday, October 29, 1992

Castle

Posters

Modeling
High Density Plasma Sources and Applications
GEC Reference Cell
Electron Collisions: Experiment

Chair
J.W. McConkey, University of Windsor

LA-1 Two Dimensional Calculations of the Free Radical Concentrations in an ECR Processing Plasma,* K. ASHTIANI, J.L. SHOHET, and R.E.P. HARVEY, Engineering Research Center for Plasma-Aided Manufacturing, Univ. of Wisconsin-Madison - A two dimensional plasma-chemistry model for calculation of the steady-state densities of neutral radicals in a CF_4 electron-cyclotron resonance (ECR) plasma has been developed. The model is based on a detailed particle balance equation in which the particle production and loss through electron impact and heavy-particle collisions as well as diffusion and flow of species are taken into account. The chemical reaction rate coefficients are calculated by convolving the electron energy distribution function with the appropriate cross sections. The electron energy distribution is assumed to be Maxwellian. Whenever such cross sections are not available, the best available rates are taken from the literature. The electron densities and temperatures are input to the code. The wall reactions are included by considering the sticking coefficients of different species. The densities of F, CF_3, and CF_2 radicals are plotted vs. pressure and power and are then compared with the experimental measurements. Initial runs show good agreement with the measurements in describing the pressure and power variations of the radical densities. The absolute magnitudes of the radical densities as predicted by the code are within an order of magnitude of the experimental values.

*Work supported by the National Science Foundation under Grant ECD-8721545

LA-2 Modeling of ECR Processes, M. MEYYAPPAN, Scientific Research Associates - Electron cyclotron resonance (ECR) processing has been receiving attention as a technique to deposit dielectrics at low temperatures and etch anisotropic features with low damage. In the present work, a simple model has been developed to predict process figures-of-merit such as deposition/etch rate and film composition. A power balance and number density balance have been used to determine the electron density and electron mean energy in the reactor. These quantities are used in a reactor model based on the assumption of well-mixed contents. The rate constants have been evaluated from known cross-sections and an assumed EEDF. The model has been applied to ECR deposition of silicon nitride, and steady state concentration of various species have been obtained. Deposition rate and film composition have been determined as a function of silane/nitrogen ratio and input microwave power.

LA-3 The RF Resonant Mode in an Elliptical Cavity
H.M.Wu, DAVID B.GRAVES, University of California at Berkeley. Based on self-confined plasma ball lightning theory,[1,2,3] a radio frequency (rf) cavity resonance mode breakdown for elliptical ball lightning is studied. Using the variational method, we have calculated several resonance modes in an elliptic plasma ball. It is shown that for m=0 (symmetric case), the resonant frequency of the TM mode shifts about 90% when the ellipticity of the ball (h=a/b) change from 1 to 10. It is shown that this method can be applied to solving the eigenvalue problem with an arbitrary boundary shape.

[1] H.M.Wu and M.E.Oakes, *Physics of Fluid* B, 3,2113(1991).
[2] H.M.Wu and Y.M.Chen, *Physics of Fluid* B,1,1753(1989).
[3] H.M.Wu etc. *IEEE tran. on Plasma Science*,20,19(1992).

LA-4 Simulation of the cathode fall region of a cylindrical magnetron discharge. I.S. FALCONER, T.A VANDER STRAATEN and B.W. JAMES, School of Physics, U. of Sydney, Australia and I.J. DONNELLY, Australian Nuclear Science and Technology Organisation, Lucas Hts, Australia - Monte Carlo calculations of electron trajectories in the cathode region of a cylindrical magnetron discharge have been used to determine ionisation densities and light emission profiles for an argon gas fill. The ionisation density increases with distance from the cathode, reaches a maximum near the edge of the cathode fall region (width 2 mm for our standard conditions) and then decreases over the next 15 mm. Excitation and light emission profiles have a similar shape near the cathode fall region. The dependence of these results on the width of the cathode fall region, the magnetic field, the cathode fall voltage and the filling gas pressure are calculated and compared with experiment.

LA-5 Modelling an Improved Spiral Loop Antenna for Inductively Coupled Plasma Sources [1]

T. INTRATOR, J. MENARD and N. HERSHKOWITZ
Dep't Nuclear Engin. & Engin. Physics, Univ. of Wisconsin

We have developed and characterized a spiral loop antenna that is useful as an inductively coupled plasma source. It has enhanced plasma confinement due to multi-dipole magnetic cusp fields on the boundary, and is very efficient at low neutral pressures. We have modelled the antenna with a computer code [2] that includes near fields, radiated far fields, image currents in a cylindrical boundary and currents in the antenna feeds, as well as kinetic effects due to finite temperature plasma. Among the interesting results are two dimensional plots of the antenna fields including the sheath regions, the size of the near field region, and non symmetric fields due to antenna feeds embedded in the net uniform field pattern.

[1] supported by NSF Grant ECD-8721545
[2] B. McVey, ANTENA User Guide, Rep't PFC/RR-84-13, Mass. Inst. Tech., Cambridge, Mass. (1984)

LA-6 Simulations of an RF Inductively Coupled Reactor*

R. K. Keinigs and T. A. Oliphant, Los Alamos National Lab., Los Alamos, NM 87545
H. M. Anderson and R. C. Sierocinski, Univ. of New Mexico.

Several types of plasma sources are being considered for implementation in etching reactors. The desired characteristics for these sources include ion flux uniformity and low ion impact energy at the water surface. We are performing particle-in-cell simulations of a simple RFI coupled reactor using the 2-½ code, MERLIN. The exciting coil is approximated by a set of concentric current carrying coils having rectangular cross-sections. The vacuum fields for a specified current are analytically calculated and introduced into the particle push routine in MERLIN. Preliminary results pertaining to the electron and ion energy distribution functions in an argon discharge will be presented. Future work will be described.

*Work supported by U.S. D.O.E.

LA-7 RF Discharge Model Comparisons T.E. NITSCHKE, D.B. GRAVES, Dept. of Chem Engr., University of California, Berkeley - One-dimensional PIC / Monte Carlo simulations have been made to compare directly with results of other modeling groups and experimental results of Godyak, et al.[1]. These simulations were run using two model gases, helium and argon, with elastic, ionizing, and excitational collisions under several operating conditions. Predictions are made for plasma densities, eedf's, average electron energy, voltage characteristics (at a given current density), and total power.

[1] V.A. Godyak, R.B. Piejak, and B.M. Alexandrovich, Plasma Sources Sci. Technol. 1, 36-58 (1992).

LA-8 Semi Analytic, Hybrid Fluid-Particle Model of 1-D Glow Discharges, R. BENDAHAN, I. PERES, J.P. BOEUF, and L.C. PITCHFORD, CNRS, Centre de Physique Atomique, Toulouse, France - We have previously reported analytic forms of the ionization source term[1],which appear in the fluid equations for electron and ion transport, for several simple gases. These analytical forms were determined by fitting the results of numerous Monte Carlo simulations of ionization produced by cathode emitted electrons in electric fields which decrease linearly from the cathode to a position d_c, the cathode sheath length. The introduction of these source terms in a fluid model of glow discharges results in analytical expressions for the sheath length and the position of the field reversal in the negative glow as functions of the applied voltage and the product of the gas pressure and the electrode separation. Assuming a constant ion density in the cathode sheath, the electron and ion densities as functions of distance, and the V-I characteristic can also be derived. Excellent comparison with results from full numerical calculations is found.

1. I. Pérès, et al, 44rd GEC, paper JB-5, Albuquerque, NM 1991.

LA-9 Rf Discharge Modeling: Moment Equations Approach, M. MEYYAPPAN and T.R. GOVINDAN, Scientific Research Associates - Continuum modeling approach has proved to be a valuable technique to examine the physics of rf discharges used in materials processing. It has been shown[1] that retaining the particle inertia term in the momentum equation and solving the time-dependent momentum equation for electrons and ions without any approximation is essential to model low pressure discharges. The discharge physics, as predicted by such a three-moment continuum model is well known. The predictive capability of this approach and how well it compares against self-consistent PIC simulations and experiments depends strongly and exclusively on the EEDF used in the simulation. Continuum models need this information as input. In the present work, EEDF from a zero-dimensional Boltzmann solver[2] and also from published MC results have been used to model 13.56 MHz argon discharges. The results are compared against previous simulation studies. Also, numerical details on stability and convergence are discussed, as these are critical and practical issues.

[1]M. Meyyappan, J. Appl. Phys., 69, 8047 (1991).
[2]W.L. Morgan, Comput. Phys. Commun., 58, 127 (1990).

LA-10 A Bounded Two Dimensional PIC-MCC Code for Simulating Processing Plasmas,[1] V. VAHEDI, C. K. BIRDSALL, M. A. LIEBERMAN, University of California, Berkeley, G. DIPESO, T. D. ROGNLIEN, J. R. HISKES, and R. H. COHEN, Lawrence Livermore National Laboratory- We have developed a bounded two dimensional particle-in-cell simulation code with a Monte Carlo Collision (MCC) handler to study processing discharges. The MCC package models the collisions, between charged and neutral particles, which are needed to obtain a self sustained plasma and the proper electron and ion energy loss mechanisms. The simulations are aimed at determining uniformity of particle fluxes (magnitude and angle) across a typical target. Some early results are obtained from an *x-y* model with electrode area ratio of 6:1; a similar *r-z* model is in progress which can be used to study cylindrical chambers.

---

1. Work performed for USDOE by LLNL under contract W-7405-ENG-48; a portion of the UCB work performed for NSF under grant ECS-8910827.

LA-11 Bounded PIC-MCC Simulation of an Electronegative RF Discharge,[1] V. VAHEDI, M. A. LIEBERMAN, C. K. BIRDSALL, University of California, Berkeley, T. D. ROGNLIEN, J. R. HISKES, and R. H. COHEN, Lawrence Livermore National Laboratory- We have developed a Monte Carlo Collision (MCC) scheme, as an addition to the Particle-in-Cell (PIC) method, to study oxygen RF discharges. The presence of negative ions and their effect on the plasma is being investigated at various pressures and input powers. Simulation results show that for low input powers, the negative ion density can be an order of magnitude higher than the electron density. This high concentration of negative ions affects the ambipolar diffusion conditions which can lead to lower ion loss rates and higher ion densities than in electropositive discharges. In this model, electrons, O_2^+, O^-, and O are evolved as particles. These models can be used to model other processing discharges.

---

1. Work performed for USDOE by LLNL under contract W-7405-ENG-48; a portion of the UCB work performed for NSF under grant ECS-8910827.

LA-12 Single Particle Monte Carlo Models and Nonlinearity as Tools to Undertand the Measured EEDF Shape in RF Discharges, S.LONGO, University of Bari and Centro Studio Chimica Plasmi (CNR) Italy - It is shown that the experimental shape of electron energy distribution function (eedf) in RF discharges in atomic gases can be rationalized by using either very simple single particle Monte Carlo calculations or concepts from nonlinear dynamics and nonlinear stochastic processes. In particular the RF discharge in helium studied by Dilecce et al.[1] is modeled by using a Single Particle Monte Carlo Method and a space- and time-dependent imposed sheath field which approximates the one calculated with a fluid model. Despite of the many approximations involved, this method gives eedf's near the experimental one. Thereafter, the use of different ideas from nonlinear mathematics is analized. For example, it is shown that the concept of nonlinear fluctuation amplification, leading in a natural way to Pareto-Levy asymptotic distributions, also allows for a better undertanding of the measured eedf shapes. The relation of this last point of view with the collisionless chaotic dynamics one, leading to similar results for different conditions is discussed.

[1]G. Dilecce, M. Capitelli, S. De Benedictis, J. Appl. Phys. 69, 121 (1991)

LA-13

PIC Monte Carlo / Fluid Model Comparison for Low Pressure RF Glow Discharges. T.E. NITSCHKE, D.B. GRAVES, Dept. of Chem Engr., University of California, Berkeley, and M. SURENDRA, IBM T. J. Watson Research Center - PIC / Monte Carlo simulations of helium RF glow discharges show that in the low pressure regime (< 250 mtorr) sheath heating becomes the dominant electron heating mechanism. This phenomenon is attributed to the presence of a group of relatively high energy non-maxwellian electrons which travel out of phase with the total current and gain momentum by impact with the oscillating sheath. A fluid model, which represents the electrons as maxwellian with no inertial effects (drift-diffusion), relies on ohmic heating to heat the electrons and therefore breaks down at lower pressures. One way of improving the behavior of fluid models is to include an analytical sheath heating analog in the electron energy balance equation. This results in better agreement between the PIC / Monte Carlo and the fluid model simulations.

LA-14 A Highly Flexible Framework for Modeling of Plasma Processing* , E.R. Keiter, K.M.Kramer, andW.N.G. Hitchon. Engineering Research Center for Plasma-Aided Manufacturing, U. of Wisconsin--Madison. A numerical procedure has been developed which greatly facilitates solution of many of the complex partial differential equations arising in modeling processing plasmas. The construction of a detailed 2D plasma model is illustrated. Finite difference forms of the continuity equations for charged and neutral species and Poisson's equation, including the relevant chemistry, are specified in a relatively simple 'input' file. A kinetic module is being coupled to the fluid equations to provide a 'hybrid' description of the plasma. The input file is 'translated' to code which solves the system using a Newton method. This provides an implicit solution of the fluid equations. Dense and sparse matrix solvers are available. The input can be easily modified to handle different chemistries; an example of a long-mean-free-path formulation of the neutral transport will also be given. Applications to CF_4 deposition will be presented.

* Work supported by NSF grant # ECD-8721545

LA-15 A Hydrodynamic-Monte Carlo Simulation for Neutral Radical Transport in Remote Plasma Reactors, Michael J. Hartig and Mark J. Kushner, University of Illinois, Department of Electrical and Computer Engineering, Urbana, IL 61801 * - In low pressure remote plasma reactors (a few mTorr to 10's mTorr), the mean free path of radicals and excited neutrals can be commensturate with the size of the vessel. In this regard, their transport is essentially in a molecular flow regime. In the intermediate pressure regime, though, there is a net advective flow field with which radicals collide and exchange momentum. To address these conditions, a hybrid hydrodynamic-Monte Carlo model has been developed. An advective flow field is calculated to form the basis of a momentum "bath". Radical transport is then simulated using Monte Carlo techniques. Elastic collisions with the bath exchange momenta with the MC particles; inelastic collisions (chemical reactions) of the particles with the bath and other particles change the identity of the radicals. Results will be discussed for Ar/SiH_4 gas mixtures in a remote plasma CVD reactor demonstrating hot atom and shadowing effects of the flux of radicals onto the substrate.

* Work supported by SRC, NSF, and Sandia National Lab.

LA-16 Numerical simulation of electrical arc including the Continuous Phase Transition (CPHT) model, A.KADDANI, C.DELALONDRE and O.SIMONIN, LNH, Chatou, France, H.MINOO, L.P.G.P, Univ. Paris-Sud, Orsay, France.

The CPHT model is based on the fact that all thermodynamical variables vary continuously from the solid state cathode region to the arc column plasma. The thickness of the transition region is a function of the temperature. This model predicts a region with a high density of metallic vapour near the cathode, coming from the evaporation of the cathode material. This approach for the cathode region with metallic vapour permits to satisfy both the continuity of electrical current and the continuity of temperature in the proximity of the wall. The CPHT one dimensional model was coupled to the two dimensional electrical arc simulation developped in the thermohydraulic numerical code Mélodie (orthogonal finite differences). This model was applied to a transferred electrical arc with a high current intensity (I = 287 A) in argon at atmospheric pressure. The cathode material is tungsten. The results of the CPHT model coupled with the other parts of the simulation show that the pressure and temperature are high in the near cathode region. The electrical and thermal transfer at the electrode are assured by the presence of dense metallic vapour in this region. The results for the arc column are in a good agreement with experiments.

LA-17 Two-Dimensional, Self-Consistent, Three-Moment Simulation of RF Glow Discharges,* Fongray Young and Chwan-Hwa Wu, Dept. of Electrical Engineering, Auburn University - For the first time, a two-dimensional, self-consistent, nonequilibrium fluid model[1,2] is used in simulations of radio frequency (rf) glow discharges to evaluate the quantitative effects of the radial and axial flow dynamics in a cylindrically symmetric geometry. The configuration is referred to the GEC RF reference cell. This model is based on the three moments of the Boltzmann equation and Poisson's equation. Thirty Cray X-MP CPU hours is required for each simulation to reach a low convergence rate, 0.01%. Spatial-temporal plasma density, electric field, velocity, mean energy and ionization rate distributions are presented. Radial-axial flow dynamics of plasma in low-pressure parallel plate rf glow discharges are investigated. As a result, nonuniform density profiles along the radial direction are observed from simulations.

*This work is supported by NSF under ECS-9009395.

[1] E.E.Kunhardt, C.Wu, B.Penetrante, Phys. Rev. A 37, 1654 (1988)
[2] B.E.Cherrington, *Gaseous Electronics and Gas Lasers* (Pergamon Press, New York, 1979)

LA-18 2-D fluid model of radio-frequency discharges, M. DALVIE and M. SURENDRA, IBM T. J. Watson Res. Ctr. — A coupled solution of the time-dependent electron and ion continuity (incorporating the drift-diffusion approximation), Poisson, and electron energy balance equations in a 2-d, bounded domain will be shown. Boundaries of the domain include conducting as well as insulating surfaces. The algorithm is adapted from earlier work on on 1-d fluid solutions. We use a time-dependent 2-d finite element formulation to solve the equations. Since direct integration in time requires too much CPU time to be feasible, the solution is obtained iteratively through: a) a rate solver, wherein the electron continuity and electron energy balance equations are solved in a time-dependent, but fixed, electric field; b) a density solver in which the time-averaged continuity equations are solved with Poisson's Equation, using the time-average of the ionization rate obtained from the rate solver, yielding the time-averaged density profiles; c) a field solver in which the time-dependent continuity equations and Poisson's equations are solved, using the time-dependent ionization rate from the rate solver, to yield the time-dependent electric field and densities. We examine the effects of domain geometry on the discharge structure, e.g., steps on the substrates representing wafer edges. Specifically, we test for the presence of electrostatic particulate traps.

LA-19 A moment analysis of Particle-in-Cell / Monte Carlo simulations of rf parallel-plate discharges, M. SURENDRA and M. DALVIE, IBM Thomas J. Watson Research Center – Self consistent Particle-in-Cell / Monte Carlo simulations of rf parallel-plate discharges are used to explicitly calculate terms in the moment (1^{st} and 2^{nd}) equations derived from the Boltzmann equation. Electron-neutral elastic and ionizing collisions (isotropic), and ion-neutral charge exchange collisions are included in the simulation. Results indicate that the convective term in the electron momentum balance can be neglected under a wide range of conditions for electrons. The range is more restrictive with the ion momentum balance. The primary contributions to electron joule heating come from the friction (ohmic) and pressure terms. The friction term is generally dominant for conditions where *pressure* $\times$ *gap* is greater than approximately 0.2 torr-cm. Common expressions for heat conduction (e.g. *thermal conductivity* $\times$ *temperature gradient*, where *thermal conductivity* $\propto$ *density* $\times$ *temperature* $\div$ *collision frequency*) are found to be only rough approximations of the heat conduction term calculated directly from the simulation.

LA-20 2-D Model of Low Pressure Glow Discharges in Plane-Plane and Rod-Rod Geometries, A. FIALA, L.C. PITCHFORD, J.P. BOEUF, CNRS, Centre de Physique Atomique, Toulouse, France - A self consistent, hybrid fluid-particle model in cylindrical coordinates has been used to study the properties of normal and abnormal glow discharges in argon at steady state for different geometries. Ionization due to the cathode emitted electrons is determined through a Monte Carlo (MC) simulation. Voltage-current characteristics were calculated for pd=1torr cm by varying the resistance of the external circuit. A description of the transition between normal and abnormal regime is thus obtained, and the role of radial electric field for the stabilisation of the normal regime will be discussed. All calculations were performed using a floating potential along the dielectric walls of the discharge tube.

LA-21 **Non-linear Circuit Model of Plasma Loaded RF Electrodes**
John Forster, IBM Technical Products Division, Hopewell Junction, NY 12533. A non-linear circuit model has been used to study the electrical characteristics of RF driven, plasma loaded electrodes. A harmonic balance technique is used to obtain voltage and current waveforms on the electrode. The circuit model was used to observe the effect of varying the driving frequency and plasma density on the driving point impedance of the electrode. As expected, the impedance becomes less capacitive and more resistive as the frequency decreases or the plasma density increases. Also, as the frequency increases, the harmonic content of the voltage at the electrode increases, while that of the current decreases. Harmonic content is strongly affected by the circuitry between the generator and the electrode.

LA-22

Nonlinear Gaseous Electric Discharge - Mathematical Modeling. M. KUMAN, Department of Electrical Engineering, University of Tennessee, Knoxville. TN 37996 --- A nonlinear equation is offered for description of the gaseous dynamic of a specific nonlinear electric discharge field. Nonlinear characteristics, specific for this type of field, can be expected. Sich nonlinear field could be used for separation of components in a gas mixture or enrichment of some of the components.
The model leads to consequences that can be tested experimentally.

LB-1 **Plasma Wave Fields in a Helicon Plasma Source,** A.R.Ellingboe, R.W. Boswell, Space Plasma and Plasma Processing, the Australian National University, Canberra, Australia

Inductive loops are used to measure wave fields in the source and down stream from the source of an inductively coupled plasma. Comparison with wave fields calculated using the ANTENA[1] computer code is made. Good agreement between vacuum measurements and theoretical calculations are found. Asymmetries measured are in agreement with theory when radial antenna leads and the ground plate at the top end of the source are included in the calculation. Plasma measurements of the experimental wave fields are being made and compared with theoretically calculated fields. A flux loop and current detector on the antenna are used to measure net power flux and plasma loading and compared to calculated values[2].

1. McVEY, B., ANTENA User Guide, Rep. PFC/RR-84-13, Massachusetts Institute of Technology, Cambridge (1984).

2. Cekic, M., Nelson, B.A., Ribe, F.L., Phys. Fluids B 4 (2), February 1992.

LB-2 Etching and Deposition in the Helicon Reactor with $SiCl_4$. M.A. JARNYK , R.W. BOSWELL, K.G. ORRMAN-ROSSITER*, and J.S. WILLIAMS, Plasma Research Laboratory, Australian National Univeristy, *Materials and Microelectronics Technology Centre, Royal Melbourne Institute of Technology — Experiments in the helicon reactor have demonstrated that etching in a $SiCl_4$ plasma competes with a deposition process. Adjusting any of the operating parameters — gas flow, source power, bias voltage or target temperature — can determine whether etching or deposition occurs. This process has been characterized for a wide range of operating conditions. Plasma parameters, SEM, RBS, AES and XPS measurements of the deposited films and the etched surfaces will be presented together with etch rates of GaAs and GaAlAs.

LB-3 Theoretically Exploring the Experimentally Observed V-B Transition Between the Conventional Magnetron and Anode Obstructed Hollow Cathode Discharge Modes, *B.Shi, Z.Yu, L.Li and G.J.Collins, Colorado State University - The transition between the magnetron and the anode obstructed hollow cathode discharge modes has been explored using the Monte Carlo method. Illustrative electron trajectories below, at and near the critical magnetic fields are presented. The calculated required sustaining voltage versus applied longitudinal magnetic field (V-B) transition curves are in agreement with the experimentally measured bimodal V-B characteristics. The calculated discharge voltage in the obstructed hollow cathode mode increases with increasing magnetic field up to a critical value. Above this critical value, the voltage required to sustain a discharge is dramatically lower and invariant to further increases in B. The latter behavior is that of the well known magnetron discharge mode.

*Work supported by NSF Grants # INT-8913426, #INT-90079031, and #DDM-9108531.

LB-4

Large Area ECR Plasma Source with a New Type of Microwave Window Utilizing a Multipolar Line Cusp Magnetic Field*, W. GETTY and J. GEDDES**, University of Michigan, Ann Arbor, MI, 48109-2122. — Conventional ECR plasma divergent field sources utilize a dielectric vacuum window between the plasma chamber and the waveguide. The cyclotron resonance surface is usually located in the vacuum close to the surface of the window, leading to bombardment of the window by the densest part of the plasma. In the present work, a metal grill has been developed which consists of 5 metal bars and covers 31% of the area of the window without affecting the transmission of the microwaves through the window. A special mode converter and mode mixture is used to obtain a microwave field pattern at the grill which is minimally reflected. In addition, the metal bars are filled with permanent magnets to form line cusps. Two modes of operation are possible. The first uses a symmetric or asymmetric mirror field with an 875 G resonance surface between the window and the field minimum. The second mode uses the resonant surfaces produced along each line cusp, permitting operation at solenoidal field strengths as low as 30% of the usual value. Results of argon plasma operation in a 20 cm diameter vessel using a 16.5 cm diameter ceramic window and a variety of magnetic field configurations will be presented. The primary advantage of this source is that a large area ECR plasma can be produced without using a large volume 875 G magnetic field.

*Work supported by IBM Corp., E. Fishkill, NY Facility
**DoE MFET Fellow

LB-5 Extended Pressure Range for Planar Inductive RF Processing Discharges through Pulsed Operation,* A. E. WENDT, L. J. MAHONEY and J. L. SHOHET, Engineering Research Center for Plasma-Aided Manufacturing, U. of Wisconsin-Madison — A planar rf (13.56 MHz) inductive plasma source has been constructed for the purpose of depositing barrier coatings. We have found that the operating range of the source can be extended to higher pressures (roughly >100-200 mTorr, depending on the gas) through operation of the rf power supply in a burst mode, and believe that operation in this mode has significant positive implications for properties of deposited films. The rf power is modulated on and off at 100 Hz-10 kHz with variable duty cycle. The range of operating conditions of interest for this study are 50-200 watts of rf power and 100-300 mTorr Ar pressure. Time-resolved Langmuir probe measurements in Ar will be presented, with sufficient time-resolution to show buildup and decay of the discharge over the pulse cycle. Probe measurements of the time evolution of electron density, temperature, energy distribution and spatial distribution are aimed at understanding the physical mechanisms which allow higher pressure operation.

*Work supported by NSF Grant #ECD-8721545

LB-6 A Comparison between Inductively-Coupled Hydrogen and Argon RF Discharges, C.S.CUI, R.K. PORTEOUS, R.W. BOSWELL, Plasma Research Laboratory, Australian National University, Canberra, Australia. Hydrogen and argon rf discharges have been experimentally compared in the WOMBAT aparatus. This is a large rf plasma device with separate source and diffusion regions. Using a planar Langmuir probe and interferometry of electron cyclotron harmonic waves, the electron density, the electron energy distribution function, the floating and plasma potentials are determined as functions of experimental conditions, including pressure and input rf power. The results show that, in general, the hydrogen discharge has lower temperature and density than the argon discharge. The electron energy distribution function in argon is very close to Maxwellian, while that of hydrogen has a pronounced hot tail.

LB-7 ECR Microwave Power Absorption in Plasma Deposition and Etching Devices - R. Veerasingam, C .A Outten, J. C. Barbour, R. B. Campbell and R. T. McGrath, Sandia National Laboratories, Albuquerque, New Mexico - Calculations of absorbed power in an ECR deposition experiment are presented. The calculations use a geometrical optics approximation in which rays are launched into the plasma from poynting flux surfaces generated from vacuum waveguide modes. The numerical results are compared to measured values of the electron density, n_e, for a helium plasma, and, to the theory for non-adiabatic power absorption. The experimental n_e is related to the absorbed power. The upstream plasma density is approximately $10^9 - 10^{10}$ cm^{-3} and the electron temperature outside the ECR region, varies little about 13 eV. The rectangular TE_{10} mode is launched at a frequency of 2.45 GHz from the waveguide. The wave-vectors so calculated are used to launch rays and determine the fractional absorption and the absorption layer. We will attempt to measure the $|E|^2$ variation in the plasma and compare it to the calculated absorption profile.

LB-8 Investigation of Spatial and Temporal Plasma Uniformity in an E.C.R. Plasma Etch Tool,* J.E.STEVENS, Princeton Plasma Physics Laboratory, Y.C.HUANG, and J.L.CECCHI, Dept. of Chemical Engineering, Princeton Univ.- Experiments using various combinations of TE_{11} and TM_{01} waveguide modes show that the coupler waveguide mode has a strong effect on the plasma uniformity in a divergent field ECR plasma only when the microwaves damp near the vacuum window ($B_{win} \lesssim 1.15\ B_{res}$). The combination of TE_{11} and TM_{01} modes produces an incident power profile which is approximately uniform, and the resulting density profile is indeed an average of both modes taken individually. However, uniform plasma density profiles do not result from the input of a uniform microwave power density. More uniform density profiles occur when the magnetic field is raised above $B_{win} \gtrsim 1.15\ B_{res}$, regardless of coupler mode. Simultaneous probe measurements of microwave-power and ion-saturation-current fluctuations show that plasma waves duct in low density regions and modeling suggests that this ducting improves plasma radial uniformity. Density fluctuations are large for parameters near the transition from peaked to flat mode.
*Work supported by SRC/SEMATECH within the New Jersey SEMATECH Center of Excellence for Plasma Etching.

LB-9 Comparison Between Measured and Predicted Spatial Variation of Plasma Parameters in an ECR Reactor. R. A. Stewart, H.-M. Wu, M. A. Lieberman, and D. B. Graves, U.C. Berkeley – Plasma density, electron temperature and plasma potential were obtained from Langmuir probe measurements of an argon discharge in the process chamber of an ECR reactor. The ECR reactor consists of a 40 cm long, 14 cm diameter aluminum source chamber and an 82 cm long, 44 cm diameter aluminum process chamber. Radially varying probe measurements were taken (1 and 5 mTorr pressure, 800 W microwave power) at several axial positions in the process chamber in order to obtain the axial and radial variation of the plasma parameters. Comparisons between the measured plasma parameters and results from two 2D models[1,2] will be presented. The first model represents the electrons as a strongly magnetized, two-dimensional fluid with conservation equations for both mass and energy. The ions are weakly magnetized and are modeled using a 2D3V particle-in-cell technique. The second, and simpler, model treats the process chamber plasma transport as governed by ambipolar diffusion with an anisotropic diffusion tensor perpendicular to and parallel to the spatially varying magnetic field lines.

[1]R. K. Porteous and D. B. Graves, Gaseous Electronics Conference, October 1991.
[2]R. A. Stewart, B. Troyanovsky, and M. A. Lieberman, IEEE Conference on Plasma Science, June 1991.

LB-10 Ion transport in a non diverging magnetically assisted surface-wave produced plasma (SWP) under ECR conditions, J. MARGOT and C. BARBEAU, U. de Montréal- Because of their rather unique flexibility in terms of operating conditions, we have recently proposed to use magnetically assisted surface-wave produced plasmas as a tool to achieve a unified picture of the whole class of magnetically assisted high frequency plasmas.[1,2] In this presentation, we report the first measurements of ion velocity distribution functions (IVDF) obtained in a low-pressure magnetically assisted surface-wave-produced plasma at 2.45 GHz under ECR conditions by means of a laser-induced-fluorescence technique. We determine the relation between the IVDF and the spatial distribution of plasma parameters as electron density and temperature. Finally, we examine the role played by the magnetic field line configuration on the ion transport.

[1] J. Margot and M. Moisan, Chap. 8 in "Microwave Excited Plasmas", Elsevier (1992)
[2] J. Margot and M. Moisan, "Modeling of surface-wave-produced plasmas in static magnetic fields: a tool for the study of magnetically assisted HF plasmas", NATO advanced Research Workshop on Microwave discharges (Portugal, May 1992), Plenum, to appear

LB-11 Electrical Characteristics of Low Pressure Inductive RF Discharges in Argon. V.A. GODYAK, R.B. PIEJAK and B.M. ALEXANDROVICH GTE Laboratories Inc., Waltham MA - The electrical characteristics (rf voltage, current and phase shift) of an induction coil that maintains an inductive low pressure rf discharge have been measured over a wide range of parameters. The discharge vessel is a 6.7 cm long glass cylinder with an ID of 14.3 cm around which a two turn induction coil is wrapped. Measurements were made in argon gas at 13.56 MHz over a power range between 25 and 150 W and at gas pressures that range from 3 mTorr to 3 Torr. Based on a recently developed analysis[1], the discharge current, the effective electric field and the equivalent radius of the current path have been inferred from the measured discharge electrical characteristics. The ratio of discharge power to total power delivered to the induction coil was also determined and was found to increase from 0.7 to 0.9 with rising gas pressure. General trends in the electrical characteristics and the plasma parameters inferred from the analysis will be discussed along with the apparent existence of strong non-collisional rf power transfer in inductive rf discharges at lower gas pressures.

[1]R.B. Piejak, V.A. Godyak, and B.M. Alexandrovich, talk given at this conference.

LB-12 **Self-accelerating Electric Field in Gridless ECR Ion Source,***
T. AKITSU, E. OGAWA, and H. MATSUZAWA, Dept. of Electrical Engineering and Computer Science, Yamanashi Univ., In a gridless ECR ion source, the accelerating field was self generated at an extracting aperture. Stationary double layers with $e\phi / kT_e = 2 - 3$ were generated at the exit of a micro wave cavity, where ϕ is the sheath potential in volts and kT_e is the kinetic energy in eV. The ion energy spectrum showed reasonable correlation with the potential difference of the layers. Although the accelerating mechanism had been explained on the base of the single fluid model in the magnetic field gradient, the present work showed that the double layer at the boundary accelerated ions. The operational characteristics of the ECR ion source were observed with and without a surface magnetic multipole confinement.

* Work realized by the courtesy of the ANELVA LTD. Dry Etching Division.

LB-13 **Modelling Plasma-Neutral Interactions in a High Density ECR Argon Discharge.** R.K. PORTEOUS and R.W. BOSWELL, Plasma Research Laboratory, Australian Nat'l Univ., Canberra, Australia. – Inductively coupled discharges often operate at low pressures (less than 1 Pa) and high plasma densities (~10^{18} m^{-3}), and the fractional ionization becomes appreciable. One clear manifestation of a high degree of ionization is the plasma density saturation, at low pressure, with increasing applied power. However, even at more modest fractional ionization the plasma can affect the neutral dynamics. Ion pumping (depletion of the neutrals through ionization) can dominate the average gas flow since the flux of neutrals from the the walls, due to neutralization of the ion wall current, can exceed the gas flow into the reactor. Other important effects are the momentum exchange between the ion flux and the gas (ion wind) and the heating of neutrals by the ions. Plasma-neutral interactions have been modeled in a 2D simulation of an ECR argon discharge. Results showing rarefaction in the source and pressure effects on the ion anisotropy and incident energy distribution at the substrate will be presented.

LB-14 A Cesium Plasma Ion Source, A J T HOLMES, M INMAN and E SURREY, AEA Technology, Culham Laboratory, Abingdon, Oxfordshire, OX14 3BD, England - Plasma volume sources have been used very successfully to produce positive or negative ion beams for many applications. The development and testing of a 2.5 litre plasma source working in pure cesium vapour is described and this is mounted on a 25keV accelerator to produce a collimated beam of Cs^+. The beam divergence in this system varies with the ratio of $I_{beam}/V^{3/2}_{beam}$, the characteristic geometrical perveance of the accelerator. A measurement of the optimum ratio and the beam divergence is reported as a function of the discharge arc current. The plasma parameters of the source are measured with a planar Langmuir probe and this is compared with the extracted beam current. The behaviour of the plasma is described using a model based on thermal electron ionisation. This type of ionisation is unusual in dc discharges as it is normally carried out by fast electrons from the discharge cathode and this effect can lead to very dense cold plasmas being formed even when the plasma density approaches the vapour density.

LC-1 GEC Reference Cell to Model Comparisons T.E. NITSCHKE, D.B. GRAVES, Dept. of Chem Engr., University of California, Berkeley - A one-dimensional fluid model has been developed to predict voltage-current characteristics in a GEC reference cell. Plasma densities, excitational emission profiles, sheath thickness, and other discharge quantities, are also predicted.

LC-2 Importance of Boundary Conditions for Breakdown in the Helium RF Discharge,* M. E. RILEY, K. E. GREENBERG, and G. A. HEBNER, Sandia National Laboratories - Our Boltzmann equation theory and computational procedures can be used effectively for transient plasma simulations. The simulations indicate that various secondary electron emission processes at the electrode surfaces can greatly influence both the low-density plasma growth rate when an rf discharge is initiated, as well as the steady-state plasma density. We have compared the simulation results with experimental measurements of the threshold for rf breakdown in a "GEC Reference Cell," (the threshold being defined as the voltage required to initiate a discharge at a given pressure). The Boltzmann simulations, which include a full five-level model of the Helium atom, do not predict a self-sustaining discharge at the correct threshold when secondary electron production from ion bombardment is the only process included. Secondary emission at the electrodes from both metastable and electron surface interactions must be included to achieve agreement with the experimental results for helium.

*This work was performed at Sandia National Laboratories and supported by the U.S. Department of Energy under contract No. DE-AC04-76DP00789.

LC-3 A Comparison of Etching Results of the GEC Reference Cell With a Commercial Etcher. J. Pender, M. Buie, M. Beauvais, M. Brake and M. Elta. University of Michigan- Results of etching of silicon wafers in the GEC Reference Cell will be presented. The wafers were etched in a mixture of CF_4 and O_2 (4%) under the following conditions: pressures from 0.2 to 0.3 torr, flows from 20 to 40 sccm and measured peak to peak driving voltages from 150 to 280 V. These etching results were compared to similar etches in a commercial, parallel plate, 30 cm diameter electrode RIE (SEMI Group 1000 TP/CC). Power, plate spacing and gas flow in the RIE were adjusted to obtain similar power densities, bias voltages and reactive species concentrations in the two systems. A one dimensional, particle-in-cell code (PDP1) was also used to simulate plasma conditions. Etching trends have been monitored for changes in power, pressure and gas flow in both etchers. The results show etch rates from 67 to 435 Å/min.

Supported by NSF CTS9009899 and equipment support SRC 90-MC-085

LC-4 Measurement of Ion Kinetic Energy Distributions from an Argon Discharge in the GEC rf Reference Cell, J. A. REES, *Univ. of Liverpool*, J. K. OLTHOFF, R. J. VAN BRUNT, *NIST*, and S. B. RADOVANOV *Institute of Physics, Belgrade* — The translational kinetic energy distributions of ions impinging on the grounded electrode of an asymmetric parallel plate discharge cell (GEC rf Reference Cell) have been measured for 13.56 MHz rf glow discharges in argon. The observed ions were sampled through a small orifice in the electrode and filtered according to both their energy and mass using a combined electrostatic energy analyzer and quadrupole mass spectrometer. The required modifications to the grounded electrode assembly did not significantly affect the electrical characteristics of the discharge. The energy distributions for Ar^+, Ar^{++}, Ar_2^+, and ArH^+ were recorded for gas pressures in the range of 1.3 to 33 Pa (10 to 250 mTorr) over a range of applied voltages from 50 to 200 V. The profiles of these distributions and their dependences on pressure and voltage are similar to those observed when ions are sampled through the sheath formed in front of a grounded orifice positioned at the side of the plasma on the mid-plane between the electrodes.

LC-5 Spatial Distribution of Densities of the Metastable $3p^54s$ State of Argon in a GEC Reference Cell, * EDWARD AUGUSTYNIAK, SERGUEI FILIMONOV and JACEK BORYSOW, Physics Department, Michigan Tech. University - Spatial distribution of $3p^54s$ metastable state of *Ar* has been measured in RF argon plasma in a GEC reference cell by means of high resolution absorption spectroscopy. Single-mode, tunable diode laser has been used to obtain absorption profiles at 801 *nm*. Spatial profiles across the gap between electrodes with 1 *mm* resolution for various pressures (0.15 to 1.0 *Torr*) and plasma powers (1 *W* to 40 *W*) were measured. The densities of $3p^54s$ metastable were obtained from integrated absorption profiles at low RF power and from analysis of the absorption line shape in the far wings for high RF power, when plasma becomes optically thick. Velocity-changing collision (VCC) effects have been observed in saturated absorption spectroscopy at low pressures (from 0.006 to 0.1 *Torr*). The pressure and power dependance of the dip shape may allow to separate electron and ground state argon atoms contribution to the VCC kernel.

* Supported by The State of Michigan Research Excellence Fund

LC-6 Comparison of microwave interferometer and langmuir probe results in the GEC reference reactor.* MIKE HOPKINS† AND LAWRENCE J. OVERZET University of Texas at Dallas, Richardson, TX 75083. — A Langmuir probe and microwave interferometer have been combined to measure the electron density in the GEC reference reactor. It was found that the two techniques track one another in predicting the electron density. In addition, interferometer does not detect significant perturbation of the electron density in rf discharges by the Langmuir probe even when biased significantly above the plasma potential. The presence or absence of a floating probe does not appear to influence the characteristics of the glow, either in terms of the electron density or the voltage and current. This is not the case for a dc discharge in the GEC reactor, where the probe can deplete over 50% of the electron density if biased near or above the plasma potential. Finally, radial scans indicate that the electron density at the chamber wall is nearly a factor of 10 less than that in the discharge center, and that the discharge itself has a smaller electron density in the center than near the electrode edge.

* Work supported in part by the National Science Foundation, Texas Instruments Incorporated, and the Royal Irish Academy.

† Dublin City University, Dublin, Ireland

LC-7 Spatial Argon Optical Emission Distributions in the GEC RF Reference Cell, S. DJUROVIĆ* and J. ROBERTS, NIST - **Spatially resolved spectral emission data are presented for reference-condition Ar discharges in the NIST GEC Reference Cell with a filter box[1] in external electric circuit. The Ar I 750.4 nm and the Ar II 427.8 nm lines were observed. We report here the spatially resolved optical emission between the electrodes defined by the dark space (DS) and the bright space (BS), measured at the half maximum intensity level, and the maximum intensity (MI) position. These parameters show some difference between the Ar I and Ar II line distribution, especially the MI position of Ar II emission. We observe no additional bright space near grounded electrode, as in our previous measurements or as previously reported.[2]**

*Visiting Scientist from The Institute of Physics, Novi Sad, Yugoslavia.

[1]P. Miller, H. Anderson and M. Splichal, J. Appl. Phys, 71, 1171 (1992).

[2]P. Bletzinger and C. A. DeJoseph, Jr, IEEE Trans. on Plasma Science, 14, 124 (1986).

LD-1 Cross Sections for Electron Excitation of Singlet Levels from the 2^3S and 2^1S Metastable levels of He.* R. B. LOCKWOOD, FRANCIS A. SHARPTON, L. W. ANDERSON, and CHUN C. LIN, University of Wisconsin-- Electron excitation cross sections in He for $2^1S \rightarrow n^1L$ and $2^3S \rightarrow n^1L$ excitations are reported. The cross sections are obtained by observing the optical emission from a target that contains a low density of metastable He atoms. The intensities of the $n^1S \rightarrow 2^1P$, $n^1P \rightarrow 2^1S$ and $n^1D \rightarrow 2^1P$ emission lines are measured. The excitation of the n^1L level is due to both the excitation out of the 2^3S and 2^1S levels. The fraction of the excitation from each of the metastable levels is determined from the energy dependence of the optical emission. The absolute cross sections are obtained with the aid of laser-induced fluorescence to measure the metastable density. Some of the cross sections are

$Q(2^1S \rightarrow 3^1S) = 5.2\times10^{-16}$ cm^2 at 10 eV,
$Q(2^1S \rightarrow 3^1P) = 13\times10^{-16}$ cm^2 at 10 eV,
$Q(2^1S \rightarrow 3^1D) = 32\times10^{-16}$ cm^2 at 10 eV,
$Q(2^3S \rightarrow 3^1S) = 0.9\times10^{-16}$ cm^2 at 3.2 eV,
$Q(2^3S \rightarrow 3^1D) = 1.5\times10^{-16}$ cm^2 at 4.2 eV.

*Supported by the National Science Foundation.

LD-2

Differential Vibrational and Electronic Excitation Cross Sections of Molecular Oxygen by Electron Impact

Tong W. Shyn and Christopher J. Sweeney
Space Physics Research Laboratory
University of Michigan
Ann Arbor, MI 48109-2143

Abstract

We have measured the vibrational excitation cross sections (v=1, 2, 3 and 4) and the $a^1\Delta$ and $b^1\Sigma$ electronic states of molecular oxygen by electron impact. A crossed-beam method was used. The incident energies used were 5, 7, 10, 15 and 20 eV. The angular range covered was from 12 to 156°. A maximum in both the vibrational and electronic excitation cross sections was found near 10 eV impact energy.

This work was supported by NSF-ATM-9020626.

LD-3 Further Studies of the Dissociative Excitation of CF_4[#], K. BECKER and J. DIKE, City College of New York, U. MÜLLER, Universität Freiburg, Germany and G. Schulz, Universität Saarbrücken, Germany — We will discuss recent measurements aimed at a further analysis of the intense continuous UV emission produced by electron impact on CF_4. The results of our experiments support the notion that the emission consists of a single fluorescence contribution due to the excited $(CF_3^+)^*$ fragment ion which is produced via two channels. An attempt is made to relate the measured absolute emission cross section for the UV continuum to existing cross sections for the ionization, dissociative ionization, double ion formation and dissociation of the CF_4 molecule.

[#]Supported by the NSF, by PSC-CUNY and by NATO.

LD-4 Elastic Electron Scattering by Laser-excited Sodium, * C. H. YING, Z. SHI, W. TAN, L. VUŠKOVIĆ, and B. BEDERSON New York U,– Extensive study of elastic electron scattering by polarized excited sodium in the range of 0.5-3.5 eV is performed in the standing wave laser field arrangement perpendicular on the atomic beam in the recoiled atom technique where an averaging over azimuthal scattering angle is minimized. For this case, the first time the fraction of atoms in the excited state during the scattering is determined from the horizontal atomic beam dispersion, while the vertical profile suffers contraction due to laser cooling effects resulting into an increase of the central atomic beam intensity. Results of absolute differential cross sections will be presented for the low angular range up to 90°, depending on the electron energy. Comparison with previous measurements[1] and close coupling calculation[2] will be discussed in light of the recent understanding of that scattering process.

* Research supported by U.S. National Science Foundation.

[1]T. M. Zuo et al., Phys. Rev. A 41, 2489 (1990); T. Y. Jiang et al., XVII ICPEAC (1991); C. H. Ying et al., DAMOP (1992).

[2]H. L. Zhou et al., 6th Int. Sym. on Cor. and Pol. in Elec. and Atomic Coll., Adelaide, Australia, July (1991).

LD-5 Elastic Electron Scattering by Hydrogen Sulphide

R.J. Gulley, S.J. Buckman and M.J. Brunger* Electron Physics Group, Australian National University As part of a series of experiments on low energy (1-20 eV) electron scattering by polar molecules we are measuring elastic differential cross sections for the H_2S molecule. These measurements are carried out on a crossed electron-molecule beam apparatus and the angular distributions obtained are placed on an absolute scale by use of the relative flow technique[1], in conjunction with the known elastic cross sections for helium[2]. The angular range covered is 15-130° and the absolute uncertainty on the cross sections varies between 6-10%. In general the cross sections exhibit the strong forward peaking characteristic of electron scattering from polar systems and a subsidiary maximum at mid angles (80-100°). Where possible, comparison will be made with theory and with the one previous absolute experiment[3].

* School of Physical Sciences, Flinders University of South Australia

[1] S.K. Srivastava *et al. J. Chem. Phys.* **64** 1340 (1976)

[2] R.K. Nesbet *Phys. Rev.* A**20** 58 (1979)

[3] K. Rohr *J. Phys. B.* **11** 4109 (1978)

LD-6 Hydrogen Atom Yield in Surface-Wave-Sustained Hydrogen Discharges, L. ST-ONGE and M. MOISAN, U. de Montréal - The need to produce large amounts of hydrogen atoms arises for example in the synthesis of diamond thin films from hydrogen-hydrocarbon plasmas. These atoms serve to stabilize the diamond (metastable) phase, and to simultaneously etch the graphite which is inevitably deposited. Using emission spectroscopy (actinometry), the relative density of atomic hydrogen in a surface-wave-sustained hydrogen discharge has been measured as a function of electron density and pressure, for plasma excitation frequencies ranging from 40.68 to 2450 MHz. The process can thus be optimized in frequency. With an increase in pressure (or correspondingly a decrease of the average electron energy), we observe at constant electron density a decrease in the hydrogen atom fraction. At constant pressure, to an increase in electron density (or equivalently of power density) corresponds an increase in hydrogen atom density. This increase is however limited by losses of H-atoms due to recombination on the walls of the discharge vessel (fused silica tube). This loss mechanism gains importance as the wall temperature is elevated, in particular when an increase in electron density causes an elevation of gas temperature. Externally cooling the discharge vessel can therefore dramatically improve the yield of atoms (in some cases, by a factor of 3). These measurements qualitatively confirmed the results of a simple particle balance model. Depending on the discharge conditions, the hydrogen atom fraction calculated from the model can vary from fractions of 1% to about 10% at a pressure of 1 torr and an electron density of 7×10^{11} cm^{-3}.

LD-7 Ion Chemistry of Tetra-Ethoxy Silane (TEOS) J. HOLTGRAVE, K. RIEHL and P. HAALAND, Air Force Institute of Technology – Tetra-ethoxy silane (TEOS) has emerged as an environmentally *green* precursor for plasma enhanced chemical vapor deposition of SiO_2 films. We report here the cross sections for total and dissociative ionization of (TEOS) as well as dissociative attachment from threshold to 50 eV using Fourier Transform Mass Spectrometry. The partitioning among ionic products is quantified. Ion-molecule reactions, which would perturb the ion composition in a real deposition reactor, are probed at low pressure as a function of the electron energy from which parent ions are generated.

LD-8 Optical Emissions from Electron-Impact Excited TEOS*, M. DUCREPIN, J. DIKE, R.B. SIEGEL and K. BECKER, City College of New York — Tetraethoxysilane, TEOS, has become a convenient and easy-to-handle substitute for silane in the plasma-assisted deposition of SiO_2 and amorphous Si films. There are essentially no collision data available for electron or ion collisions with TEOS. We report the first studies of optical emissions produced by electron impact on TEOS. The measurements which cover the spectral range from the vacuum ultraviolet (VUV) to the near-infrared were caried out in our well-characterized crossed electron-beam - gas-beam apparatus[1,2]. Photoemission cross sections and appearance potentials for the most intense emissions will be reported and discussed.

*Supported by the NSF.

1. K. Miller Jr. and K. Becker, Can. J. Phys. 65, 530 (1987)
2. M.B. Roque et al., J. Chem. Phys. 94, 341 (1991)

LD-9 Molecular Beam Profile Measurements - Investigating the Validity of the Relative Flow Normalisation Technique
R.J. Gulley, S. Bennett and S.J. Buckman, Electron Physics Group, Australian National University Many collision experiments rely on a combination of the relative flow technique[1] and a well-known cross section for the establishment of an absolute normalisation. Central to this approach is the notion that, provided great care is taken with establishing the flow conditions for both the target and "standard" gases, the collision volume is independent of gas species and the cross section can be directly related to a ratio of scattered signals and relative flow rates. We are conducting a series of beam profile measurements to test this hypothesis near (2-5 mm) the exit of both a capillary array and a single capillary beam source for a variety of gases. Such distances are typical of those used in collision experiments and initial data highlights the advantages in beam collimation that can be achieved by using a capillary array source for the formation of such effusive molecular beams. Comparison is also made between the experimentally determined distributions and those predicted by theoretical approximations[2].

[1] S.K. Srivastava *et al. J. Chem. Phys.* **64** 1340 (1976)
[2] D.R. Olander and V. Kruger *J. App. Phys.* **41** 2769 (1970)

LD-10 Electron Impact Ionization Covariance Mapping Spectroscopy of N_2. M.R. Bruce, L. Mi, and R.A. Bonham, Dept. of Chemistry, Indiana University, Bloomington, IN 47405.- Using a pulsed-electron-beam time-of-flight (TOF) apparatus, covariance mapping spectroscopy has been applied to dissociative ionization of N_2. In covariance mapping spectroscopy, the flight time of two ions in coincidence relative to the electron pulse are recorded on individual time axes (flight time of the fastest ion vs. the flight time of the later ion). This technique is experimentally the same as the PEPIPICO experiments[1] and has enabled us to clearly discern true coincidences for $e^- + N_2 \rightarrow N^+ + N^+ + 3e^-$ from accidental coincidences (ie. $2e^- + 2N_2 \rightarrow 2N^+ + 2N + 4e^-$) based upon the readily distinguishable temporal distributions for the two different reactions. Also, true coincidences are observed between N^{2+} and N^+ in the fragmentation of N_2 ($e^- + N_2 \rightarrow N^{2+} + N^+ + 4e^-$). The theory behind covariance mapping is discussed, as well energy and momentum distributions along with appearance potentials are obtained for the observed coincidences.

1. K. Codling et al., J. Phys. B **24**, 951 (1991).
* Work supported by NSF grant PHY-8913096.

LD-11 Triple Coincidence Measurements of Electron Impact Double Ionization*, M. J. FORD, J. P. DOERING, Johns Hopkins U., Baltimore, M. A. COPLAN, J. W. COOPER, J. H. MOORE, U. of Maryland at College Park - Double ionization provides a means of investigating electron-electron correlations within atoms as well as the mechanism of ionization itself. Coincidence measurements, where the kinematics of the collision are completely specified, are a very sensitive probe of these phenomena. The feasibility of applying triple coincidence, or (e,3e) measurements, to double ionization has recently been demonstrated[1]. An (e,3e) spectrometer has been developed capable of measuring the five-fold differential cross-sections for double ionization over a range of angles simultaneously. The multichannel design employed is relatively simple yet gives nearly two orders of magnitude improvement in sensitivity over conventional coincidence experiments; such considerations are crucial in performing these experiments where count rates are extremely low.

*Work Supported by NSF Grant No. PHY-9107337.

[1]A. Lahmam-Bennani, C. Dupre and A. Duguet, Phys. Rev. Letts. 63(15) 1582 (1989).

LD-12 The Angular Distribution of Low-Energy Secondary Electrons in the Ionization-Excitation of N_2.* J. P. DOERING and L. GOEMBEL, Johns Hopkins U. -- Angular distributions of low-energy (5 eV) secondary electrons associated with the production of N_2^+ in the X $^2\Sigma_g^+$, A $^2\Pi_u$, and B $^2\Sigma_u^+$ states from N_2 by 100 eV electron impact have been measured in a coincidence experiment. The scattered "primary" and low energy "secondary" electrons were energy analyzed and detected in coincidence for the asymetric energy sharing regime characteristic of most ionizing collisions. The results show that that electrons associated with production of N_2^+ in the X $^2\Sigma_g^+$ state are characteristically ejected at a smaller (~50°) angle to the incident beam than those associated with production of N_2^+ in the A $^2\Pi_u$ state which are centered on ~75°. This difference is apparently due to the fact that different molecular orbitals of N_2 have been ionized to produce these final states. The backward or "recoil" ejection of secondary electrons has also been measured.

*Work supported by NSF Grant ATM-8915375.

LD-13 Electron Impact Ionization of APSM(2Acryloyloxy Propionic Acid Methylester) R.BASNER, M.SCHMIDT INP H.DEUTSCH Univ O-2200 GREIFSWALD; H.STEINHAUSER,A.HARTWIG GFT W-6680 Neunkirchen
The optically active monomer APSM is in discussion for coating of membranes by plasma polymerization, therefore data of electron impact induced fragmentation and ionization probabilities are of interest.For the measurements is used the double focussing mass spectrometer MCH1310. The ion currents are measured in the electron energy range of 5-100 eV in the peak maxima and we get the ionization cross section by calibrating with the simultaneously measured Ar ion current using the cross sections of Rapp Englander-Golden /1/ .The mass spectrum, ionization (10.9 eV) and appearance energies ,the partial and total (70 eV: $7.9*10^{-16}cm^2$) ionization cross sections are presented. The total ionization cross section is compared with calculations by the additivity rule in different modifications.
Work supported by BMFT Fed. Rep. of Germany Contract No 13 N5939
/1/ D.Rapp et al, J.Chem.Phys.43(1965)1464

LD-14 Electron Impact Ionization of WF6

R.BASNER,M.SCHMIDT INP O-2200 Greifswald,
H.DEUTSCH University O-2200 Greifswald

WF6 is the reaction product of plasma etching of W in fluorine containing gases (CF4,SF6). A detailed modelling of the plasma demands knowledge of data of electron induced fragmentaion and ionization in the energy range of the plasma electrons. The measurements were carried out with the double focussing mass spectrometer MCH1310 (E,H configuration) in the electron energy range of 5-100 eV. The ion current measurements were performed by integration over the beam cross section behind the magnetic field. We get the ionisation cross-section by calibration wih the simultaneously measured Ar ion current using the cross section of Rapp Englander-Golden/1/. The mass spectrum, the partial and total ionization cross sections are presented. The experimental results are compared with calculations by a modified additivity rule.

Work supported by the NATO CRG 9220089

/1/ Rapp et al, J.Chem.Phys.43(1965)1464

LD-15 Electron-Impact Ionization of CF_x and NF_x (x=1-3)*,

V. TARNOVSKY and K. BECKER, City College of New York, H. DEUTSCH, Universität Greifswald, Germany and T.D. Märk, Universität Innsbruck, Austria -- We report absolute partial ionization and dissociative ionization cross sections for NF_3 and for the free radicals CF_3, CF_2, CF, NF_2 and NF. The measurements were carried out using the fast-beam technique[1,2]. We found comparatively small cross sections (< 1 $Å^2$ at 70 eV). Dissociative ionization was identified as an important mechanism in all cases with cross sections for dissociative ionization typically exceeding the parent ionization cross section by up to a factor of 2. Where possible, measured cross sections will be compared to cross sections obtained from an improved additivity rule.

*Supported by the NSF, by PSC-CUNY and by NATO.

1. R.C. Wetzel et al., Phys. Rev. A 35, 559 (1987)
2. V. Tarnovsky and K. Becker, Z. Phys. D 22, 603 (1992)

LD-16 Electron Impact Ionization Cross Sections for NO and N_2O from Threshold to 1 KeV*, I. Iga, M. V. V. S. Rao, and S. K. Srivastava, Jet Propulsion Laboratory, California Institute of Technology - Cross sections for the formation of ions by electron impact on NO and N_2O have been measured by utilizing the crossed beam collision geometry and relative flow technique. Appearance potential for each ion has also been measured. Hess' law has been used to predict appearance energies for various channels of dissociation. Total ionization cross sections have been obtained by adding individual cross sections. Cross sections for fragment ion formation from these species have not been measured so far. Previously reported cross sections for direct ionization cover an energy range of 0 eV to 180 eV. Present work extends this range to 1 KeV. Total ionization cross sections and cross sections for the production of all ions born with kinetic energies larger than 0.25 eV have also been reported previously. At the conference we will present our data and compare them with previous measurements.

*Work supported in part by Airforce Wright Aeronautical Laboratories and in part by National Aeronautics and Space Administration.

LD-17 Electron-impact ionization cross-section measurements for In^+ and Te^+ using crossed beams,* N. ĐURIĆ, E. BELL and G. H. DUNN, JILA, U. of Colorado and NIST— The crossed beams technique has been used to measure for the first time the absolute cross sections for electron impact ionization of In^+ and Te^+ at electron energies ranging from threshold to 200 eV. Target ions were selected for their particular electronic configuration and large number of inner-shell electrons. Excitation-autoionization significantly contributes to ionization of Te^+, but it is not so evident for In^+. Results are compared to the semiempirical prediction formula of Lotz. Ionization rates for a Maxwellian electron-temperature distribution calculated from the data will also be presented.

*Work supported in part by the Office of Fusion Energy of the U.S Department of Energy under Contract No. DE-A105-86ER53237 with NIST.

LD-18 Electron Recombination of $CO^+ \cdot CO$ and H_3O^+,* R. Johnsen, Y.S. Cao, L.A. Weber, and M.F. Golde, U. of Pittsburgh- The recombination of $CO^+ \cdot CO$ ions has been studied using the photoionized, stationary afterglow technique and emission spectroscopy. CO band emissions were observed in the third positive ($b^3\Sigma$-$a^3\Pi$), the Angstrom ($B^1\Sigma$-$A^1\Pi$), and the Herman ($e^3\Sigma$-$a^3\Pi$) systems. The measured recombination coefficient, $\alpha = (2.5 \pm 0.1) \times 10^{-6}$ cm^3/s at T=300 K, is significantly larger than that obtained an earlier experiment[1]. In a second, flowing-afterglow experiment, we used laser-induced fluorescence (LIF) to determine yields of OH (v=0,1) products from recombination of H_3O^+. We find that the OH(v=0) yield is approximately 0.6 while that of v=1 is only 0.12. These results are close to the FALP results of Herd et al.[2].

*Work supported, in part, by NASA

1 M. Whitaker, M.A. Biondi, and R. Johnsen, Phys. Rev. A 24, 743 (1981)

2 C.R. Herd, N.G. Adams, and D. Smith, Ap.J. 349, 388 (1990)

LD-19 **Dissociative Electron Attachment in S_2F_{10}, S_2OF_{10}, and $S_2O_2F_{10}$**, J. K. OLTHOFF, K. L. STRICKLETT, R. J. VAN BRUNT, *NIST*, J. H. MOORE, *UMD*, and I. SAUERS, *ORNL* — The absolute cross sections for dissociative electron attachment to S_2F_{10}, S_2OF_{10}, and $S_2O_2F_{10}$ are measured in an electron transmission experiment using a trochoidal monochromator. The corresponding negative ion fragments are identified by a separate measurement using a time-of-flight mass spectrometer. For S_2F_{10}, attachment of thermal electrons results in the formation of F^-, SF_4^-, SF_5^-, and SF_6^-. Two higher energy resonances near 4.5 and 9.5 eV yield F^- and SF_4^- fragments. Both S_2OF_{10} and $S_2O_2F_{10}$ have unusually large dissociative attachment cross sections ($> 10^{-12}$ cm^2) peaked at energies below 0.1 eV. Electron attachment to S_2OF_{10} yields primarily SOF_5^-, while for $S_2O_2F_{10}$, SF_5^-, SOF_5^-, SOF_3^-, and F^- are formed.

Work partially supported by NSF Grant No. CHE-91-20504.

LD-20 Low-Energy Electron Attachment to Molecules Studied by Pulse Radiolysis Microwave Cavity Technique Combined with Microwave Heating,* H. SHIMAMORI, Y. TATSUMI, Y. OGAWA, T. SUNAGAWA, Fukui Institute of Technology, Japan - Rate constants have been measured for electron attachment to SF_6, CCl_4, $CHCl_3$, $CFCl_3$, CF_3I, CF_3Br, $C_2F_3Cl_3$, and $C_2H_3Cl_3$ in Xe buffer gas (70 Torr) in the mean electron energy from thermal to about 2 eV. Time-dependence of electron density is measured by pulse-radiolysis microwave-cavity method, and a microwave heating technique is additionally applied in order to vary mean electron energies. The calibration of electron energy is made by analyzing the time-profile of microwave conductivity signals for thermalizing electrons produced by pulsed x rays in gaseous Xe that shows the Ramsauer minimum in the momentum-transfer cross sections for collisions with electrons. The data of electron-energy dependence for SF_6, CCl_4, $CHCl_3$, $CFCl_3$, $C_2F_3Cl_3$, and $C_2H_3Cl_3$ are generally in good agreement with those obtained previously by the electron swarm (ES) method. The present thermal values for SF_6, CCl_4, CF_3I, and CF_3Br are in good agreement with previous ones, but those for $CHCl_3$, $CFCl_3$, $C_2F_3Cl_3$, and $C_2H_3Cl_3$ are approximately a half or 60 % of the ES values. The electron-energy-dependence data obtained by the threshold photoionization technique, normalized to the present values at thermal energy, also fit very nicely to our data. In light of present results the rate constants obtained by using high-Rydberg atoms appear to be too high at very low electron energies and too low at electron energies above thermal.

*Work supported in part by a Grant-in-Aid for Scientific Research on Reactive Plasma in Priority Areas from the Ministry of Education, Science and Culture.

LD-21 **Neutral Metastable Fragments from Electron Collisions with Ar Clusters*** P J M van der Burgt and J W McConkey University of Windsor, --A new apparatus has been developed to enable studies of van der Waals clusters and clustering phenomena to be carried out. Features include pulsed supersonic gas injection, pulsed electron beam excitation or ionization, mass detection using quadrupole mass spectroscopy and neutral detection using time-of-flight techniques. V.U.V. photons can also be detected. The performance of the apparatus has been tested using Argon. Time-of-flight spectra recorded for neutral metastable fragments indicate significant contributions from clustered parent species.

* Research supported by the Natural Science and Engineering Research Council of Canada.

LD-22 Angular correlations between sequential cascading photons from $n = 3$ atomic hydrogen. J.F. WILLIAMS, M. KUMAR, *Center for Atomic, Molecular and Surface Physics, University of Western Australia*, AND A. T. STELBOVICS *, *ITAMP, Harvard-Smithsonian Center for Astrophysics*—We report the first measurements of angular correlations of sequential cascading photons for an atomic system excited by electron impact in which a scattering plane is defined. The cascade radiation from the $n = 3$ levels of atomic hydrogen is observed. The measured angular correlations and the deduced multipole moments agree well with Glauber, Born and six state close coupling model predictions at an excitation energy of 290 eV. The first values of a rank-4 multipole and the magnetic sublevels of the $3d$ state are reported.

*Permanent address: Murdoch University, Perth Australia

Session MA

1:30 p.m. – 3:30 p.m.
Thursday, October 29, 1992

Georgian Room

Excited Atoms and Electron Collisions

Chair
W.A.M. Blumberg, Phillips Laboratory

MA-1

Electron Collisions with Excited Atoms*, S. Trajmar**, J. C. Nickel, K. Fujii and M. Johnston, Deptm. of Phys, Univ. of Calif., Riverside - A brief review on electron collision cross section measurements involving excited atoms will be given. Preparation of metastable rare gases by various discharge, electron beam, and charge exchange methods and short-life atomic species (Na, Ba) by laser excitation techniques for cross section measurements, as well as available cross setion data will be briefly summarized. Special considerations concerning these measurements and the nature of resulting cross sections will be discussed and some new results on electron impact ionization of metastable rare gases will be reported.

* Work supported by the National Science Foundation, NATO and

** Premanent address: Jet Propulsion Laboratory, California Institute of Technology

MA-2 Excitation from Metastable He Levels by Electron Impact.* L. W. ANDERSON and CHUN C. LIN, University of Wisconsin--Experiments on the electron excitation of He metastables to higher levels are described. Our measured cross sections for electron excitation of $2^3S \rightarrow n^3L$, $2^3S \rightarrow n^1L$, and $2^1S \rightarrow n^1L$ show that the excitation out of the metastable levels is qualitatively different from the excitation out of the ground level. For example for excitation out of the ground level the cross sections for the optically allowed n^1P levels are larger than those for the n^1S or n^1D levels. One might expect therefore that cross sections out of the 2^3S (2^1S) level and into the n^3P (n^1P) levels would be larger than the cross sections into the n^3S (n^1S) or n^3D (n^1D) levels. This is experimentally not true. In addition the cross sections for excitation out of the 2^3S level into the n^3L levels are qualitatively different from the cross sections for the excitation out of the 2^1S level to the corresponding n^1L levels. This indicates that a systematic study of excitation from metastable levels over a wide energy range is essential for basic understanding of excitation processes.

*Supported by the National Science Foundation.

MA-3 Distorted Wave Approach for (e-2e) Scattering with the Proper Asymptotic Boundary Conditions*, D.H. MADISON AND S. JONES, University of Missouri-Rolla - Over the last several years there has been intense interest and activity in the field of atomic ionization by electron impact. Much of the interest has concentrated on triple differential cross sections for which the energy and angular distributions of both final state electrons are measured (the e-2e problem). It has now become apparent that any reliable theoretical description of this problem must include the final state interaction between the two outgoing electrons and it has been shown that the asymptotic wavefunction for the system must contain a coulomb wave for these two electrons. In this paper we report our progress in incorporating this boundary condition into the distorted wave treatment of the problem.
*Work supported by the National Science Foundation.

MA-4 The Use of Distorted Green's Functions for Electron Scattering from Heavy Atoms*, D.H. MADISON and J. MITCHELL, University of Missouri-Rolla - We have recently performed exact second order distorted wave calculations for electron-hydrogen scattering[1]. In that work, it was shown that the distorted wave series converged to the second term at about 2-3 times the ionization energy and that the use of distorted Green's functions instead of the usual free-particle Green's function caused the series to converge faster. We have now extended this method to the treatment of electron scattering from heavier atoms. The use of distorted Green's functions for heavy atoms is complicated by the fact that the usual static distorting potentials contain natural bound states corresponding to negative ions. This problem will be discussed and results will be shown for electron-sodium scattering.
1. D.H. Madison, I. Bray, and I.E. McCarthy, J. Phys. B 24, 3861 (1991).
*Work supported by the National Science Foundation.

MA-5 Electron Collision Cross Sections for He and Ar — Compilations of DCS —, M. Hayashi, Gaseous Electronics Institute, Nagoya- Electron collision cross section sets for He and Ar were compiled from available experimental values of differential cross sections for elastic scattering and electronic level excitations by smoothly connected method[1]. Recommended DCS values were determined and then integrated. We compiled excitation cross sections for 25 levels in both gases. For Ar, we revised the DCS values of Chutjian et al.(1981) to obtain consistency. Electron collision cross sections for metastable He(2^3S)atoms were also compiled.

[1]M. Hayashi, Gaseous Electronics and Its Applications, Ed. by R.W. Crompton, et al., Kluwer, 9-33 (1991).

MA-6

Measurement of Dielectronic Recombination in a Known External Electric Field, D. W. SAVIN, L. D. GARDNER, J. C. RAYMOND, D. B. REISENFELD, and J. L. KOHL, Harvard-Smithsonian Center for Astrophysics — Dielectronic recombination (DR) tends to be the dominant recombination mechanism for non-hydrogenic ions in low- to medium density ($n_e \lesssim 1 \times 10^{18}$ cm^{-3}), high temperature ($T_e \gtrsim 1 \times 10^4$ K) plasmas. Because electric fields, which are often found in such plasmas (*e.g.* plasma microfields), can significantly enhance the DR process, measurements of DR in fields of known strength are needed. We have used an inclined beams arrangement and a photon/recombined-ion coincidence technique to measure the C^{3+} DR rate coefficient through the 2s-2p core transition in an electric field of 12 V cm^{-1}. Our preliminary result of $(2.8 \pm 0.8) \times 10^{-10}$ cm^3 sec^{-1}, at the 1σ confidence level, is 5.6 ± 1.6 times larger than calculated zero field values. Our new value agrees well with a previous measurement from this laboratory[1] and, to within the experimental uncertainties, at the 90 percent confidence level, with calculations which include the effects of an external electric field. We will demonstrate the need for accurate DR rate coefficients as a function of field strength by showing that solar transition region models which include field-enhanced DR rates lead to as much as a factor of 4 reduction in previously reported C^{3+} fractional abundances.[2] Progress towards measurements of the C^{3+} DR rate coefficient at other field strengths will also be reported.

This work was supported by NASA under grant number NAGW-1687 to Harvard University.

1. A. R. Young, Ph. D. Thesis, Harvard University, 1990.

2. D. B. Reisenfeld, J. R. Raymond, A. R. Young, and J. L. Kohl, Astrophys. Lett. **389**, L37.

Session MB

1:30 p.m. – 3:30 p.m.
Thursday, October 29, 1992

Arlington Room

Plasma Etching

Chair
T. Sommerer, GE Corporate Research

MB-1 A Simple Rule for the Etch Rate of SiO_2 in CF_4 Plasmas,* N. HERSHKOWITZ and J. DING, University of Wisconsin-Madison — Measurements of SiO_2 etch rate by CF_4 plasmas in an ECR tool operated at 0.5 - 2.5 mTorr and in a parallel plate RIE etcher at 37 mTorr both find over a very wide range of conditions the etch rate is proportional to the ion energy flux (i.e. the ion power/cm^2) delivered to the wafer. The remarkable result is that the constant of proportionality appears to be the same for both tools. Measurements were carried out with mixtures of $CF_4/O_2/CHF_3/Ar$. As long as adequate fluorine is available, the etch rate only depends on the ion energy flux to the wafer. Ion power to the wafer was determined by measuring the ion saturation current multiplied by the ion energy at the wafer surface. In the ECR tool the ion energy is equal to the difference in the plasma potential and the rf self bias voltage. At high pressure it is necessary to correct for collisions within the plasma-wafer sheath.

*Work supported by NSF Grant No. ECD-8721545 for the Engineering Research Center for Plasma-Aided Manufacturing.

MB-2 Investigation of Ion-Enhanced Fluorocarbon Etching Kinetics at Near-Threshold Ion Energies, David C. Gray and Herbert H. Sawin, MIT Dept. of Chemical Engineering, Cambridge MA 02139-
Due to increasing concern over substrate surface damage and anisotropy requirements in submicron dry etching, development of a number novel high density plasma tools such as ECR, helicon, and RFI is occurring rapidly. These sources all offer low mean ion energies, typically 10 to 30 eV, in comparison to conventional parallel plate etching tools. However, little information is available regarding etching rates where the bombarding ion energies are near the sputtering threshold energy of the substrate materials. We have measured etching rates of silicon and silicon dioxide exposed to simultaneous fluxes of atomic fluorine, and nominal 20 eV ions produced in a compact ECR source. The effectiveness of inert Ar^+ ions in enhancing etching was compared to a mixture of carbonaceous (CF_x^+) ions. In the presence of reactive free radical species, the threshold energies for ion-induced etching processes are shown to be in the range of 1-5 eV, an order of magnitude lower than physical sputtering threshold energies. These rate measurements should provide insight regarding wafer throughput in low energy plasma processes.

MB-3 Microtrench Formation During Plasma Etching*, T.J. DALTON**, J.C. ARNOLD, & H.H. SAWIN, Massachusetts Institute of Technology, S. Swan & D. Corliss, Digital Equipment Corporation - The opening of a sub-micron window in polysilicon over a thin gate oxide, using an existing etching process, produced an unusual microtrenching phenomenon. The micro-trenches were formed by higher local etching rate of the oxide, resulting in "punch-through" of the oxide and rapid etching of the silicon substrate below. These microtrenches differed from those reported previously in that they were located several hundred angstroms away from the foot of the sidewall. Examination of the literature revealed three possible causes of microtrenching: surface diffusion of reactants along the sidewalls, specular reflection of ions from the sidewalls, and localized charging of the feature surface. Ion reflection was thought to be the most promising of these. A simple model was constructed, which considered only single specular reflection of ions where the reflection probability decreased with incidence angle. The angular distribution of ions arriving from the plasma was estimated from the work of Liu, et al[1]. An existing string model was used to simulate profile evolution in time. The modelling results indicated that ion reflection was the dominant cause.

*Work supported by SEMATECH, at the Mass. SCOE
**Supported by National Science Foundation

1. J. Liu, G.L. Huppert & H.H. Sawin, J. Appl. Phys., 68(8), 3916 (1990).

MB-4 Parametric Study of the Influence of the Wafer Biasing Frequency and Voltage upon Etching of Polyimide, F. BOUNASRI, G. SAUVE AND M. MOISAN, U. DE MONTREAL - In RF capacitive discharges, the wafer biasing voltage results from discharge conditions and cannot be adjusted independently from plasma parameters such as density. In contrast, in electrodeless HF sustained plasmas, one can use a biasing frequency different from that stimulating the plasma, and the biasing voltage can be set at different values with respect to plasma potential. It has already been shown that biasing the wafer at 13.56 MHz in a 2.45 GHz microwave sustained plasma can substantially increase the etch rate. We show that varying the biasing frequency when etching polyimide allows one to identify two types of plasma surface interaction, depending on the gas composition: i) with an inert gas such as argon, the etch rate is higher when the biasing frequency f_b is below the ion plasma frequency; ii) with reactive gases (CF_4, SF_6, O_2), the etch rate is independant of f_b. In the latter case, we have further identified two etching regimes, depending on the biasing voltage: regime I: chemical etching and regime II: ion assisted chemical etching. Although the etch rate is independent of f_b in case ii), XPS analysis of the polyimide surface shows that the surface treated at 13.56 MHz is different than that etched at 100 kHz; for example, fluorine contents are reduced by approximately 50% at 100 kHz.

MB-5 Spatially and Temporally Resolved Profiles of O atoms in Etching Plasmas,*A.D TSEREPI, B.L. PREPPERNAU, and T.A. MILLER, The Ohio State University-The detection of atomic O by two-photon laser-induced fluorescence has been employed to obtain the spatial distribution and the temporal behavior of oxygen atoms in a 10 MHz parallel plate rf discharge. Absolute concentrations have been determined via a titration technique throughout the range of intensities typically found in 20-100 W, 0.1-4 Torr O_2 discharges. We find the O concentration to vary, depending on the discharge conditions, in the range 5-20x10^{14} atoms/cm^3. The spatial O distribution is mostly uniform under both steady state condition and after initial turn-on, which indicates a nearly uniform production of O atoms throughout the interelectrode space. Furthermore, the decay of the O concentration near surfaces reveals information about the reaction of O atoms with materials in the plasma environment. Specifically, we study the concentration decay rates over a photoresist surface in pure oxygen plasma and over a Si wafer in CF_4/O_2 mixture, because of their significance to materials etching.

*Work supported by Air Force Wright Research and Development Center.

MB-6 High Sensitivity Absorption Spectroscopy for Low Pressure Plasma Etching Diagnostics. E. A. WHITTAKER, H. C. SUN, V. PATEL, B. SINGH, New Jersey Sematech Center of Excellence in Plasma Etch.--- We report on the performance of a tunable lead salt diode laser absorption spectrometer capable of detecting absorbances as small as a few parts in 10^{-7} with a detection bandwidth of several kiloherz. To achieve such a high performance, we have implemented a novel laser modulation scheme which allows us to selectively reject interference fringes induced by reaction chamber windows and other optical surfaces through which the probing beam must pass. The method also allows us to lock the laser to the resonance line of the species being probed and to measure its absorbance in real time. We present data taken from SF_6 and C_2F_6 plasmas used for polysilicon and oxide etching. The high dynamic range and wide detection bandwidth allow us to measure SF_6 and C_2F_6 concentrations in real time as various etching reactor parameters are varied. We have also measured concentrations of SiF_4, and a number of intermediate reaction species.

MB-7 Surface Charging Effects During Plasma Etching,* J.P. MCVITTIE, S. FANG and S. MURAKAWA, CIS, Stanford Univ.
Charging is important in IC fabrication since it can both damage thin gate oxides [1] and affect etch profiles[2]. Recently, we reported [3] a model which relates charging to differences in the local electron and ion currents caused by plasma nonuniformity. Using a magnet to create a nonuniform plasma, this model was used to explain damage in both ashing where MOS gates are directly exposed to a plasma and in etching where the gates are mostly protected by a resist mask. In addition, for the same magnetron system, this charging model with ion trajectory simulations was be used to explain differences in etch profile shape across a wafer. In this system insulating surfaces on a grounded wafer can charge up to nearly 20 volts which is a sizable fraction of the plasma potential. Note that this charging mechanism is significantly different than that proposed in [2] where an uniform plasma is assumed and charging is caused by the angular distribution difference between ions and electrons.

*Work supported by DARPA and SRC

[1]S. Fang, and J.P. McVittie, IEEE Elec. Dev. Lett.,13, 288 (1992).

[2]J.C. Arnold et al, J.Appl. Phys., 70, 5314 (1991).

[3]S. Fang, and J.P. McVittie, IEEE Elec. Dev. Lett.,13, 347 (1992).

MB-8 **Electron Collection at the Gate Edge During Overetching***, SHIGEMI MURAKAWA**, SYCHYI FANG AND JAMES P. MCVITTIE, Center for Integrated Systems, Stanford University, Stanford, CA94305 ---
Recently, we reported [1] that the local imbalance of electron and ion currents causes wafer charging and subsequent thin gate oxide damage to MOS gates exposed to a non-uniform plasma. In this work, we investigate the electron current flow to the exposed edges of a poly-Si gate during gate etching. Electrons are attracted to the side wall of the resist-covered gate by the potential difference between the gate and the more negatively charged nearby insulator surface. Electron trajectories in the plasma sheath were calculated and found to be deflected to the gate side wall from as much as 10μm away. However, the net current to the gate by this mechanism was still found to be 50 x too small to account for actually measured oxide damage. These results show why charge damage during overetch is not significant in most cases.

* Work supported by Kawasaki Steel Corp., DARPA and SRC.

** on leave from Kawasaki Steel Corp., LSI Research Center, Technical Research Div.,1,Kawasaki-cho,Chuo-ku,Chiba260, JAPAN

[1] S. Fang and J. P. McVittie, IEEE EI. Dev. Let.,13, 347 (1992)

Session NA

3:45 p.m. – 6:15 p.m.
Thursday, October 29, 1992

Georgian Room

CF_4 Workshop

Chair
R.A. Bonham, Indiana Unviersity

NA-1 Cross Sections for Scattering of Low- and Intermediate-Energy Electrons from CF_4* M. A. DILLON, MINEO KIMURA, Argonne National Laboratory, Argonne, IL 60439, L. BOESTEN, H. TANAKA, and A. KOBAYASHI, Sophia U., Tokyo--Differential cross sections[1] (DCS) for e-CF_4 collisions with incident electrons of 1.5-100 eV were recorded over an angular range of 15-130°. Relative measurements were made absolute by applying the relative flow method with He as the comparison gas. Integral and momentum transfer cross sections obtained from the DCS are compared with theoretical calculations, past experimental results, and values derived from swarm experiments. The integrated DCS show a broad structure at 7 eV of symmetry T_2, as predicted by theory, and one broad peak at 15-25 eV. Evidence of shape resonance of T_2 symmetry was observed in the recorded angular distributions for vibrational modes ν_0, ν_1, ν_3, and ν_4. In addition, a large cross section for ν_3 excitation with 2-eV electrons was found to occur by a direct mechanism.

* Work supported in part by the U.S. Department of Energy, Office of Energy Research, Office of Health and Environmental Research, under Contract W-31-109-Eng-38 (MK), and by the Office of Basic Energy Sciences (NFL).

1 L. Boesten, H. Tanaka, A. Kobayashi, M. A. Dillon, and M. Kimura, J. Phys. B 28, 1607 (1992).

NA-2 Calculation of Elastic and Momentum Transfer Cross Sections for CF_4, C. WINSTEAD, Q. SUN, and V. McKOY, Caltech—We have calculated fixed-nuclei elastic cross sections for electron scattering by CF_4 from 0–40 eV. Differential and integral cross sections will be compared with recent experimental determinations and with previous calculations. Assignments will be given for several shape resonances evident in the cross section. We will discuss the relationship of our results to the vibrationally elastic and inelastic cross sections and to the total inelastic cross section. The momentum transfer cross section determined from our differential cross section will also be presented.

NA-3 Dissociative Attachment and Ionic Dissociation Cross Sections of CF_4*, S. K. Srivastava, Jet Propulsion Laboratory, California Institute of Technology- First measurements of cross sections for the production of negative ions by electron attachment to CF_4 will be presented. Energies at which various negative ions appear and the positions at which ionization efficiency curves peak have been obtained and compared with previous measurements. Cross sections for the formation of positive ions by electron impact on CF_4 have also been measured.The cross section data will be presented for electron impact energy range of 0 to 1 KeV for the formation of various fragemnt ions. Thermochemical data have been employed to predict and identify the various channels of dissociation.

*Work supported in part by Airforce Wright Aeronautical Laboratories and in part by National Aeronautics and Space Administration.

NA-4 Dissociative Ionization Cross Sections for CF_4. M.R. Bruce and R.A. Bonham, Dept. of Chemistry, Indiana University, Bloomington, IN 47405.- The cross section data for dissociative ionization of CF_4 is critically reviewed. Recent re-examinations by Poll et. al[1] and Bruce et al.[2] of the results by Stephan et al.[3] and Ma et. al.[4], respectively, have determined several error sources, and have now brought the results of these two groups into excellent agreement except for the double charged cross sections. Also, corrections are applied for multiple ion formation[5].

1. H.U. Poll et. al., Int. J. Mass Spectrom. Ion Processes **112**, 1 (1992).
2. M.R. Bruce and R.A. Bonham, Int. J. Mass Spectrom. Ion Processes (in press 1992).
3. K. Stephan et. al, J. Chem. Phys. **83**, 5712 (1985).
4. Ma et. al, Phys. Rev. A **44**, 2921 (1991).
5. M.R. Bruce et. al, Chem. Phys. Lett. **190**, 285 (1992).
* Work supported by NSF grant PHY-8913096.

NA-5 Measured and Calculated Cross Sections for the Electron-Impact Ionization of CF_3, CF_2 and CF*. V. TARNOVSKY and K. BECKER, City College of New York, H. DEUTSCH, Universität Greifswald, Germany and T.D. MÄRK, Universität Innsbruck, Austria -- We present a summary of recent measurements of absolute partial cross sections for the electron-impact ionization of the free radicals CF_3, CF_2 and CF carried out in our laboratory. The measurements will be compared with calculated cross sections obtained on one hand from an improved additivity rule and on the other hand from the recently proposed semi-classical DM approach. The inherent and general problems of cross section determinations for free molecular radicals will be discussed.

*Supported by the NSF, by PSC-CUNY and by NATO.

NA-6 **Dissociative Excitation of CF_4 Following Electron Impact*** S Wang†, P J M van der Burgt, L Forand** and J W McConkey University of Windsor, Canada.--The breakup of CF_4 following electron impact has been studied using two different techniques, V.U.V. spectroscopic analysis and time-of-flight detection of metastable fragments. Absolute cross-section data for production of many excited neutral and ionized species of both C and F have been measured at an incident electron energy of 200 eV and excitation functions of the most intense emissions were measured from threshold to 600 eV. Detailed studies of the near-threshold excitation cross-sections revealed that many different dissociation channels were involved. In some cases these could be unambiguously identified.

* Work supported by the Natural Science and Engineering Research Council of Canada.

† Present address: Jet Propulsion Laboratory, Pasadena, CA 91109.

** Present address: Defence Research Board, Valcartier, Quebec.

NA-7 Polarization Calculations for Electron-Molecule Scattering Employing the Schwinger Multichannel Method with *VGV* Insertion. J. A. SHEEHY* and W. M. HUO, NASA Ames Research Center. – – – The idea of evaluating the matrix elements $\langle \Psi_m | V G_p^{(+)} V | \Psi_n \rangle$, which arise in the Schwinger multichannel method for calculating electron-molecule scattering cross sections, employing a Gaussian insertion technique has recently been revived. This approach is applied to low-energy elastic scattering from CO and CF_4, at the static-exchange level as well as with target polarization effects included, and the results are compared with experiment. It is seen that reliable cross sections may be obtained in a reasonable amount of computer time with appropriate choices for the target and insertion basis sets, where the latter is defined as the additional basis functions used only in the evaluation of the aforementioned matrix elements. Moreover, computing polarization cross sections is no more demanding on the one-particle basis set than are static-exchange calculations.

* NRC/NASA Research Associate

NA-8 Initial Modeling Results of rf Discharges in CF_4 Gas Mixtures Using a New Cross Section Set, Helen H. Hwang, Debbie S. Thomas and Mark J. Kushner, University of Illinois, Department of Electrical and Computer Engineering, Urbana, IL 61801 * – The use of CF_4 as an etching gas in microelectronics fabrication has motivated a number of experimental measurements of electron impact cross sections. Recently, Bonham[1] has evaluated and compiled all currently available cross sections for CF_4 into a new cross section set. We have incorporated those cross sections into a hybrid Monte Carlo-fluid model for rf discharges, and investigated discharge properties for CF_4 gas mixtures. Initial results from that study will be presented, and comparisons will be made to results obtained using the CF_4 cross section set proposed by Hayashi.[2]

* Work supported by U of Wisconsin ERC, NSF and SRC.

[1] R. Bonham, unpublished.

[2] M. Hayashi, in Swarm Studies and Inelastic Electron-Molecule Collisions, edited by L. C. Pitchford, 1986.

Session NB

3:45 p.m. – 5:45 p.m.
Thursday, October 29, 1992

Arlington Room

Plasma Assisted Deposition

Chair
E.E. Kunhardt, Stevens Institute of Technology

NB-1 Absolute CH_3 Densities in a Diamond Growth Environment by Ultrasensitive Absorption Spectroscopy,* K. L. MENNINGEN, M. A. CHILDS, P. CHEVAKO, N. W. SPELLMEYER, L. W. ANDERSON, AND J. E. LAWLER, University of Wisconsin. - Absorption spectroscopy using an ultrastable xenon arc lamp and a multielement photodiode array is used to determine the CH_3 density above a hot filament in a H_2 (98% by volume) and CH_4 (2%) gas mixture. The tungsten filament temperature is kept at 2150°C. The total gas pressure is 20 torr with a mass flow rate of 100 sccm. The absorption was observed on the $\tilde{B}\leftarrow\tilde{X}$ transition at 216nm. The total fractional absorption along a 10 cm path is 2×10^{-3}. The CH_3 density is determined to be 5×10^{12} per cm^3 about 0.5 cm above the filament. Signal to noise ratios of about 50 to 1 indicate that it should be possible to detect as few as 10^{11} CH_3 radicals per cm^3.

*Work supported by the Army Research Office.

NB-2 Microwave Perturbation and Langmuir Probe Measurements in Methane/Hydrogen Discharges, C. B. FLEDDERMANN and H. R. SNYDER, Center for High Technology Materials, U. of New Mexico- Measurements of electron density, electron density decay time, electron temperature, and floating potential in methane/hydrogen discharges excited by an rf helical resonator are reported. These studies were undertaken for up to 5% methane diluted in hydrogen, the range of gas mixtures that correspond to those used for plasma deposition of diamond thin films. Measurements of the effect of added oxygen are also reported. Studies were performed using microwave cavity perturbation to measure electron density and decay time constants, and a Langmuir probe to measure electron density, electron temperature, and floating potential. It is shown that there is little variation in electron density and decay times over the range of gas mixtures used, which indicates that negative ion formation through dissociative attachment is not a significant process in these discharges. Electron temperature measurements showed little variation with gas mixture for both methane and oxygen incorporation into the plasma. Floating potential did show a large variation with methane percentage, but was insensitive to oxygen content of the plasma.

NB-3 Ultraviolet Photoacoustic Detection of Gas Phase Precursors of Diamond,* M. A. CHILDS, K. L. MENNINGEN, P. CHEVAKO, N. W. SPELLMEYER, L. W. ANDERSON, and J. E. LAWLER, University of Wisconsin. - Photoacoustic detection of C_2H_2 and CH_3 in a diamond growth environment is attempted near 216nm. Detection of the $V_0^4K_0^1$ bandhead of the $\tilde{A}\leftarrow\tilde{X}$ transition of acetylene at 46304 cm^{-1} is limited to volume densities greater than about 1×10^{15} C_2H_2 molecule/cm^3. Detection of the $\tilde{B}\leftarrow\tilde{X}$ transition of CH_3 at 46205 cm^{-1} is limited to about 1.6×10^{13} CH_3 radicals/cm^3. No radicals were detected. An unexplained broadband absorption signal was observed. Two absorption cross sections of C_2H_2 are measured with a spectral limit of resolution of 0.5 cm^{-1}. The cross sections are 1.5×10^{-20} cm^2 for the $V_0^4K_0^1$ bandhead and 6×10^{-21} cm^2 for the $2_0^1V_1^3K_1^2$ bandhead.

*Work supported by the Army Research Office.

NB-4 Oxidation and Reduction of Carbonous Impediments to the Low Temperature Growth of Diamond Films, F. V. Wells, R. Rodriguez, D. W. Warner, and S. Johnson, Idaho State University, Pocatello, ID 83209. The quality of low pressure diamond films prepared at temperatures less than 880 K is typically deteriorated by the competing deposition of graphite and amorphous carbon. The results of a temperature dependent study for oxidation and reduction reactions of graphite in the plasma environment using partial pressure mass spectroscopy will be presented. The reactions were studied by monitoring the carbon containing products of rf excited Argon plasmas containing low concentrations of H_2, Cl_2, F_2 and O_2. The temperature dependent behavior for the removal of graphite deposits in the range of 300 to 800 K will be presented.

Work supported by Air Force Office of Scientific Research and Gould Electronics, Semiconductor Division.

NB-5 A Comparison of $He/O_2/SiH_4$ and $He/N_2O/SiH_4$ Gas Mixtures for Remote Plasma Deposition of SiO_2, Mark J. Kushner, University of Illinois, Department of Electrical and Computer Engineering, Urbana, IL 61801 *

- In Remote Plasma Enhanced Chemical Vapor Deposition (RPECVD) a subset of the deposition gases are flowed through a plasma zone with the remainder being injected downstream. Mixing between the activated gases and injected deposition gases produce precursor radicals for the deposition. RPECVD of SiO_2 can be performed using $He/O_2/SiH_4$ or $He/N_2O/SiH_4$ mixtures. It has been proposed that $O_2(^1\Delta)$ and $SiH_4(v)$, or species such as SiH_2O and HSiO are the deposition precursors. A 2-dimensional plasma chemistry model has been developed to investigate the production of deposition precursors using these mixtures. Results comparing these two systems will be made. In this paper we will also propose a new reactor configuration using pulsed plasma/pulsed injection of gases to maximize the isolation between the injected gases and the plasma. An animation of this system will be shown using $Ar/H_2/SiH_4$ chemistry to demonstrate the ability to selectively produce radicals.

* Work supported by SRC, NSF, IBM and the University of Wisconsin ERC for Plasma Aided Manufacturing

NB-6 Low temperature plasma assisted deposition of thick SiO2 layers using the helicon reactor.

H. Persing, G. Giroult-Matlakowski, S. Armand, R.Boswell, Plasma Research Laboratory - The Australian National University - Canberra - Australie.

In the production of both electronic and optical device structures it is necessary to be able to deposit high quality SiO2 films at low temperature. Previous results presented on the deposition of silicon dioxide from a silane - oxygen plasma using the helicon reactor dealt with silicon substrates which were neither externally biased nor cooled. This paper will show the first results concerning a low temperature (T=60°C) deposition process. Deposition rates, optical and physical properties of the deposited layers will be presented.

NB-7 Deposition of a-Si:H Films by Glow Discharge Method with SiH_4-He System, Y. NAKAMURA, S. SUNAGO, Y. SAKAI, N. KUTSUWADA and T. SEKINE, Nippon Inst. of Tech. - OES for pure He and SiH_4(40%) - He(60%) were observed at 1.0 Torr with the gas flow rate of 140 (cc/min). A relative intensity of SiH^* at 414 (nm) to HeI at 706.5 (nm) was about 10 and stronger than that for usually used SiH_4 - H_2 system. Deposition rate was measured in the range of SiH_4 concentration between 2 and 40% in this system. While below 20% the rate increased proportionally with the concentration, deposition rate of a-Si:H saturated in the upper region of 20% which was about 5μm/hr and relatively higher than that of SiH_4 - H_2. Dark conductivity on the film was reduced to 10^{-13}(S/cm) by doping of B_2H_6 with B_2H_6/SiH_4 ratio of 10^{-6}. Photo conductivity, optical band gap, FT-IR and ESR measurements for the films were also done.

Keywords : Silane, amorphous Silicon, Glow discharge, Plasma - CVD.

NB-8 Time Dependent Analysis of Velocity distribution and Transport Coefficients of electrons in SiH_4 under RF Field S.NAKAJIMA and N.Ikuta Tokushima U.Jpn.--- Adopting the principle of the path integral solution of the Boltzmann equation, the time dependent behavior of electrons in SiH_4 gas has been accurately analysed under RF electric fields of 19.8, 198 and 626 Td at 13.56 MHz for various gas densities. Not only the velocity distribution and transport coefficients, many quantities such as the gain rates of energy and momenta, random and drift components of mean energies etc. are precisely calculated. When the gas density is high, the relaxation time is short, and the higher terms in Fourier series of transport coefficients are observed. Decreasing the gas density, the situation shifts to non-equilibrium. The phase lag in the Fourier components increases and the energy input for electrons decreases. The lower limit of the field E for the constant mean energy under constant E/N is given by the decrease of energy input over one cycle below the level of the mean energy.

1 S.Nakajima, Y.Seki and N.Ikuta, Bulletin of Faculty of The University of Tokushima, 27, 49 (1990).

Session PA

8:00 a.m. – 9:45 a.m.
Friday, October 30, 1992

Georgian Room

Recent Advances in Electron Atom Collisions

Chair
D.H. Madison, University of Missouri

PA-1 Advances in the Theory of Electron-Atom Collisions, H.R.J. WALTERS, The Queen's University of Belfast -

Latest developments in the theory of electron-atom collisions will be described with particular emphasis on the intermediate energy region. Amongst the topics to be addressed are perturbative methods, optical potentials, coupled pseudostate methods and the new intermediate energy R-matrix theory. Problems associated with pseudothreshold and pseudoresonant behaviour will be discussed. The different methods will be illustrated by applications principally to electron scattering by atomic hydrogen and outstanding discrepancies between theory and experiment will be highlighted. Future directions will be discussed.

PA-2 Unpolarized Electron Scattering as a Stringent Test of Theory,* L. VUŠKOVIĆ, New York U,- Recent progress in the experimental investigation of unpolarized electron scattering by ground state (3^2S) and polarized excited sodium ($3^2P_{3/2}$) will be reported for the threshold region up to several times ionization potential. Extensive measurements[1a] of differential cross sections for scattering from both 3^2S and $3^2P_{3/2}$, generally support close coupling calculation[1b]. Substantial disagreement exists for the elastic scattering by $3^2P_{3/2}$ laser-excited sodium, and developments toward a picture of the underlying physical mechanisms are stressed. Second example are high electron energy resolution measurements[2a] of the angular intensity distribution for various excitation processes, such as $3^2S \rightarrow 4^2P$ scattering which serve as a test of distorted wave calculation[2b] for effect of polarization on the projectile and exchange distortion.

* Research supported by U.S. National Science Foundation.

[1](a) T. Y. Jiang et al., Phys. Rev. Lett. 68, 915 (1992); C. H. Ying et al., GEC 44 (1991) and GEC 45 (1992); (b) H. L. Zhou et al., 6th ISCPEAC, Adelaide, Australia, July (1991).

[2](a) B. Marinković et al., Submitted to J. Phys. B (1992); (b) D. H. Madison et al., Submitted to J. Phys. B (1992).

PA-3

Electron-Impact Excitation from Excited Atomic Systems.
G. CSANAK (1), D. C. CARTWRIGHT, R. E. H. CLARK, and J. ABDALLAH, JR., Los Alamos National Laboratory---
Fundamental equations for Many Body Theory (MBT) will be derived for electron impact excitation from excited atomic systems. First-order results for excitation from the 2-3-S and 2-1-S of He atom will be compared to experimental differential (DCS) and integral cross section (ICS) data. Higher-order MBT contributions to the scattering matrix will be described and it will be shown that the usual DWA can be obtained by selectively summing certain terms to infinite order. Our DWA results for the above He excited state targets will be compared to MBT results and to experimental and other theoretical data. DWA results for electron impact excitation from the laser-pumped 6-1-P state of Ba will also be presented and compared to experimental DCSs.

(1) on sabbatical, University of Tsukuba, Tsukuba, Ibaraki 305, Japan

PA-4 Polarized Electron-Noble Gas Collisions*,
T.J. GAY, J.E. FURST, and W.M.K.P. WIJAYARATNA, University of Missouri-Rolla - In electron-atom collisions, spin-dependent effects can be caused either by spin-orbit forces exerted by the atom on the continuum electron (Mott scattering), or by spin-orbit splitting of the atomic target states (the "fine-structure" effect). We have performed a series of experiments designed to identify effects due exclusively to continuum electron-spin orbit coupling. These involve measurement of the Stoke's parameters of light emitted by the $np^5(n+1)p[5/2]_3$ states of heavy noble gases excited by impact of polarized electrons. Our studies indicate that such effects are small, even for relatively heavy Xe targets. Implications of our work for optical electron polarimetry will be discussed.

*Work supported by National Science Foundation Grant PHY-9201289.

PA-5 R-Matrix Calculations for Electron Impact Ionization of Complex Atoms*. K. BARTSCHAT, JILA and University of Colorado†. — A newly developed method [1, 2] for calculating total and single differential (with regard to energy loss) cross sections for electron impact ionization within the R-matrix (close-coupling method) will be presented. This approach includes channel coupling, autoionizing resonances and a multi-configuration expansion of the initial state in an *ab initio* manner. Sample results for ionization of inert gases as well as open-shell systems such as chromium will be shown at the meeting.

[1] K. Bartschat and P.G. Burke, J. Phys. B **20** (1987), 3191
[2] K. Bartschat (1992), submitted to Computer Physics Communications

* Work supported by the National Science Foundation, the Research Corporation, and a JILA Visiting Fellowship

† Permanent Address: Physics Department, Drake University

PA-6 Time-Dependent Approach to Electron-Hydrogen Collisions.* D. R. SCHULTZ AND C. BOTTCHER, ORNL, and D. H. MADISON, University of Missouri-Rolla – As an alternate and complementary approach to close coupling and perturbative treatments, we have developed a method utilizing a Hylleraas representation of the Hamiltonian and the basis-spline collocation technique to numerically evolve the time-dependent Schrödinger equation describing the collision of an electron with atomic hydrogen. In comparison to these other methods, the present treatment has the potential advantages of a more flexible expansion of the wavefunction and a more complete representation of the correlation of the two electrons over the entire collision regime. We also present the results of a time-dependent, statistical, and quasi-quantal model based on classical electron trajectories, illustrating the regimes in which classical dynamics play the dominant role in electron-hydrogen collisions.

*Research sponsored by the Office of Basic Energy Sciences, U.S. Department of Energy under contract No. DE-AC05-84OR21400 managed by Martin Marietta Energy Systems, Inc.

Session PB

8:00 a.m. – 10:00 a.m.
Friday, October 30, 1992

Arlington Room

Electrical Characterization of Plasmas

Chair
W. Lapatovich, GTE Laboratories Incorporated

PB-1 Probe Diagnostics of Non-Maxwellian Plasmas. V.A. GODYAK, R.B. PIEJAK and B.M. ALEXANDROVICH GTE Laboratories Inc., Waltham MA - A comparison of the results from various probe diagnostic methods has been performed for rf plasmas with non-Maxwellian electron energy distribution functions (EEDF). Measurements were done in a 13.56 MHz capacitive argon rf discharge at two gas pressures: p=30 mTorr, corresponding to stochastic electron heating and p=300 mTorr, corresponding to collisional electron heating. At these two gas pressures the measured EEDF manifests a departure from thermodynamic equilibrium being bi-Maxwellian at 30 mTorr and Druyvesteyn-like at 300 mTorr. Plasma density, N and effective electron temperature, T_e were obtained using standard procedures from the intermediate (classic Langmuir method) part, the ion saturation part and the electron saturation part of the measured probe I/V characteristic. Considerable differences in N and T_e were obtained from the different parts of the probe characteristic and these values differ dramatically from those found from integration of the measured EEDF's. This demonstrates that using standard procedures in non-Maxwellian plasma can give misleading results.

PB-2 Electron Energy Distribution Function in Plasma Etching System

K.F. Al-Assadi, M. Boudiaf and N.M.D. Brown
The Joint Ceramics Research Centre, Dept. of Applied Physical Sciences, University of Ulster, Coleraine BT52 1SA

Abstract

An rf self-compensated Langmuir probe technique has been used to measure the electron energy distribution function (EEDF) using the second differential of the (I-V) characteristics in an rf (13.56 MHz) argon gas discharge under constant pressure - variable power (10 - 100 watts), and constant power - variable pressure (2 - 50 mtorr) conditions.

It is found that the EEDF can be represented as a sum of two Maxwellian distributions with two values of electron temperature. The electron temperature of each group is directly proportional to the rf power at constant pressure, where the high-energy electrons having a temperature more than four times those of low-energy group. The measurement shows that the high - energy tail of the EEDF extends to higher energies as the rf power increases. At constant power, it is found that the electron temperature increases with gas pressure.

PB-3 Mapping of Plasma Densities, Potentials, and Electron Energy Distribution Functions in a Low Pressure DC Discharge, R. CLAUDE WOODS and ISAAC D. SUDIT, Department of Chemistry, University of Wisconsin-Madison — Plasma parameters have been mapped in a large low pressure DC discharge with a hollow cathode. These discharges, intended to produce molecular ions for study by microwave spectroscopy, have been studied using cylindrical Langmuir probes. Electron energy distribution functions (EEDFs) , plasma densities, and plasma potentials have been determined in helium and nitrogen discharges. Electron energy distribution functions in the negative glow are Maxwellian and show very cold (0.25 eV in nitrogen) and very dense (10^{11} cm^{-3}) electrons. Double layers (approximately 20 V in voltage change) appear a few tens of centimeters from the negative glow in both helium and nitrogen. The EEDFs in this region are very complex, exhibiting several distinct populations of electrons. These double layers connect with the positive column where the electron density decreases by two orders of magnitude and the electron temperature increases by one. In the case of the nitrogen positive column, the EEDFs are highly non-Maxwellian, and agree very well with the theoretical results of Pitchford and Phelps[1]. Stationary striations are present in both the helium and nitrogen columns, with wavelengths of approximately 15 cm and 30 cm respectively in a 200 mA discharge. The phase relationships between the density, field and electron temperature spatial variations depend on the gas.

[1]L. C. Pitchford and A. V. Phelps, Phys. Rev. A 25, 540 (1982).

PB-4 A Study of the Accuracy of Various Cylindrical Probe Theories, ISAAC D. SUDIT and R. CLAUDE WOODS, Department of Chemistry, University of Wisconsin-Madison — The applicability of different methods of extracting plasma parameters from cylindrical Langmuir probe data has been investigated using a workstation based probe system. The plasmas used in this study are nitrogen and helium DC discharges, with pressures ranging from 10 to 50 mTorr and plasma densities from 10^9 to 10^{11} cm^{-3}. Electron densities were determined from the saturation current at the plasma potential, from integration of the electron energy distribution function, and from a power-law approximation of Laframboise's theory[1]. These were compared with microwave interferometer measurements and with densities derived from a combination of published electron-drift velocities and electric field measurements. All these methods agree well with each other. Ion densities deduced from ion saturation currents using Laframboise's theory agree with the electron densities at the very dense and very low electron temperature negative glow, but overestimates the plasma density by up to an order of magnitude in the positive column. This overestimation is attributed to ion-neutral collisions. The solution of the differential equation for ion collection as proposed by Chen[2] underestimates the electron density, but the disagreement is much smaller than Laframboise's. This disagreement can be reduced considerably by applying the correction suggested by Shih and Levi[3].

[1]J. G. Laframboise, Univ. of Toronto Inst. Aerospace Studies Rept. No. 100 (1966).

[2]F. F. Chen, Plasma Phys. 7, 47 (1965).

[3]C. H. Shih and E. Levi, AIAA J. 9, 1673 (1971).

PB-5 Plasma-Sheath Approximate Solutions for Cylindrical Probes, O. BIBLARZ and G. S. BROWN, Nav. Postgrad. Sch., Monterey, CA - Anode sheaths are explored for low-temperature plasmas. The approach involves postulation of an electric field distribution[1]. A ratio (z), specifying plasma composition and condition, groups diverse plasmas with similar sheath characteristics. Another ratio, electrical energy to thermal energy in the sheath, represents the discrete temperatures studied: 6000°K, 3000°K, and 300°K. Charge production in the outer sheath is somewhat generic to the electric field distribution with sheath lengths unaffected by the changes in temperature. Conversely, sheath densities and extent are shown to vary for differing z values. Only anodes with radii comparable to a plasma 'peculiar radius' must be treated with the cylindrical formulation; low to moderate pressure plasmas would require micron-diameter anodes to be thus affected.

[1]O. Biblarz, "Approximate Sheath Solutions for a Planar Plasma Anode", IEEE Trans. Plasma Sci., 19, 1235 (1991).

PB-6 Electron temperature measurements in a magnetized surface-wave-produced plasma (SWP) under ECR conditions, J. MARGOT, M. MOISAN and R. GRENIER, U. de Montréal, M. CHAKER and F. GOLDBERG, INRS-Énergie et Matériaux- Magnetically assisted high frequency plasmas exhibit attractive characteristics for plasma deposition and etching. To take advantage of these interesting properties, one still needs to perform exhaustive studies to reach a better understanding of these plasmas. For this purpose, it is essential to have access to a plasma source whose external parameters can be systematically varied. Generalized SWP offer such a possibility since they can be operated in an extremely broad range of experimental conditions.[1] In this presentation, we report measurements of the electron temperature obtained from both electrostatic probes and ion acoustic waves in a generalized SWP obtained at 2.45 GHz under ECR conditions. We examine the spatial distribution of the electron temperature as well as its anisotropy. From the ion acoustic wave diagnostic, we also determine the bulk plasma velocity along and across the static magnetic field and we estimate the ion temperature.

[1] J. Margot and M. Moisan, Chap. 8 in "Microwave Excited Plasmas", Elsevier (1992)

PB-7 Charged Particle Dynamics Inside the Sheath of a Spherical Electrode in the Presence of Axial Magnetic Field. * - S. Popovic and E. Kunnhadt, Stevens Inst. of Tech., Hoboken, N.J. - Charged particles which move inside the sheath around a biased spherical electrode in the presence of space charge are exposed to a strong central field. The effective trapping of a particle moving in the field of the central force in the presence of axial magnetic field is, however, still possible. It depends on the canonical angular momentum of the particle, character of the central force, and on the magnetic field strength. On their way toward the electrode, located at the center of the discharge, charge particles with angular momentum larger than a critical value, are faced with an effective potential barrier, with a finite amplitude. The barrier increases with the canonical angular momentum of the particle. In front of the barrier, a potential well is created, which tends to keep charged particles from moving straight to the electrode. In the case of the Coulomb force the amplitude of the barrier is infinite and the barrier is located along the central axis parralel to the direction of the magnetic field. The effective trapping of charged particles inside the sheath is shown to influence their transport toward the electrode, and, consequently, the development of the discharge, and the current collected by the electrode.
* Work supported by SDIO/DNA

PB-8 Thomson Scattering Measurements of T_e and n_e in an ECR Discharge. M.D. BOWDEN, F. KIMURA, K. MUTA, K. UCHINO, K. MURAOKA, M. MAEDA, Y. MANABE, M. KITAGAWA and T. KIMURA, Kyushu U and Matsushita Electric - Electron temperature T_e and density n_e in the source region of an ECR discharge have been measured by incoherent Thomson scattering[1] of the beam from a 0.5 J YAG laser. This is the first experiment in which this technique, routinely used on fusion plasmas, has been applied to a processing plasma. Measurements were made in an argon discharge at pressures from 0.3-2mTorr and microwave powers from 250-1000W. Velocity distributions were measured both parallel and perpendicular to the magnetic field and the measured distributions were carefully checked for deviations from a Maxwellian distribution. Temperatures in the range of 1-5 eV and densities in the range of 2-10 x $10^{17}m^{-3}$ were measured. T_e and n_e were found to strongly depend on pressure but only weakly on the input power and discharge magnetic field.

[1]D.E. Evans and J. Katzenstein, Rep. Prog. Phys. 32, 207 (1969).

Session QA

10:15 a.m. – 11:15 a.m.
Friday, October 30, 1992

Georgian Room

Electron Attachment

Chair
F.W. Meyer, Oak Ridge National Laboratory

QA-1 Enhanced Electron Attachment to Laser-Irradiated Molecular Hydrogen*, L. A. Pinnaduwage and L. G. Christophorou, ORNL and University of Tennessee, Knoxville - Efficient H^- formation in laser-irradiated hydrogen is reported. The electrons produced by laser photoionization are converted to negative ions via dissociative electron attachment. The observed H^- signal is more than two orders of magnitude larger than the maximum possible H^- signal that can be expected via electron attachment to high-vibrational states of the ground electronic state that may be indirectly populated. Dissociative electron attachment to superexcited states is proposed as a possible mechanism.[1,2]

*Research sponsored by the Office of Health and Environmental Research, U.S. Department of Energy, under Contract DE-AC05-84OR21400 with Martin Marietta Energy Systems, Inc., and the National Science Foundation.

1. L. A. Pinnaduwage, L. G. Christophorou, and A. P. Bitouni, *J. Chem. Phys.* **95**, 274 (1991).
2. L. A. Pinnaduwage and L. G. Christophorou, *Chem. Phys. Lett.* **186**, 4 (1991); **189**, 486 (1992).

QA-2 Temperature Dependence of the Cross Section for Dissociative Attachment in Methyl Chloride,* D.M. Pearl and P.D Burrow, U. of Nebraska, Lincoln - Datskos et al,[1] using electron swarm methods, have observed a strong temperature dependence for peaks near 0 eV and 0.8 eV in the cross section for dissociative attachment (DA).[2] These peaks increase by more than two orders of magnitude from 400 K to 750 K. We have examined this temperature dependence using electron beam methods and find that the 0.8 eV peak arises from the DA of HCl produced from dissociation of CH_3Cl, presumably on the walls of the oven. Similar effects were found in other saturated monochloroalkanes, such as ethyl and t-butyl chloride, at even lower temperatures.

*Supported by NSF.

[1]P.G. Datskos et al, Chem. Phys. Lett. 168, 324 (1990).

[2]S.C. Chu and P.D. Burrow, Chem. Phys. Lett. 172, 17 (1990).

QA-3 Variation with Temperature of the Dissociative Electron Attachment to CH_3Br[#], P. G. Datskos, L. G. Christophorou, and J. G. Carter, Oak Ridge National Laboratory and The University of Tennessee. --The dissociative electron attachment to CH_3Br exhibits a remarkable dependence on the gas temperature. Low energy electrons ($\leq$1 eV) attach very weakly and dissociatively to CH_3Br at T=300 K but as T is increased to 700 K the electron attachment rate constant, $k_a(<\varepsilon>,T)$ increases by more that 2 orders of magnitude; the thermal value of k_a is 1.08×10^{-11} cm^3s^{-1} at 300 K and increases (by more that 300 times) to 3.28×10^{-9} cm^3s^{-1} as T is raised to 700 K. The profound increases in k_a with small changes in the internal energy of CH_3Br (which may be induced also with infrared excitation) make this molecule a potential candidate for pulsed power switching applications.

[#]Research sponsored by the Office of Health and Environmental Research, U.S. Department of Energy under contract No. DE-AC05-84OR21400 with Martin Marietta Energy Systems, Inc.

QA-4 Effect of Temperature on the Autodetachment of $C_6F_6^{-*}$ P. G. Datskos, L. G. Christophorou, and J. G. Carter, Oak Ridge National Laboratory[#] and The University of Tennessee--At room temperature the C_6F_6 molecule attaches slow ($\leq$1 eV) electrons nondissociatively producing long-lived parent anions. We studied the electron attachment and detachment properties of C_6F_6 in a buffer gas of N_2 for mean energies below 1 eV as a function of temperature T in the range 300 to 575 K. We found that the electron attachment rate constant initially increases slightly with T for T$\leq$450 K and subsequently decreases with increasing T and the autodetachment rate constant of $C_6F_6^{-*}$ increases monotonically as T is raised from 300 to 575 K.

[#]Research sponsored by the Aero Propulsion and Power Directorate, Air Force Wright Laboratory and the Office of Health and Environmental Research, U.S. Department of Energy under contract No. DE-AC05-84OR21400 with Martin Marietta Energy Systems, Inc.

Session QB

10:15 a.m. – 12:00 p.m.
Friday, October 30, 1992

Arlington Room

Optical Diagnostics

Chair
T. Fohl, Technology Integration Group

QB-1 Radical Density Measurements in RF Reactive Plasmas by IR Diode Laser Absorption Spectroscopy, T. GOTO, Dept. of Quantum Eng., Nagoya University - Measurement methods of radicals using infrared diode laser absorption spectroscopy (IRLAS) have been developed and various radicals in processing plasmas have been measured.

In Table 1, the radicals are listed whose densities and rotational temperatures were measured in processing plasmas using IRLAS. The SiH_3, CF_3 and CH_3 radical densities were first measured by the development of IRLAS. They were shown to be of the order of 10^{11-13} cm^{-3} which are much higher than other radical densities.

The diffusion coefficients of SiH_3 and CF and the reaction rate constant of SiH_3 were also measured.

The recent developments of radical measurements by IRLAS described above are reviewed.

Molecule	Radical	Plasma
SiH_4	SiH_3 SiH_2 SiH	RF, P
CF_4	CF_3 CF_2 CF	ECR RF, P
CHF_3	CF_3 CF_2 CF	RF
CH_4	CH_3	RF

QB-2 Spectroscopic study of metastable oxygen in point-to-plane corona discharges, I.S. FALCONER, G.P. TIMMS, L.Y. MONTUNO and B.W. JAMES, School of Physics, U. of Sydney, Australia, and J.J. LOWKE, CSIRO Division of Applied Physics, Lindfield, Australia - A recent theory of the electrical breakdown of air for non-uniform electrical fields[1] proposes that the $a^1\Delta g$ metastable states of molecular oxygen, produced in the pre-breakdown corona and streamer processes, have a dominant role in determining the breakdown voltage. The detachment of O_2^- ions by these $a^1\Delta g$ molecules is of central importance to this theory. The long radiative lifetime of these states (45 minutes), together with their low quenching rate by collisions with oxygen and nitrogen, suggests that the density of these metastable molecules will be sufficiently high for their reactions to be a significant factor in determining the breakdown characteristic, but make their detection a difficult task. We report the result of a spectroscopic study of the dimole emission from these metastable states at 634 nm for point-to-plane corona discharges in both air and oxygen.

[1] J.J. Lowke, J. Phys. D: Appl. Phys. **25** 202-210 (1992)

QB-3 Time-Delayed Fluorescence from the 2px States of Pulse-Irradiated Argon and Neon: The Role of Subexcitation Electrons,* M. A. DILLON, MINEO KIMURA, Argonne National Laboratory, Argonne, IL 60439, and M. M. BURGERS, U. of Melbourne, Australia--In an effort to observe, indirectly, the degradation spectrum of initially fast electrons, radiation from the $2p_1$ level of neon and argon, A, has been measured as a function of time subsequent to excitation by a nanosecond pulse of high-energy electrons. Although the dominant mode of populating the $2p_1$ state is thought to be direct excitation by cascading electrons, the monitored fluorescence arises from

$$A^*(2p_1) \rightarrow A^*(1s_2, 1s_4) + h\nu. \qquad (1)$$

Intensity profiles of reaction 1 for both Ar and Ne reveal an after pulse with a maximum at approximately 100 ns after the initial excitation. One possible mechanism for this phenomenon is reexcitation of the $2p_1$ state by electron impact excitation of the metastable states $1s_3$ and $1s_5$:

$$A^*(1s_3, 1s_5) + e(\text{subexcitation}) \rightarrow A^*(2p_1) \qquad (2)$$

This reaction must be induced by electrons of low kinetic energy, resulting in delayed fluorescence.

* Work supported in part by the U.S. Department of Energy, Office of Energy Research, Office of Health and Environmental Research, under Contract W-31-109-Eng-38.

QB-4 High Sensitivity Absorption Spectroscopy in Glow Discharge Plasmas, J. E. LAWLER, K. MITSUHASHI, R. C. WAMSLEY, University of Wisconsin--A highly sensitive absorption experiment for diagnosing glow discharge plasmas is described. This experiment is applicable from the vuv to the ir. A very stable Xe Arc lamp is used as a source of continuum radiation. An echelle spectrometer equipped with a gated, image intensified, CCD detector array is used to disperse and detect the continuum, with absorption features, after it has traversed the glow discharge. Digital subtraction is used to discriminate against the line emission from the glow discharge and detect only the continuum emission from the arc discharge. Estimates of the relative spectral radiance of glow and arc discharges suggests the subtraction technique is broadly applicable to glow discharge studies. Signal-to-noise ratios and detection limits are discussed. Further improvements in the experiment are proposed.

*Work supported by the General Electric Co.

QB-5 Optogalvanic Effect as a Probe for Plasma Processes,* D. KUMAR, R. R. ZINN and S. P. MCGLYNN, Department of Chemistry, LSU, Baton Rouge, LA - The utility of laser optogalvanic (LOG) effect as a weakly-perturbative probe for low-power plasma processes is demonstrated. The LOG effect in an rf-driven plasma exhibits some unique features when the rf frequency is tuned/detuned relative to the matching-network/plasma resonance. Investigation reveals the presence of two distinct, often overlapping yet separable components in the temporal profile of a LOG signal: one mediated by ionization rate changes and the other by acoustic (e.g., ion-acoustic) effects.[1] Selective laser excitation of appropriate transitions with different decay branching ratios to metastables, to non-metastables and to levels with different radiation trapping effects reveals the importance of this technique. The processes which can be monitored include: direct and collisional photoionization from metastable and non-metastable states, radiation trapping, and accoustic effects. Some sample results in neon, helium, iodine and bromine will be presented.

*Work supported by grants from U. S. Department of Energy and the LSU Center for Energy Studies.

[1]D. Kumar and S. P. McGlynn, J. Chem. Phys. 93, 3899 (1990); Chem. Phys. Lett. 176, 536 (1991).

QB-6 Temporal and Spectral Characteristics of Laser Optogalvanic Signals in an Argon RF Discharge,* D. KUMAR, R. R. ZINN and S. P. MCGLYNN, Department of Chemistry, LSU, Baton Rouge, LA - Temporal and spectral characteristics of pulsed-laser induced optogalvanic signals in some $1s_j \rightarrow 2p_k$ (Paschen notation) excitations in a low power ~30 MHz rf discharge in ~5 torr argon have been investigated. In the tight-coupling regime, the rf plasma behaves as an integral part of the rf resonator. A recently developed method[1] permits separation of two distinct components in the optogalvanic signal, one generated by laser-induced changes in the equilibrium ionization rate (which shifts the rf resonance frequency), and the other generated by a photoacoustic effect (which launches an ion-acoustic wave without producing any change of the net ionization rate). Separability of these two components, which may exhibit temporal overlap, permits the study of acoustic waves in the plasma, and the differentiation of such various plasma processes as radiation trapping, collisional energy transfer, the role of metastable states, low-energy and high-energy (i.e., near ionization threshold) excitation, etc. The ionization and acoustic components will be separated and shown for all of these processes.

*Work supported by grants from U. S. Department of Energy and the LSU Center for Energy Studies.

[1]D. Kumar and S. P. McGlynn, J. Chem. Phys. 93, 3899 (1990).

INDEX OF AUTHORS

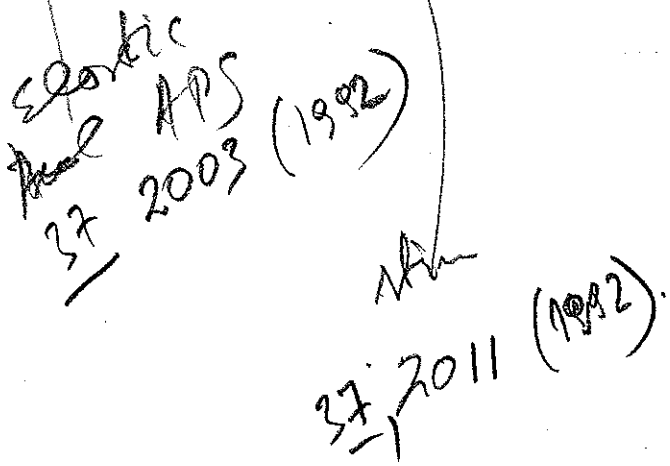

45th Annual Gaseous Electronics Conference

October 27–30, 1992 • Boston Park Plaza Hotel • Boston, Massachusetts

Tuesday, October 27		Wednesday, October 28		Thursday, October 29		Friday, October 30	
AA. 8:00–10:00 Streamers and Time Dependent Discharges Georgian Room	AB. 8:00–10:00 Plasma Modeling Arlington Room	EA. 8:00–10:00 Electronic and Atomic Collision Processes Georgian Room	EB. 8:00–10:00 Radiation, Metastables and Lasers Arlington Room	KA. 8:00–10:00 Collisions of Laser Cooled Atoms Georgian Room	KB. 8:00–10:00 Sheaths and Cathodes Arlington Room	PA. 8:00–9:45 Recent Advances in Electron Atom Collisions Georgian Room	PB. 8:00–10:00 Electrical Characterization of Plasmas Arlington Room
Break							
BA. 10:15–12:00 Atomic and Molecular Collisions Georgian Room	BB. 10:15–12:15 RF Discharge Modeling and GEC Reference Cell Arlington Room	F. 10:30–11:30 Plenary Lecture G. 11:30–12:00 Business Meeting Georgian Room		L. 10:15–12:15 • Posters • Modeling • High Density Plasma Sources and Applications • GEC Reference Cell • Electron Collisions: Experiment Castle		QA. 10:15–11:15 Electron Attachment Georgian Room	QB. 10:15–12:00 Optical Diagnostics Arlington Room
Lunch							
CA. 1:30–3:30 Electron Molecule Collisions Georgian Room	CB. 1:30–3:30 High Density Plasma Arlington Room	HA. 1:30–3:00 Surface Interactions Georgian Room	HB. 1:30–3:00 Novel Plasma Applications Arlington Room	MA. 1:30–3:30 Excited Atoms and Electron Collisions Georgian Room	MB. 1:30–3:30 Plasma Etching Arlington Room		
D. 3:30–5:30 • Posters • Heavy Particle Collisions • Diagnostics • Plasma Surface Interactions Castle		J. 3:30–5:30 • Posters • Glow Discharges • Electron Transport • Ion Transport • Laser Kinetics • Lamps and Switching Arcs • Electron Collisions: Theory • Breakdown Castle		NA. 3:45–6:15 CF_4 Workshop Georgian Room	NB. 3:45–5:45 Plasma Assisted Deposition Arlington Room		
		Social Hour 6:30–7:30 Banquet 7:30–9:30					